Transaldolase 1 is required for Neutrophil Extracellular Trap (NET) Formation

DISSERTATION

zur Erlangung des akademischen Grades

Doctor rerum naturalium

(Dr. rer. nat.)

eingereicht an der

Lebenswissenschaftlichen Fakultät der Humboldt-Universität zu Berlin

von

Jakob Paul Steffen Morath, M. Sc.

Präsidentin

der Humboldt-Universität zu Berlin

Prof. Dr.-Ing. Dr. Sabine Kunst

Dekan der Lebenswissenschaftlichen Fakultät

der Humboldt-Universität zu Berlin

Prof. Dr. Bernhard Grimm

Gutachter/innen

1. Prof. Arturo Zychlinsky, Ph.D.
2. Prof. Dr. Simone Reber
3. PD Dr. med. Robin Kobbe

Tag der mündlichen Prüfung: 17. März 2020

Contents

Zusammenfassung

Transaldolase-Mangel (TALDO) ist ein extrem seltener, angeborener Stoffwechseldefekt, von dem weltweit nur 34 Fälle bekannt sind. Der Defekt geht auf den Verlust des Enzyms Transaldolase 1 aus dem nicht-oxidativen Pentosephosphat-Weg (nicht-oxPPW) zurück und äußert sich in einem weiten Spektrum klinischer Symptome. Die schwerwiegendsten Folgen sind Leber- und Nierenmangelfunktionen, die zum sehr frühen Tod führen können. Desweiteren leiden 15 % der Patienten an wiederkehrenden Infektionen, unter anderem der Atemwege. Neutrophile Granulozyten (Neutrophile) sind die häufigsten weißen Blutkörperchen im Menschen und essentiell für die angeborene Immunantwort gegen Infektionserreger wie Bakterien oder Pilze. Auf dieser Grundlage habe ich funktionale Aspekte von TALDO-Neutrophilen untersucht. Der oxidative Pentosephosphat-Weg (oxPPW) stellt das Reduktionsäquivalent NADPH bereit, welches von der NADPH-Oxidase für den oxidativen Burst in Neutrophilen benötigt wird. Sauerstoffradikale (ROS) aus dem oxidativen Burst sind ihrerseits für die Entstehung von Neutrophil Extracellular Traps (NETs) verantwortlich. Der Beitrag des nicht-oxPPW zur ROS-abhängigen NET-Bildung ist bislang nicht bekannt.

In dieser Arbeit konnte ich für Neutrophile aus drei TALDO-Patienten eine jeweils komplett abwesende Entstehung ROS-abhängiger NETs und einen deutlich verringerten oxidativen Burst nach PMA-Stimulation zeigen. Um diese Beobachtungen in einem unabhängigen Modelsystem zu bestätigen, habe ich mit Hilfe des CRISPR-Cas9-Systems, ‚knock-out' Mutanten von Transaldolase 1 und dessen Partnerenzym Transketolase in der Neutrophil-ähnlichen Zelllinie PLB-985 hergestellt. Die dergestalt genetisch manipulierten Zellen waren nicht mehr zu PMA-induziertem Zelltod in der Lage und wiesen einen deutlich verringerten oxidativen Burst auf. Dies ist somit der erste auf genetischer Evidenz basierende Beweis für die Abhängigkeit des oxidativen Burst und der Bildung von NETs vom nicht-oxPPW. Diese Erkenntnis trägt zum einen zum mechanistischen Verständnis der NET-Entstehung bei und liefert zum anderen eine potentielle Erklärung für einige der bei TALDO beobachteten Symptome.

Ausgehend von der Bedeutung von Transaldolase für die Bildung von NETs wurde eine massenspektrometrische Messung des globalen Metaboloms von PMA-aktivierten Neutrophilen durchgeführt, sowie einige der metabolischen Erfordernisse für die Bildung von NETs mit Hilfe von pharmakologischen Inhibitoren untersucht. Zusammengenommen zeigen die erhaltenen Erkenntnisse, dass das initiale Maximum des oxidativen Bursts für NET-Bildung

unerheblich ist und vielmehr die ROS-Generierung nach ca. 50 Minuten entscheidende Bedeutung für diese hat. Außerdem weisen die gewonnenen Daten darauf hin, dass der bekannte inhibitorische Effekt von 2-Deoxyglucose auf die NET-Bildung nicht zwingendermaßen, wie in der Literatur angenommen, durch Inhibition von Glycolyse und ATP-Produktion verursacht wird, sondern durch Inhibition des PPW und damit der NADPH-Generierung.

Abstract

Transdaldolase 1-deficiency (TALDO) is an extremely rare genetic disease with only 34 described cases globally. It manifests in a missing transaldolase 1 protein, an enzyme of the non-oxidative pentose phosphate pathway (non-oxPPP) and leads to a plethora of clinical symptoms including kidney and liver failure, which can lead to early child mortality. Furthermore, 15 % of the patients suffer from recurrent infections, including infections of the respiratory tract. Neutrophils are the most abundant white blood cells and essential for the innate immune defence against bacterial and fungal pathogens. These observations led me to investigate functional aspects of TALDO neutrophils. The oxidative (ox)PPP generates the reducing equivalent NADPH which is crucial for the NADPH-consuming NOX2-dependent ROS-generation that is essential for neutrophil extracellular trap (NET) formation in neutrophils. The involvement of the non-oxPPP however has not been assessed.

I observed a complete defect of ROS-dependent NETs upon PMA stimulation in 3 TALDO patients and a strong reduction in the oxidative burst. In order to confirm those results in a different system, I knocked out transaldolase 1 and its partner enzyme transketolase in the PLB-985 cell line using the CRISPR-Cas9 system. PLB-985 cells deficient in each enzyme showed a strongly reduced PMA-induced cell death and ROS generation. Thus, I confirmed that transaldolase-1 is required for PMA-induced NET formation in primary neutrophils and the neutrophil-like cell line PLB-985. Accordingly, I provide the first genetic evidence that the non-oxPPP is required for ROS generation and NET formation. Besides providing insights into the mechanistic understanding of NET formation, these results could provide a potential explanation for some of the clinical observations in TALDO patients.

Furthermore, I performed a global mass spectrometry-based metabolome study on PMA-stimulated neutrophils and assessed the metabolic requirements of NET formation by pharmacological inhibition. Taken together, I showed that only the ROS formation after approximately 50 minutes of PMA-stimulation is relevant for netosis whereas the initial oxidative burst peak does not affect NET formation. Moreover, the obtained data indicate that 2-DG´s previously reported inhibitory effect on NET formation could be mediated by inhibition of the PPP and NADPH production rather than as commonly assumed by inhibition of glycolysis and ATP-production.

Table of Figures

Table of Tables

Abbreviations

Abbreviation	Full word or phrase
2-DG	2-deoxyglucose
6-AN	6-aminonicotinamide
Aka	Also known as
ANOVA	Analysis of variance
Au	Arbitrary units
BSA	Bovine serum albumin
Cas9	CRISPR-associated protein-9 nuclease
CL	Cell lysate
Cntr	Control
Conc	Concentration
CPS	Counts per second
CRISPR	Clustered Regularly Interspaced Short Palindromic Repeats
DALY	Disease-adjusted life years
DAPI	4', 6-diamidino-2-phenylindole
ddH_20	Double-distilled water
DMF	N, N-Dimethylformamide
DMSO	Dimethyl sulfoxide
DNA	Deoxyribonucleic acid
DPBS	Dulbecco's phosphate-buffered saline
DPI	Diphenylene iodonium
DSMZ	Deutsche Sammlung von Mikroorganismen und Zellkulturen (English: German Collection of Microorganisms and Cell Cultures)
ECAR	Extracellular Acidification Rate
EDTA	Ethylenediaminetetraacetic acid
Eg	Exempli gratia, latin for *for example*
FCS	Fetal calf serum
GSDMD	Gasdermin D
GSH	Glutathione
HEK	Human embryonic kidney
HRP	Horse Radish Peroxidase
HSA	Human serum albumin
Ie	Id est, latin for *that is to say*
KO	Knock-out
Mol	Molecular
MPO	Myeloperoxidase
MS	Mass spectrometry
NAD	Nicotinamide adenine dinucleotide
NADP	Nicotinamide adenine dinucleotide phosphate
NCBI	National Center for Biotechnology Information
NE	Neutrophil Elastase
NETs	Neutrophil Extracellular Traps
NMR	Nuclear magnetic resonance
NOX2	NADPH Oxidase 2
OCR	Oxygen Consumption Rate
P/S or Pen/Strep	Penicillin/Streptomycin
PBMC	Peripheral blood mononuclear cell
PBS	Phosphate buffer saline
PCR	Polymerase chain reaction
PFA	Paraformaldehyde
PI	Propidium iodide
PMA	Phorbol 12-myristate 13-acetate
PMNs	Polymorphonuclear leukocytes
PPP	Pentose Phosphate Pathway
RNA	Ribonucleic acid
RNAi	RNA interference

Abbreviation	Full word or phrase
ROS	Reactive Oxygen Species
RPMI 1640	Roswell Park Memorial Institute (Cell Culture Medium)
RPMI 1640 wo	RPMI 1640 without phenol red
SDS	Sodium dodecyl sulfate
SDS-PAGE	SDS-polyacrylamide gel electrophoresis
SgRNA	Single guide RNA
TAL	Transalolase 1 (protein)
TALDO1	Transaldolase 1 (gene)
Temp	Temperature
TKL	Transketolase (protein)
TKT	Transketolase (gene)
V	Volt
Vs	Vide supra aka see above
WB	Western blot
Wo	Without
WT	Wild type

1 Introduction

Infections account for a major portion of the global burden of disease which manifests in a staggering amount of disease-adjusted life years (DALY) mainly in low-income countries (WHO 2004). Autoimmune diseases are globally on the rise, with a much higher prevalence in high income countries as compared to middle and low income countries (Agmon-Levin et al. 2011; Selmi 2010).

1.1 Neutrophils

Neutrophils are innate immune cells crucial for the host's response to microbial infections and increasingly reported to take part in pathological over-activation of the immune system.

These cells have several names that are in use and collectively reflect Paul Ehrlich's methodology and observation when he first managed to describe neutrophils and differentiate them from other blood leukocytes (Ehrlich 1880). At the time, and to Paul Ehrlich's disliking, the term *granular* was frequently used in histology. He referred to the term as "a not quite fortunate choice" since it was used to describe a kind of cellular appearance which in fact is caused by a plethora of different cellular characteristics and in his opinion should have been described in a more differentiated way (Ehrlich 1879). When experimenting with more refined staining methods he noticed that not all granular cells (granulocytes) that he identified could be stained with either acidic or basic stains. As opposed to eosinophils (acidic) or mast cells (basic), staining of the remaining granulocytes required a mix of both, and thus *neutral*, stain, hence the name *neutrophil* or *neutrophil granulocyte*. In the same article he described the lobulated nuclei of neutrophils as "peculiarly polymorph nucleus figures" which is already close to the currently used *polymorphonuclear* leukocyte (PMN) (Ehrlich 1880).

Neutrophils are the most abundant type of leukocyte in circulation and form part of the myeloid branch of the hematopoietic system. Blood PMN are terminally differentiated, post-mitotic and very short lived which makes them a cell that is notoriously hard to study due to the difficulty of performing genetic manipulations.

An abnormally low concentration of neutrophils (i.e. neutropaenia) leads to severe bacterial and fungal infections with potential fatal consequences if no counter measures are taken. Neutrophils are *first-responders* and very quick in migrating out of blood vessels

through the tissue towards the source of bacterial dissemination. Their antimicrobial repertoire consists mainly of phagocytosis, degranulation and production of reactive oxygen species (ROS). Besides these direct antimicrobial measures, neutrophils regulate other immune cells such as dendritic cells, T-cells, B-cells, natural killer cells, macrophages as well as endothelial and epithelial cells (Amulic et al. 2012; Mayadas et al. 2014).

1.1.1 Neutrophil Functions

Despite neutrophils' recently increasingly recognized immune regulatory role, their arguably most important functions are those directly addressing and eliminating pathogens. As previously mentioned, those functions include phagocytosis, degranulation, generation of ROS and the formation of neutrophil extracellular traps (NETs); the latter will be introduced in more detail in the next section.

After developing in the bone marrow and entering the blood stream, neutrophils are ready to go but per se quiescent under healthy conditions. Notwithstanding neutrophil activity within blood vessels, it is widely assumed that Neutrophil´s main work load takes place outside of them. Neutrophils are recruited from the blood stream to tissues with an ongoing infection or inflammation. Therefore, as mentioned before, it should be emphasized that prior to most neutrophil antimicrobial effector activity, lies a sophisticated regulatory regime responsible for making the neutrophil aware of an ongoing infection, inflammation or tissue damage. This regime consists mostly of an interplay of endothelial cells and circulating PMNs that lead to neutrophil recruitment, activation and extravasation in several ways (e.g. trans- versus paracellular migration) (De Oliveira et al. 2016). Only then do neutrophils proceed to their main, pathogen-antagonizing activities.

Phagocytosis

Phagocytosis is a process of active engulfment of extracellular material and was first described by Metchnikoff in the 1880s (Tauber 2003) and is an important neutrophil function. Together with macrophages, another myeloid cell, neutrophils are part of the group of professional phagocytes (Lee et al. 2003). Opsonized and non-opsonized particles can be phagocytosed (Lee et al. 2003). Opsonisation consists in coating of a particle with antibodies or components of the complement system which are recognised by neutrophils' Fcγ or complement receptors, respectively, thus rendering the phagocytosis process more efficient (Lee et al. 2003). Opsonised particle engulfment is the quicker and better understood phagocytic process (Amulic et al. 2012). However, pathogen uptake mediated by neutrophils' pattern recognition

receptors (PRR) interaction with pathogen-associated molecular patterns (PAMPs) exists as well (Lee et al. 2003).

Uptake of an extracellular entity leads to its localization in intracellular phagosomes which are double lipid layer-separated cell compartments. Neutrophil phagosomes are subsequently supplemented with an array of antimicrobial proteins via fusion with preformed neutrophil granules and the release of their content into the phagosomes (Nordenfelt & Tapper 2011). Different from macrophage phagosome maturation which results in a strongly acidic milieu, phagosomes in neutrophils maintain a neutral to slightly alkaline pH also in its mature stage (Foote et al. 2019). NADPH oxidase (NOX2) and the intraphagosomal formation of ROS are essential for pathogen killing (Dupré-Crochet et al. 2013). Protein kinase C (PKC) is involved in the regulation of phagocytosis although its precise requirement is still to be elucidated (Lee et al. 2003; Lennartz 1999).

Degranulation

A name-giving characteristic of neutrophil *granulo*cytes are the granules they contain. Granules are cell compartments of different types which differ in their content, size and the time during neutrophil hematopoiesis when they are formed (Amulic et al. 2012). All three types of granules, i.e. primary to tertiary (azurophilic, specific and gelatinase granules, respectively), plus the much smaller secretory vesicles have in common that they contain proteins necessary for the completion of specific neutrophil tasks (Lawrence et al. 2018). To implement those tasks the granular content needs to be secreted or integrated into the plasma membrane at appropriate time points which occurs by degranulation. The ordinal numerals-based granule terminology is based on the time point during neutrophil development when the respective granule is formed and not on their sequence of release from neutrophils.

ROS generation

Nomen est omen, ROS are a diverse group of highly reactive oxidants. Whereas it is well understood that ROS originate from the mitochondrial respiratory chain, xenobiotics or dedicated cellular pathways, the precise mechanisms of their downstream effects are yet to be fully elucidated. ROS can oxidise nucleic acids, lipids or proteins (Ray et al. 2012). Therefore, oftentimes ROS are equalled to harmful oxidative stress for a particular cell or organ which needs to be defended against and which needs to be antagonized in order to reach the homeostatic redox balance. Although this notion is accurate in many circumstances, it

underestimates two important points: First, ROS are important and increasingly recognized factors in cellular regulation (Lichtenberg & Pinchuk 2015; Reczek & Chandel 2015). Second, neutrophils deliberately produce extraordinary amounts of ROS, in a very rapid reaction also termed oxidative burst, as part of their antimicrobial repertoire (Winterbourn et al. 2016).

The importance of the oxidative burst in neutrophil function is best emphasized by the clinical observations made in patients suffering from the genetic deficiency Chronic Granulamotous Disease (CGD) (Assari 2006). CGD patients carry a mutation in genes encoding for subunits of the superoxide producing enzyme NOX2. As stated above, NOX2 is essential for the oxidative burst in neutrophils and its dysfunction leads to recurrent infections and, less well understood, sterile granulomas (Assari 2006; Baehner & Nathan 1967).

NOX2 is a multisubunit complex which is rapidly assembled upon stimulation and oxidizes the reduced form of nicotinamide adenine dinucleotide phosphate (NADPH) in order to reduce oxygen (O_2), thus producing superoxide (O_2^-). Depending on NOX2's localization, superoxide is produced either in the phagosome or extracellularly. Superoxide is subsequently dismutated to hydrogen peroxide (H_2O_2), either spontaneously or superoxide dismutase (SOD)-catalysed. Hydrogen peroxide in turn is the substrate which MPO uses to generate highly reactive hypochlorous acid (HOCl). The three aforementioned oxidants superoxide, hydrogen peroxide and HOCl plus chloramines, the product of HOCl reacting with proteins or smaller molecules, are the most important ones and to varying degrees microbicidal (Winterbourn et al. 2016). Interestingly, compared to NOX2-deficient CGD patients MPO-deficient patients seem to be less vulnerable to infections (Metzler et al. 2012; Winterbourn et al. 2016). Whether this is because of compensation by other unknown factors or due to a result of the much broader immune regulatory role of NOX2 remains a topic of ongoing debate (Winterbourn et al. 2016).

Assessing the precise roles of ROS in general and individual ROS in particular, is challenging on a cellular or *in vitro* level due to their reactivity and the technical restraints when it comes to distinguishing different species. Furthermore, ROS are not only acting on their own behalf but also contribute in crucial ways to other neutrophil functions. Some of the important oxidative burst players are integral parts of degranulation (Lawrence et al. 2018). Furthermore, ROS production is essential for NOX2-dependent NET formation (Fuchs et al. 2007). The latter was nicely emphasized by using gene therapy to recover NOX2 activity in a CGD patient, thus achieving restored NET formation and controlled aspergillosis, normally the

leading cause of death for those patients (Bianchi et al. 2009). Interestingly, ROS was also found to downregulate cytokine production and life span in neutrophils by inducing DNA damage (Harbort et al. 2015).

Taken together, the critical influence exerted by ROS formation in many neutrophil functions substantially complicates the study of its individual contribution to neutrophils' antimicrobial effect.

1.1.2 NET formation

The most recently discovered neutrophil function consists of making NETs (Brinkmann et al. 2004). NET formation is generally assumed to go along with the death of the NET forming neutrophil through an active cell death process which is different from apoptosis and necrosis (Fuchs et al. 2007). This novel cell death program was subsequently termed netosis (Steinberg & Grinstein 2007). It is noteworthy however, that cell death-independent NET formation has been reported (Pilsczek et al. 2010; Tong et al. 2019; Yipp & Kubes 2013). Although, judging by the current body of NET literature, its occurrence could be less frequent or much harder to observe than that of cell death-associated NET formation.

Interestingly, neutrophil cell death caused by *Candida albicans* was already reported 16 years before NETs were observed for the first time (McNamara et al. 1988). The authors hypothesized that "neutrophil death and dissolution" may lead to release of a "substance which inhibits candidal growth" (McNamara et al. 1988).

Eight years later, a phorbol 12-myristate 13-acetate (PMA)-induced cell death different from apoptosis and necrosis and dependent on protein kinase C (PKC) and reactive oxidants was described (Takei et al. 1996). In what was likely the first description of netosis the authors observed chromatin decondensation but did not recognize the extracellular release and the antimicrobial effects (Takei et al. 1996).

Netosis is characterized by chromatin decondensation, nuclear membrane breakdown and subsequent extrusion of chromatin and attached granular proteins into the extracellular space (Brinkmann et al. 2004). NET proteomic studies have been done by our lab and others, identifying dozens of neutrophil proteins of granular or cytosolic origin (Chapman et al. 2019; Urban et al. 2009).

The fact that NETs consist mostly of chromatin and the observation that chromatin mediated antimicrobial activity exists in evolutionary distant organisms as well, led to the yet to be proven or falsified hypothesis that "Immunity is the second function of chromatin"

(Brinkmann & Zychlinsky 2012). Whereas there is an ongoing debate regarding that hypothesis, the notion that NETs are implicated in a wide range of clinically relevant processes including, but not limited to, innate immunity and autoimmune diseases is established (Papayannopoulos 2017).

The shear amount of processes that NETs are reported to be part of, raises many questions with respect to the precise mechanisms involved downstream of the formation of NETs. Some of these question have been answered on a molecular and cellular level. Two principles emerge that mediate the effects of NETs and often mutually apply.

On one hand, NETs and its components, i.e. mainly DNA, histones and granular proteins have immediate effects on the tissues or pathogens in their surroundings (Corbin et al. 2008; Halverson et al. 2015; Hirsch 1958; Silk et al. 2017; Urban et al. 2009; Villanueva et al. 2011).

On the other hand, NETs can have more indirect downstream effects. In an atherosclerosis mouse model, NETs were shown to pull the first of a pair of triggers required for the IL-1ß secretion of macrophages, one of the major drivers of atherosclerosis pathogenesis (Warnatsch et al. 2015).

Netosis is induced through several compounds and signal cascades (Hoppenbrouwers et al. 2017; Kenny et al. 2017). PMA is a plant derived mitogen and very potent netosis stimulator. The potent and robust NET formation it induces, together with the mechanistic parallels observed when comparing it to more physiological stimuli, make PMA a widely used compound when studying ‘classical’ NET formation. Activation of protein kinase C (PKC), ROS formation, phosphorylation of retinoblastoma protein and nuclear lamins as well as nuclear envelope disassembly are among the cellular events required for PMA-induced ROS-dependent NETs. The same processes are also involved in NET formation induced by less potent but more physiological inducers such as the yeast fungus *Candida albicans*, Group B Streptococcus (GBS), monosodium urate crystals or heme (Amulic et al. 2017; Chen et al. 2014; Desai et al. 2016; Kenny et al. 2017; Papayannopoulos 2017). ROS-dependent NET formation depends on the production of superoxide by the NOX2 (Brinkmann et al. 2004; Fuchs et al. 2007).

The ROS-dependent mechanism remains the up to now mostly studied one (Figure 1), although ROS-independent NET formation has been reported. NET stimuli, such as the potassium ionophore nigericin or the calcium ionophore A23187 stimulate NET formation in a ROS-independent manner (Kenny et al. 2017).

A common denominator of many of the above mentioned NET inducers (PMA, *Candida albicans*, nigericin, A23187, GBS) is their independence from *ad hoc* protein synthesis (Kenny et al. 2017; Sollberger et al. 2016).

Two early events in the NOX2-dependent pathway are the activation of the so-called molecular switch Akt (Douda et al. 2014) and of protein kinase C (PKC) (Hakkim et al. 2011). PKC is an activator of the Raf-MEK-ERK pathway (Hakkim et al. 2011) which results in NOX2 activation and subsequent superoxide production. Superoxide is then dismutated to hydrogen peroxide which is used by MPO to produce hypochlorous acid and other oxidants, collectively termed ROS (Klebanoff 2005).

Although the precise role played by ROS during NET formation is not fully elucidated, activation of granular serine proteases, such as NE is one downstream effect of NOX2 activation (Reeves et al. 2002). In addition, localization of ROS synthesis is crucial since intracellular ROS-production and MPO-activity in granules seem to be required for NET formation (Metzler et al. 2012, 2014) whereas extracellular ROS-production is not (Björnsdottir et al. 2015).

The two neutrophil granular proteins MPO and NE play a crucial role in NOX2-dependent NET formation (Metzler et al. 2012; Papayannopoulos et al. 2010). NE translocates to the cell nucleus during NET formation by an hitherto not fully understood mechanism, “where it partially degrades specific histones”, thus contributing to chromatin decondensation (Papayannopoulos et al. 2010). The peroxidase enzyme MPO is required for NET formation (Metzler et al. 2012). It oxidizes chloride to hypochlorous acid in the presence of hydrogen peroxide. Similar to NE although slightly delayed, MPO translocates to the neutrophil nucleus during NET formation (Papayannopoulos et al. 2010). MPO is required for the release of NE from the neutrophil azurophilic granules and possibly plays a dual role in NET formation by enzymatically producing hypochlorous acid as well as being a crucial structural component in chromatin decondensation (Metzler et al. 2014; Papayannopoulos et al. 2010).

Despite being post-mitotic cells neutrophils make use of the cell-cycle pathway when undergoing NET formation (Amulic et al. 2017). The reminiscence of the nuclear envelope break down of NET formation with that of mitosis, led to the identification of cyclin-dependent kinases 4 and 6 as essential enzymes for netosis (Amulic et al. 2017).

Gasdermin D plays a crucial role in netosis and leads to permeabilization of the plasma membrane and subsequent neutrophil lysis (Chen et al. 2018; Sollberger et al. 2018).

Gasdermin D (GSDMD) is cleaved by serine proteases, like NE, into a product that allows its pore-forming assembly and cell-lysing integration into the cellular membrane (Sollberger et al. 2018). Interestingly, GSDMD is prominently known for its cell death mediating role in macrophages where it is activated by the inflamasome and leads to pyroptosis via pore formation (Liu et al. 2016). Thus, GSDMD is a common denominator in two separate cell death pathways in the two myeloid cell lines neutrophils and macrophages.

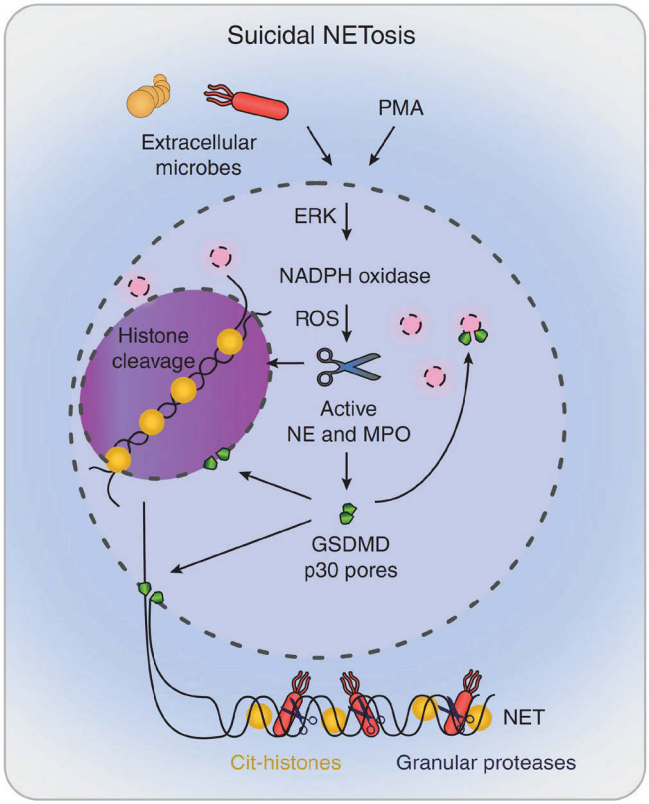

Figure 1 | Depiction of ROS/NOX2-dependent netosis pathway (aka suicidal netosis)
PMA or extracellular microbes induce suicidal netosis by inducing the extracellular signal-regulated kinase (ERK)-dependent assembly of the NOX2, which generates ROS and the cytoplasmic release of granule proteins, and leads to chromatin decondensation in the nucleus. Chromatin is then expelled into the extracellular space via GSDMD pores or GSDMD-driven membrane tears, resulting in neutrophil death. ROS, reactive oxygen sensing; NOX2, NADPH oxidase; PMA, phorbol-12-myristate-13-acetate; GSDMD, gasdermin D; NE, neutrophil elastase; MPO, myeloperoxidase; NET, neutrophil extracellular traps. (Figure and legend taken from Burgener & Schroder 2019 and adapted)

1.2 Cellular Metabolism and Transaldolase 1-deficiency

The vast network of metabolic pathways taking place in the cytosol and some of the cellular compartments is the biochemical backbone of all cellular regulation and activity. Cellular metabolism supplies energy and building blocks to the cell.

Glycolysis

Glucose is transported into the cell and subsequently enters glycolysis which takes place entirely in the cytosol and consists of ten reactions converting glucose into pyruvate. The subsequent reactions, i.e. pyruvate oxidation, Krebs cycle and oxidative phosphorylation all take place in mitochondria.

Together, glycolysis, Krebs cycle and oxidative phosphorylation provide 30-32 molecules of ATP per molecule of glucose. Oxidative phosphorylation contributes the main share of this energy conversion from glucose into ATP. Here, the reducing equivalent nicotinamide adenine dinucleotide (NADH) is used to reduce oxygen to water (H_2O) in an energy-releasing reaction that forms a hydrogen (H^+) potential which is the driving force of the ATP synthase.

Under aerobic conditions cells oxidatively decarboxylate glucose into carbon dioxide (CO_2). When oxygen is limiting cells rely on glycolysis for ATP production, recovering the NAD^+ by reducing pyruvate to lactate and consuming higher amounts of glucose per molecule of ATP.

Glycolysis is energetically less efficient than oxidative phosphorylation but it is quicker (Lunt & Vander Heiden 2011) and products of glycolysis are precursor of nucleotides, lipids and proteins. Glycolysis is intertwined with the pentose phosphate pathway (PPP) (Figure 2).

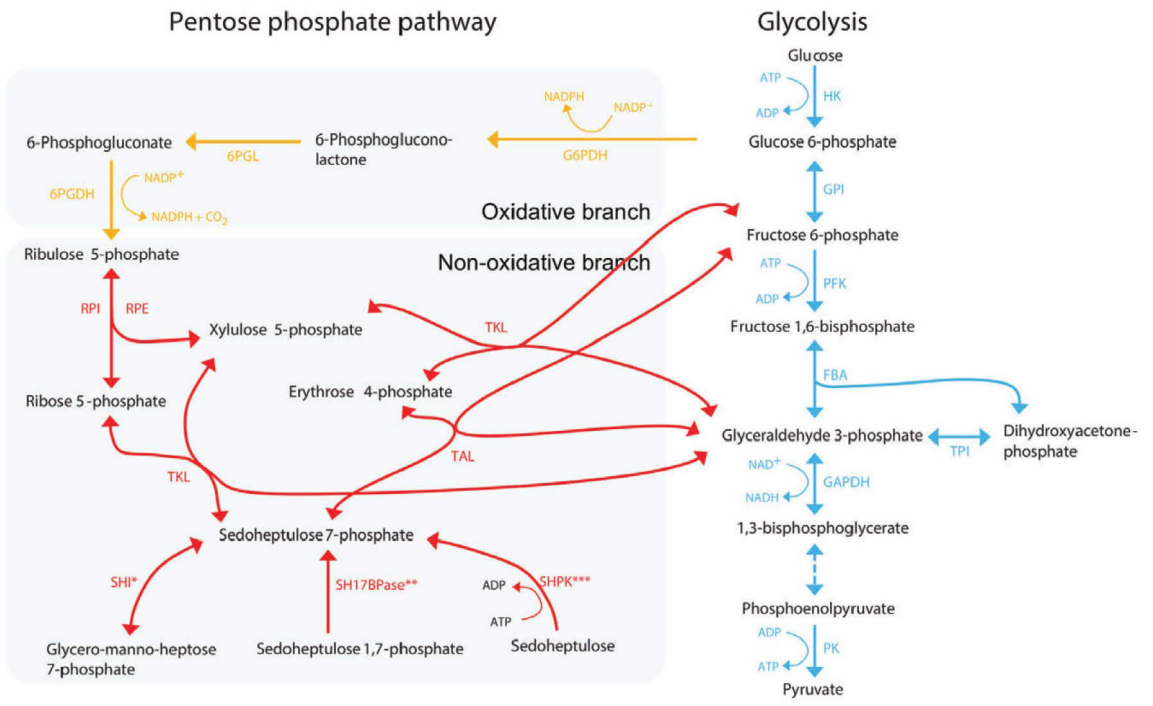

Figure 2 | Schematic representation of the PPP (left) and glycolysis (right).
The enzymatic reactions constituting both pathways are represented by double or single arrows, according to the reversibility of the reaction. The oxidative and non-oxidative branches of the PPP are highlighted by background coloring. Sedoheptulose conversion enzymes found in *bacteria; **fungi (*S.cerevisiae*) & plants and ***mammals.
Abbreviations: HK, hexokinase; G6PDH, glucose-6-phosphate dehydrogenase; 6PGL, 6-phosphogluconolactonase; 6PGDH, 6-phosphogluconate dehydrogenase; RPI, ribose 5-phosphate isomerase; RPE, ribulose 5-phosphate epimerase; TKL, transketolase; TAL, transaldolase; SHI, sedoheptulose 7-phosphate isomerase; SH17BPase, sedoheptulose 1,7-biphosphatase; SHPK, sedoheptulokinase; GPI, glucose phosphate isomerase; PFK, phosphofructokinase; FBA, fructose bisphosphate aldolase; TPI, triosephosphate isomerase; GAPDH, glyceraldehyde 3-phosphate dehydrogenase; PK, pyruvate kinase; SH17BP, SH17BPase. (Figure and legend taken from Stincone et al. 2015)

Pentose Phosphate Pathway

The PPP also occurs in the cytosol and produces ribose 5-phosphate, a precursor of nucleotides and reduces $NADP^+$ to NADPH (Stincone et al. 2015).

The PPP starts with glucose 6-phosphate (G6P) which is oxidized and decarboxylated to ribulose-5-phosphate in three sequential reactions G6P is. Those three reactions produce two NADPH molecules and are jointly called oxidative branch of the PPP (oxPPP). The reactions of the oxidative branch are irreversible.

Then the reversible non-oxidative branch (non-oxPPP) starts (Stincone et al. 2015). Here, four enzymes (ribose 5-phosphate isomerase [RPI], ribose 5-phosphate epimerase [RPE], transketolase [TKL] and transaldolase 1 [TAL]) catalyse the production of the nucleotide precursor ribose 5-phosphate as well as the glycolysis intermediates glyceraldehyde

3-phosphate (GAP) and fructose 6-phosphate (F6P). Thus, the non-oxPPP feeds back into glycolysis and, since its reactions are reversible, vice versa. This also means that both branches of the PPP combined can form a reaction cycle where the non-oxidative branch ends with G6P, the starting molecule of the oxidative branch.

Three out of the four enzymes catalysing the non-oxPPP are essential (Stincone et al. 2015). TAL is an exception, since transaldolase 1-deficient (TALDO) individuals reach adulthood but suffer from different clinical symptoms (Stincone et al. 2015). Transaldolase 1 is a ubiquitously expressed enzyme. It converts a seven-carbon sugar (sedoheptulose 7-phosphate) and a three-carbon sugar (glyceraldehyde 3-phosphate) into a four-carbon sugar (erythrose 4-phosphate) and a six-carbon sugar (fructose 6-phosphate), or vice versa (also see Figure 2, Stincone et al. 2015). Thus, transaldolase 1 provides part of the link between glycolysis and the PPP.

Transaloldase 1-deficiency

TALDO is a very rare genetic disease which has been diagnosed and reported in only 34 patients up to the beginning of this year (Williams et al. 2019). A “Clinical, biochemical, and molecular overview of transaldolase deficiency and evaluation of the endocrine function” was recently published and comprehensively reviews the current literature in addition to providing some up to date information regarding those 34 patients (Williams et al. 2019).

TALDO onset varies between *early* (before or up to one month after birth, 22 patients) and *late* presentation (three months or older, 12 patients). In total eight patients died (24 % mortality), out of which seven presented pre- (one) or neonatal (six) onset. Six patients died within six months after birth and one patient as a teenager. Also, one patient died due to terminated pregnancy, the other seven because of liver dysfunction. Of note, one TALDO patient was identified by sequencing but was asymptomatic (Williams et al. 2019). Overall, the liver was affected in over 85 % of patients some of which presented fibroses or cirrhosis leading or contributing to the lethal outcomes (Loeffen et al. 2012; Verhoeven et al. 2005).

Other frequently observed (>50 %) symptoms are dysmorphic features (triangular-shaped face, low-set ears, wide mouth), skin abnormalities (cutis laxa or wrinkled skin), anemia, thrombocytopenia and cardiac abnormalities. Of note, coagulopathy and bleeding diathesis were observed in 12 patients (35 %) (Williams et al. 2019).

Susceptibility to infections, including recurrent infections of the respiratory tract, were reported for five cases of TALDO (Balasubramaniam et al. 2011; Wamelink et al. 2008; Williams

et al. 2019; Kobbe, personal communication) which could indicate decreased antimicrobial activity of neutrophils in the affected patients.

Pathophysiologically, transaldolase 1-deficiency is thought to cause damage mainly because of the resulting lack of NADPH which leads to deficient control of oxidative stress, e.g. in the liver or hematopoietic bone marrow. Additionally, accumulation of seven-carbon sugars and polyols could potentially have toxic effects (Williams et al. 2019). The consequences of dysfunctional or absent transaldolase 1 seem to be worse in early postnatal development since most lethally affected patients died during that period. However, I am not aware of any pathophysiological hypothesis explaining this observation.

TALDO patients normally present hepatomegaly or dysmorphic features at first consultation with a medical doctor. The final diagnosis can be confirmed with biochemical analysis since polyols and seven-carbon sugars will accumulate in urine, plasma and cerebral spinal fluid. Ultimately, sequencing can provide a final confirmation (Williams et al. 2019).

Transaldolase 1 has been studied in different biological model systems. TAL overexpression in the human Jurkat T cell line leads to decreased levels of NADPH and the reduced form of glutathione (GSH) whereas impaired transaldolase 1 activity increased GSH levels (Banki et al. 1996) suggesting and increased rate or unaffected level of NET formation upon transaldolase 1-deficiency. Mice-spermatozoa lacking transaldolase 1 display reduced levels of NADPH, and GSH (Perl et al. 2006). This led to dysfunctional mitochondrial transmembrane potential and unfertility in male homozygous $TAL^{-/-}$ mice (Perl et al. 2006).

Interestingly, the *TALDO1* gene has two different translation initiation sites which are 30 nucleotides apart and result in two isoforms of TAL (Moriyama et al. 2016). The two isoforms TAL short (TAL-S) and TAL long (TAL-L) localize to the cytosol and to the nucleus, respectively and are encoded by two versions of the *TALDO1* gene, i.e. *TALDO1 short* (*TALDO1S*) and *TALDO1 long* (*TALDO1L*). Depending on their localisation the two isoforms differently influence a range of metabolites in the cell (Moriyama et al. 2016). Interestingly, this finding also shows that the PPP can take place in the nucleus and is not restricted to the cytosol as was commonly assumed until now.

1.3 NADP

NADP is an electron accepting/donating co-factor and essential for the NOX2-mediated oxidative burst in neutrophils as well as for maintaining a redox balance in many other cell types (Stincone et al. 2015). NADP is a pyridine nucleotide and serves in its reduced form

(NADPH) as an important reducing equivalent in neutrophil ROS formation, in the control of ROS-mediated damages in many other cell types and in the reductive biosynthesis of lipids (Williams et al. 2019). Conversely, its oxidized version ($NADP^+$) might possess important functions in calcium based cellular signalling (Agledal et al. 2010).

Interestingly, NADPH/$NADP^+$'s redox potential is very similar to that of NADH/NAD^+ (NADPH/$NADP^+$ without phosphate group), a closely related co-enzyme (Agledal et al. 2010). Nevertheless, the presence of both electron accepting/donating compound pairs is essential for all thus far investigated organisms (Agledal et al. 2010). *De novo* NADP is normally generated in its oxidized form $NADP^+$ by nicotinamide adenine dinucleotide kinases (NADK)-mediated phosphorylation of NAD^+; the synthesis of NADPH by phosphorylation of NADH is less common (Agledal et al. 2010). Beyond the question of *de novo* NADP synthesis and given a sufficient NADP pool, the more relevant question is how to keep a certain NADPH/$NADP^+$ ratio at all times.

Of note, NADPH is regarded to be membrane impermeable, thus rendering the subcellular localization of its generation important (Stincone et al. 2015). The oxPPP is considered to be the most important cytosolic source of NADPH, and is seen as especially crucial in situations of high NADPH demand (Stincone et al. 2015; Winterbourn et al. 2016). NADPH is used by NOX2 to reduce oxygen to superoxide in the neutrophil oxidative burst. Due to NOX2's high maximum rate of electron transfer, the required amounts of cytosolic NADPH can only be provided by the oxPPP (Stincone et al. 2015; Winterbourn et al. 2016).

Notwithstanding the assumed reliance of neutrophil ROS formation on the cytosolic PPP, other NADPH generating enzymes and pathways exist, both in the cytosol and in mitochondria (Agledal et al. 2010; Stincone et al. 2015). Isocitrate dehydrogenase, malic enzyme, aldehyde dehydrogenase, glutamate dehydrogenase, methylene-tetrahydrofolate dehydrogenase and formyl-tetrahydrofolate dehydrogenase are oxidoreductases with cytosolic and/or mitochondrial isoforms in mammalian cells capable of reducing $NADP^+$ to NADPH (Chang & Tong 2003; Donato et al. 2007; Hatefi et al. 1957; Khallaf 2017; Plaitakis et al. 2017; Tottmar et al. 1973). To my knowledge no reports regarding the expression or potential role in neutrophils of any of those oxidoreductases have been published.

1.4 Neutrophils, NETs & Cellular Metabolism

A role of the oxPPP in NET formation seems logical since netosis depends on ROS (Azevedo et al. 2015; Siler et al. 2016). Recently, Riyapa et al. showed that a presumed inhibitor of TKL, the

partner enzyme of transaldolase 1 in the non-ox PPP, blocked NET formation (Riyapa et al. 2019). Genetic evidence is lacking (Riyapa et al. 2019).

1.5 Studying Neutrophils and NET formation

Studies aiming at assessing *in vivo* netosis have been conducted in mice, zebrafish and guinea pigs (Filio-Rodríguez et al. 2017; Isles et al. 2019; Yipp et al. 2012). However, netosis is still mostly studied *in vitro* where it is induced by a range of compounds and through a variety of different pathways as described before (Hoppenbrouwers et al. 2017; Kenny et al. 2017). Netosis is potently induced by the mitogen PMA whose mitogenic properties were discovered over 50 years ago since when it is used as a tumour promoting agent (zur Hausen et al. 1978).

PMA is widely used in netosis research, especially in studies investigating the mechanism of NET formation and its downstream effects. PMA is considered a very useful compound to study the cellular regulation leading to netosis since the NET formation it induces mechanistically parallels many other, more physiological but less robust, NET inducers. An explanation for these mechanistic similarities was recently provided with the finding that the cell-cycle machinery stimulated by mitogens and normally inducing mitosis and cell proliferation is re-purposed in post-mitotic neutrophils and controls the production of NETs (Amulic et al. 2017).

Studying NET formation is complicated because of neutrophils' short life span and post-mitotic state. Mice as the most popular *in vivo* model in immunology are also used in neutrophil research. In fact, whereas traditionally mouse neutrophil function was assessed by antibody depletion, recently a sophisticated genetic model was developed for these assessments (Faget et al. 2018; Hasenberg et al. 2015). However, transferring mouse neutrophil findings to the human situation has to be done with precaution. Mouse neutrophils are very different morphologically and only represent 15-20 % of white blood cells in mice compared to 50-70 % in humans (Haley 2003). Also, neutrophil subsets that were discovered in mouse, although admittedly in the specific situation of the tumour environment, were not identified in humans (Fridlender et al. 2009). Furthermore, netosis in murine and human neutrophils is differentially affected when exposed to serum components *in vitro*, thus further complicating the study of the underlying process (Neubert et al. 2019).

Investigating the mechanism of netosis in human cells relies on pharmacological inhibition in primary cells and genetic manipulation in neutrophil-like cell lines (Hakkim et al. 2011; Kawakami et al. 2014; Sollberger et al. 2019). Although the *ex vivo* generation of

neutrophils from multipotent hematopoietic stem cells is also possible, this model has until now not been used for the study of NET formation to my knowledge (Jie et al. 2017). The HL-60 cell line and the HL-60-derived cell line PLB-985 were established from the peripheral blood of an acute myeloid leukemia patient (Collins et al. 1977; Zhen et al. 1993). Both can be differentiated into neutrophil-like cells and as such are used as a PMN model than can be genetically engineered (Kawakami et al. 2014; Sollberger et al. 2019). PLB-985 cells undergo a PMA-induced cell death that is reminiscent of netosis and therefore constitute a suitable model for investigating its mechanism (Sollberger et al. 2019).

Besides immortalized cell lines, occasionally genetically abnormal primary neutrophils can be used for the study of neutrophil biology. Patients, frequently children, with inborn errors can serve as sources of such samples which provide important insights into PMNs functioning in health and disease states (Klein 2016).

This work is primarily based on primary neutrophils of patients suffering from genetic transaldolase 1-deficiency and on genetically manipulated PLB-985 cells.

1.6 Aim of the study

The aim of this study was to assess the ability of TALDO neutrophils to forms NETs and thus to provide a potential explanation for the observed phenotype in TALDO patients as well as to contribute to the mechanistic understanding of netosis.

2 Material & Methods

2.1 Material

2.1.1 Primary Cells

Table 1| Primary cells

Primary cell type	Source
Healthy donor	Charité, Berlin
TALDO patient donor (HH)	Robin Kobbe, Universitätsklinikum Eppendorf, Hamburg
TALDO patient donor (Paris 1 & 2)	Pascale de Lonlay, Hôpital Necker-Enfants malades, Paris

2.1.2 Cell Lines

Table 2 | Cell lines

Cell line	Source
HEK-293 cells	Leibniz Institute DSMZ, Braunschweig
PLB-985 cells	Mary Dinauer, Washington University School of Medicine, St Louis (Zhen et al. 1993)

2.1.3 Bacteria

Table 3 | Bacteria

Bacteria	Catalogue Number, Supplier
Heat shock-competent Stbl3	C737303, Thermo Fisher Scientific

2.1.4 Media, buffers and other solutions

Table 4 | Base media

Name	Short name	Catalogue Number, Supplier
DMEM	DMEM	10938-025, Gibco
Optimem	Optimem	31985-070, Gibco
RPMI 1640	RPMI 1640	31870-025, Gibco
RPMI 1640, wo phenol red	RPMI 1640 wo	32404-014, Gibco
Seahorse XF RPMI, wo phenol red	XF RPMI	103336-100, Agilent

Table 5 | Media composition

Medium Name	Base medium	Final concentration					
		FCS	Glutamine	Pen/strep	DMF	HEPES	HSA
PMN/neutrophil	RPMI 1640 wo	-	-	-	-	10 mM	0.1 %
Carbonate-free assay (PMN)	XF RPMI	-	-	-	-	10 mM	0.1 %
HEK	DMEM	10 %	2 mM	100 U/ml, 100 µg/ml	-	-	-
PLB	RPMI 1640	10 %	2 mM	100 U/ml, 100 µg/ml	-	-	-
PLB thawing	RPMI 1640	20 %	2 mM	100 U/ml, 100 µg/ml	-	-	-
PLB differentiation	RPMI 1640	2.5 %	2 mM	100 U/ml, 100 µg/ml	0.5 %	-	-
PLB assay	RPMI 1640 wo	1 %		100 U/ml, 100 µg/ml	0.5 %	10 mM	-
Carbonate-free assay (PLB)	XF RPMI	1 %		100 U/ml, 100 µg/ml	0.5 %	10 mM	-

Table 6 | Buffer & Solutions

Name	Catalogue Number, Supplier
DPBS	14190094, Gibco
Histopaque-1077	10771, Sigma-Aldrich
Histopaque-1119	11191, Sigma-Aldrich
Luminol enhancer solution	1859698, Thermo Scientific
MES SDS Running buffer	NuPAGE, NP0002, Invitrogen
Peroxide solution	1859701, Thermo Scientific
UltraPure Water	L0020, Biochrom

2.1.5 Inhibitors, media supplements & other Chemicals

Table 7 | Inhibitors, media supplements & other chemicals

Name	Catalogue Number, Supplier
2-Deoxyglucose	D3179, Sigma-Aldrich
6-Aminonicotinamide	A68203, Sigma-Aldrich
Cell-Tak adhesive	354240, Corning
Diphenyleneiodonium	D2926, Sigma-Aldrich
Fetal Calf Serum	S0115, Biochrom GmbH
Glucose	G8270, Sigma-Aldrich
Glutamine	G3120, Sigma-Aldrich
Glycine	3790.2, Roth
HEPES	15630-056, Gibco
Horse Radish Peroxidase	31941, Serva
Luminol	11050, AAT Bioquest
Mowiol 4-88	17951, Polysciences
Penicillin/Streptomycin	15140-122, Gibco
Puromycin	A11138-02, Gibco
Tween20	P1379, Sigma-Aldrich

2.1.6 Antibodies and dyes for FACS, microscopy and western blot

Table 8 | FACS

Antigen	Fluorochrome (Detection channel)	Conc	Cell type	Catalogue Number, Supplier	Clone
CD15	FITC (B1)	1:40	PMN	130-081-101, Milteny	
CD3e	APC Vio 770 (R2)	1:40	T-cell	130-102-306, Milteny	
CD62L	PE (B2)	1:100	Steady-state PMN	130-113-625, Milteny	REA615
DNA	DAPI (V1)	1 µg/ml	Dead cells	D9542, Sigma-Aldrich	
Siglec 8	APC (R1)	1:100	Eosinophil	347105, Biolegend	7C9

Table 9 | Microscopy/EVOS FL

Name	Concentration	Catalogue Number, Supplier
anti-mouse Alexa 567	1:500	A11004, Life technologies
anti-rabbit Alexa 488	1:500	A11008, Life technologies
Draq5	2.5 µM	DR50050, Biostatus
Hoechst 33342	1:1500	62249, Thermo Scientific
mouse anti-PL2-3	4 µg/ml	In house (V. Brinckmann)
rabbit anti-Neutrophil Elastase	1:500	481001, Calbiochem
SytoxGreen	1 µM	S7020, Invitrogen

Table 10 | Western Blot

Name	Host	Concentration/dilution from stock	Diluent	Catalogue Number, Supplier	Clone
Anti-tubulin	mouse	1:1000	PBS-T	62204, Invitrogen	DM1A
HRP-conjugated anti-mouse		1:5000	PBS-T	115-035-166, Jackson Lab	
HRP-conjugated anti-rabbit	goat	1:2000	PBS-T	111-035-144, Jackson Lab	
Polyclonal anti-transaldolase	rabbit	0.2 µg/ml	PBS-T	ab187689, abcam	

2.1.7 Assay kits

Table 11 | Kits

Name	Catalogue Number, Supplier
CytoTox 96 Non-Radioactive Cytotoxicity Assay	G1780, Promega
DuoSet ELISA human CCL4/MIP-1 beta	DY271, R&D Systems
DuoSet ELISA human CXCL8/IL-8	DY208, R&D Systems
FITC AnnexinV Apoptosis Detection Kit I	556547, BD Pharmingen
Invisorb Spin Pasmid Mini Two kit	1010140300, Stratec Molecular
Lenti-X GoStix	631281, Clontech Laboratories
Zymoclean Gel DNA recovery kit	D4002, ZymoResearch

2.1.8 Enzymes (CRISPR KO generation related ones are listed in the methods section)

Table 12 | Enzymes (except for CRISPR KO related ones listed in the methods section)

Enzyme	Catalogue Number, Supplier
RNAse A	EN0531, Thermo Scientific
Proteinase K	EO0491, Thermo Scientific

2.1.9 Oligonucleotides used to generate CRISPR-Cas9 guide RNA

Table 13 | Oligonucleotides used to generate CRISPR-Cas9 guide RNA

Target gene (guide number-orientation)	5' overhang (generic)	20 nt specific target sequence (5'-3')	3' overhang (generic)
MPO (38F)	CACCG	TGGTGGACTTAGGACCTTGC	
MPO (38R)	AAAC	GCAAGGTCCTAAGTCCACCA	C
MPO (39F)	CACCG	AAGCTGCTTCTGGCCCTAGC	
MPO (39R)	AAAC	GCTAGGGCCAGAAGCAGCTT	C
TALDO1S (40F)	CACCG	GTAAGCGGGCATCTGTGCTG	
TALDO1S (40R)	AAAC	CAGCACAGATGCCCGCTTAC	C
TALDO1S (41F)	CACCG	GATGCCCGCTTACCAGGAGC	
TALDO1S (41R)	AAAC	GCTCCTGGTAAGCGGGCATC	C
TALDO1L (42F)	CACCG	AGCTCGACATAGCAAGACCG	
TALDO1L (42R)	AAAC	CGGTCTTGCTATGTCGAGCT	C
TALDO1L (43F)	CACCG	GCTCACCCGTGAAGCGTCAG	
TALDO1L (43R)	AAAC	CTGACGCTTCACGGGTGAGC	C
TKT (44F)	CACCG	CATCCAGGCCACCACTGCGG	
TKT (44R)	AAAC	CCGCAGTGGTGGCCTGGATG	C
TKT (45F)	CACCG	GGTCATTGTGCGGATTCCGG	
TKT (45R)	AAAC	CCGGAATCCGCACAATGACC	C

2.1.10 Plasmids

Table 14 | Plasmids

Name	Supplier
lentiCRISPR v2	Feng Zhang, Broad Institute, Boston
pMD2.G	Addgene
psPAX	Addgene

2.1.11 Primers

Table 15 | Primers for knock-out sequencing

Name	Sequence incl. overhang (5'-3')
MPO (38F)	ACACTCTTTCCCTACACGACGctcttccgatctTATCCATAGACAGGGCCCTCTGA
MPO (38R)	TGACTGGAGTTCAGACGTGTGctcttccgatctAACCACCCCAACACACCATCTTC
MPO (39F)	ACACTCTTTCCCTACACGACGctcttccgatctAGATGGGGGTTCCCTTCTTCTCT
MPO (39R)	TGACTGGAGTTCAGACGTGTGctcttccgatctAGGAAGGCCTGCTCTGAGAAAAG
TALDO1S (40F)	ACACTCTTTCCCTACACGACGctcttccgatctAAGGCCAACTAGACTAGCACGAG
TALDO1S (40R)	TGACTGGAGTTCAGACGTGTGctcttccgatctCTGGGGAATTACAGGGTTCCTTC
TALDO1S (41F)	ACACTCTTTCCCTACACGACGctcttccgatctAAGGCCAACTAGACTAGCACGAG
TALDO1S (41R)	TGACTGGAGTTCAGACGTGTGctcttccgatctCTGGGGAATTACAGGGTTCCTTC
TALDO1L (42F)	ACACTCTTTCCCTACACGACGctcttccgatctTCACCGTGGAAGTCGCCCGTGTC
TALDO1L (42R)	TGACTGGAGTTCAGACGTGTGctcttccgatctTTCGTCCAGGCGCGCAGGGACCA
TALDO1L (43F)	ACACTCTTTCCCTACACGACGctcttccgatctCCGCGCCGTCCTCACCGTGGAAG
TALDO1L (43R)	TGACTGGAGTTCAGACGTGTGctcttccgatctTTCGTCCAGGCGCGCAGGGACCA
TKT (44F)	ACACTCTTTCCCTACACGACGctcttccgatctGCACCATGGAGAGCTACCACAAG
TKT (44R)	TGACTGGAGTTCAGACGTGTGctcttccgatctCCACCTTCCTCGTCTAGGCATCT
TKT (45F)	ACACTCTTTCCCTACACGACGctcttccgatctCAGGTCTCCTCAAAGACCACTCA
TKT (45R)	TGACTGGAGTTCAGACGTGTGctcttccgatctTGCCTGTGTCTGTCTTCTCTCCT

2.1.12 Software and web tools

Table 16 | Software and web tools

Software/web tool	Supplier
Fiji	https://imagej.net/Fiji/
FlowJo_V10	Becton-Dickinson
Graph Pad Prism	GraphPad Software
http://www.browsergenome.org/	Schmid-Burgk et al. 2014
http://www.e-crisp.org/E-CRISP/	Heigwer et al. 2014
http://www.outknocker.org/	Schmid-Burgk et al. 2014
https://chopchop.cbu.uib.no/	Labun et al. 2016
https://www.ncbi.nlm.nih.gov/tools/primer-blast/	USA NCBI
MS Office	Microsoft
Adobe Illustrator CS4	Adobe
R (open source statistical programming language)	https://cran.r-project.org

2.1.13 Technical Equipment with respective software

Table 17 | Technical Equipment

Equipment	Software (if applicable)	Supplier
CASY Cell Counter		Innovatis
Confocal Microscope Leica SP 8	Leica LAS X	Leica
EvosFL Auto 2		Invitrogen
Fluoroscan Ascent	Ascent Software Version 2.6	Thermo Labsystems
MAQS Quant		Milteny Biotec
Microplate Reader Versa Max	SoftMax Pro 7	Molecular Devices
Nanodrop		Thermo Fisher
Seahorse		Agilent
Thermal Cycler S1000		Biorad

2.1.14 Plastic ware

Table 18 | Plastic ware

Plastic ware	Supplier
µ-slide 8 well ibiTreat dishes	Ibidi
12-well plate	Sarstedt
15 & 50 ml falcon tubes	Corning
2, 5, 10, 25 & 50 serological pipettes	Corning
24-well plate	Sarstedt
5 ml FACS tubes	BD Biosciences
6-well plate (adherent cells)	Sarstedt
6-well plate (suspension cells)	Sarstedt
Cryotubes	Nunc
Pasteur pipette	VWR
PCR plates	Eppendorf
PCR tubes	Life technologies
T25 flask	Sarstedt
T75 flask	Sarstedt
Transparent flat bottom 96-well plate	Sarstedt
Transparent round bottom 96-well plate	Sarstedt
White flat bottom 96-well plate	Nunc

2.1.15 External measurements

Table 19 | Commissioned companies to do external measurements

Measurement type	Company
Metabolome mass spectrometry	Metabolon
Next generation sequencing	Atlas Biolabs
Sanger Sequencing	Eurofins Genomics

2.1.16 Other Material

Table 20 | Other Material

Name	Catalogue Number, Supplier
High Performance Chemiluminescence Film	28906837, GE Healthcare
NuPAGE 4-12% Bis-Tris Gel	NuPAGE, NP0336BOX, invitrogen
Precision Plus Protein Standards Dual Color	161-0374, Biorad
PVDF Membrane	1060023, GE Healthcare

2.2 Methods

2.2.1 Neutrophil Isolation

Blood sampling was approved by the ethics council of the Charité Hospital Berlin or the institutions of our collaboration partners; all donors gave informed consent according to the Declaration of Helsinki.

Human neutrophils were isolated using a two-step density separation. Blood was collected in 9 ml EDTA-treated tubes (S-monovette, 02.1066.001, Sarstedt) and layered on top of 7.5 ml histopaque-1119 in a 15 ml falcon tube filling it up to the top. The tubes were centrifuged for 20 minutes at 800 xg at room temperature, acceleration 7, deceleration 4. Subsequently, the two top layers (plasma & peripheral blood mononuclear cells (PBMC)) were removed using a vacuum pump. The third layer (i.e. neutrophils) was transferred with a Pasteur pipette to 50 ml tubes and washed once in at least 3 times the volume of Dulbecco's phosphate-buffered saline (DPBS) incl. 0.1 % human serum albumin (HSA) at 300 xg for 10 minutes at room temperature.

The resulting supernatant was discarded; the pellet was resuspended in 1 ml DPBS incl. 0.1 % HSA, carefully layered on top of a discontinuous Percoll gradient (65 % - 85 % in 2 ml layers) and centrifuged for 20 minutes at 800 xg at room temperature, acceleration 7, deceleration 4. The resulting supernatant was discarded; the pellet was washed in 10 ml DPBS incl. 0.1 % HSA at 300 xg for 10 min at room temperature.

This supernatant was discarded; the pellet was resuspended in 2-6 ml DPBS incl. 0.1 % HSA. Subsequently, isolated neutrophils cells were counted using a CASY cell counter system.

2.2.2 Neutrophil Phenotyping by Flow Cytometry

Neutrophils were blocked in 1:67 Fc blocking reagent (130-059-901, Milteny) in phosphate buffered saline (PBS) at a concentration of $5*10^5$ cells/ml in 100 µl volume in Eppendorf tubes placed on ice for 5 minutes. An equal volume of antibody dilution in PBS at 2 x concentration was added and cells were incubated for 30 minutes on ice.

Subsequently, cells were washed three times in PBS at 450 xg and resuspended in 200 µl PBS per tube. 4', 6-diamidino-2-phenylindole (DAPI) stain was added just before cells were measured in MAQS Quant. Results were analyzed using FlowJo_V10.

2.2.3 PLB-985 differentiation

PLB-985 differentiation was based on a protocol previously published by our lab (Sollberger et al. 2019). On day 0, PLB-985 cells were plated at a density of $1.2*10^6$ cell per 3 ml PLB differentiation medium per well in suspension cell 6-well plates. On day 4, 2 ml PLB differentiation medium was added per well.

On day 7, cells were harvested by centrifuging them down in 15 ml falcons at 300 xg for 10 minutes. Subsequently, cells were resuspended in 1 ml PLB assay medium and layered onto 3 ml of histopaque 1077 in 15 ml falcons and then centrifuged at 800 xg for 20 minutes (acceleration 7, brakes 7). After centrifugation, floating cells were collected using a Pasteur pipette and washed once in PLB assay medium by centrifuging at 300 xg for 10 minutes. Subsequently, cells were re-suspended in 1 ml PLB assay medium, then counted using a Casy cell counting device and used for assays.

2.2.4 Cell freezing & thawing

Freezing

HEK and PLB aliquots were frozen down in aliquots of 1 ml FCS containing 10 % DMSO in Cryotubes (082685, Nunc) stored in a Mr. Frosty-device at -80°C for at least one day before transferring aliquots to liquid nitrogen tank.

Thawing

HEK-293 cells

HEK293 cells were thawed in a water bath at 37 °C as quickly as possible and taken up in 10 ml HEK medium. Then, cells were washed once, centrifuged at 300 xg for 10 min. Resuspended in 10 ml HEK medium and plated out in T75 flask at 37 °C, 5% CO_2.

PLB-985 cells

Cells taken from liquid nitrogen were thawed in 37 °C water bath as quickly as possible and taken up in 10 ml PLB thawing medium (see Table 5). Subsequently, cells were washed three times at 300 xg in order to get rid of DMSO. Then, cells were plated out in 5ml in T25 flasks overnight at 37 °C. On the following day, medium was changed and cells were plated out in the same flask in 5 ml fresh medium and left over night at 37 °C. On the next day cells were transferred to a T75 flask and 5 ml normal PLB medium was added. From this point on, cells were used for differentiation.

2.2.5 Viability measurements

Annexin V/PI

The FITC Annexin V Apoptosis Detection Kit I (556547, BD Pharmingen) was used according to the manufacturer's instructions. Cells were measured in a MAQS Quant Flow Cytometer (Milteny). Results were analyzed using FlowJo_V10 (Becton-Dickinson).

LDH measurement

The CytoTox 96 Non-Radioactive Cytotoxicity Assay (G1780, Promega) was used according to the manufacturer's instructions. Samples were measured using a Microplate Reader Versa Max (Molecular Devices) and the corresponding software SoftMax Pro 7.

Hypodiploid DNA Content

Hypodiploid DNA content was measured based on a published protocol (Taylor et al. 2007). On respective time points, 10^5 cells per well were harvested, transferred to round-bottom 96-well plates and centrifuged at 200 xg for 2 minutes at 4 °C. Obtained supernatants were discarded and cells were briefly vortexed to disrupt the cell pellets. Subsequently, cells were resuspended in 200 µl 70 % ethanol, transferred to Eppendorf tubes and incubated on ice for 10 minutes for permeabilization. Then, cells were washed 3x by centrifuging at 500 xg at 4 °C by resuspending them in PBS. Subsequently, cells were resuspended in 0.5 mg/ml RNase A as well as 60 µl 0.1 mg/ml propidium iodide and incubate at room temperature for 25 minutes in the dark. Then, 100 µl PBS were added per tube and hypodiploid DNA content was measured using a MAQS Quant Flow Cytometer (Milteny). Results were analyzed using FlowJo_V10 (Becton-Dickinson).

2.2.6 NET measurements

PL2-3 staining

On the day of NET induction

Glass cover slips were washed in 100 % EtOH and left to dry before placing them in 24-well plate. 10^5 neutrophils were added in neutrophil assay medium and left in incubator at 37 °C, 5 % CO_2 for approximately 30 minutes. Subsequently, 100 nM PMA was added. NET formation was stopped with 2 % PFA after respective amount of time. Cells were kept at 4 °C overnight.

On the day of NET staining

Coverslips were washed in floating drops of 300 µl PBS on falcon holder lined with parafilm. Subsequently, fixed cells were permeabilized in 200 µl 0.5 % TritonX-100/PBS for 5 minutes.

Then blocked in 300 µl blocking buffer (3 % donkey serum, 3 % fish gelatine, 1 % BSA, 0.05 % Tween in PBS) for 30 minutes at room temperature.

Subsequently, each cover slip was incubated for 1-2 hours at room temperature in 50 µl primary antibody (mouse anti-PL2-3, produced in house by microscope facility, used at 4 µg/ml and rabbit anti-NE (used at 1:500 from stock) in blocking buffer.

Then, the coverslips were washed again 3 x in 300 µl PBS for 5 minutes before staining for 30 minutes to 1 hour at room temperature with 50 µl secondary antibody (anti-mouse alexa 567 and anti-rabit alexa 488, both 1:500) and Hoechst (1:1500 dilution) in blocking buffer. Subsequently, coverslips were washed again 3 x in 300 µl PBS for 5 minutes, before mounting them in 7 µl Mowiol 4-88, briefly drying them and storing them at 4 °C until proceeding to imaging. Staining, imaging and quantification was done as previously described (Brinkmann et al. 2012)

Sytox Green/Draq 5 staining (Evos)

Neutrophils plated in 1 ml neutrophil assay medium per well in 24-well plate at concentration of 10^5 cells per ml and left in incubator at 37 °C, 5 % CO_2 for approximately 30 minutes. Subsequently, NET formation was induced by adding 100 nM PMA.

After 170 minutes, 2.5 µM Draq5 and 1 µM SytoxGreen were added. After 10 minutes, incubation NET formation was visually assessed with the 20x magnification objective of the EVOS (EvosFL Auto 2, Invitrogen). The total amount of cells was counted manually based on Draq5 staining and bright field visualization. NETs were manually counted based on SytoxGreen positivity and expanded nuclei. NET positive rate was given as ratio of those two values.

Sytox Green Assay (Fluoroscan)

10^6 neutrophils per ml were suspended in medium incl. 500 nM Sytox green. Cells were distributed in technical triplicates onto flat-bottom 96-well plate, i.e. 10^5 cells in 100 µl medium per well. Then the respective inhibitors were added to appropriate wells before the whole plate was placed at 37 °C, 5 % CO_2-incubator for 30 minutes. Subsequently, 100 nM PMA were added for NET induction.

The plate was measured once just after stimulation and from there on every hour. Measurements were performed using the Fluoroscan Ascent and the corresponding software Ascent Software Version 2.6. Settings: Measurement type: single. Integration time (ms): 20. Excitation: 485 nm. Emission: 518 nm.

PMA-induced cell death at given time points is given as fold-increase compared to the first measurement.

Live Confocal Microscopy Imaging (Sollberger et al. 2018)

Live imaging was performed with help from my lab colleague Dr Alf Herzig. $5*10^5$ cells per well were distributed in µ-slide 8 well ibiTreat dishes in PMN assay medium containing 500 nM Sytox Green and 2.5 µM Draq5. Cells were inhibitor treated for 30 minutes and stimulated with 100 nM PMA. Subsequently, cell images were acquired at 37 °C in 2 minute intervals using glycerol immersion on a Leica TCS SP8 confocal microscope equipped with a Leica HC PL APO 20x/0.75 IMM CORR CS2 objective. Draq5 stains nuclei of cells with an intact cell membrane. Imaging was used for individual cell nuclei tracking and to determine nuclear area of live cells. Sytox Green measurements indicate permeability of cells.

2.2.7 ROS measurement and analysis

10^5 neutrophils in 100 µl medium per well were plated in a white, flat bottom 96-well plate (Nunc) and left in incubator for 30 minutes at 37 °C. Subsequently, 1.2 U/ml HRP and 50 µM luminol were added to each well, and incubated for 10-15 minutes. Then, 100 nM PMA was added and immediately afterwards measured in a luminometer (Victor XLight, PerkinElmer).

ROS production was measured as luminescence-reaction and is given as counts per second (CPS). Experimental measurements were normalized and are shown as regression model. Normalized CPS values (*norm CPS)* were calculated using the formula

$$norm\ CPS = \frac{CPS_x - CPS_{min}}{CPS_{max} - CPS_{min}}$$

Subsequently, *norm CPS* of independent experiments were taken together and displayed using the non-parametric local regression smoothening approach *Loess* (span = 0.1) from the ggplot package of R (statistical programming language).

2.2.8 Oxygen consumption measurement

Oxygen consumption was measured using a Seahorse device (Agilent Technologies) and the respective Seahorse equipment based on the Seahorse user guides and test kit instructions.

XF96 cell culture microplates were coated in 25 µl Cell-Tak adhesive per well for 20 minutes at room temperature (adhesive diluted to 22.4 µg/ml 0.1 M $NaHCO_3$ pH6.5-8) as indicated in the Cell-Tak adhesive's instructions for use. Subsequently, microplates were

washed twice in ddH_20 and stored for up to a week at 4 °C. 5*10^4 neutrophils in 50 µl XF RPMI wo phenol red medium (103336-100, Agilent Technologies) incl. 2 mM glutamine and 10 mM glucose were added to each well of the coated XF96 microplates. Microplates were centrifuged at 200 xg for 1 minute without breaks. Then, plates were placed into a no-CO_2 incubator at 37 °C for 25-30 minutes, before adding 130 µl medium per well and placing the plate in the no-CO_2 incubator for an additional 15-25 minutes. This happened in parallel with the XFe96 sensor cartridge (Agilent Technologies) calibration.

Subsequently, the seahorse measurement was initiated. Results are given as pmol/min (oxygen consumption rate, OCR) or mpH/min (extracellular acidification rate, ECAR).

2.2.9 Cytokine measurements

10^5 cells in 200 µl medium per well were seeded in flat bottom 96-well plates. Cells were incubated for 5 hours before collecting supernatants. Secretions of cytokines IL-8 and MIP-1ß was assessed using the commercially available DuoSet ELISA kits human CXCL8/IL-8 (DY208) and human CCL4/MIP-1 beta (DY271, both R&D Systems). Plates were measured at a Microplate Reader Versa Max (Molecular Devices) and the protocol 'ELISA-Endpoint HRP TMB' of the corresponding software SoftMax Pro 7.

2.2.10 Western Blot

Lysate generation

2*10^6 cells were taken up in 200 µl hot 2 x SDS buffer and left for 10 minutes at 95 °C on heat block. Then, lysates were sonicated for 5 seconds, aliquoted and stored at -20 °C.

Preparation of 10 ml 6 x SDS: 1.2 g SDS, 6 mg bromphenol blue, 4.7 ml glycerol, 1.2 ml 0.5 M Tris HCl 6.8, 2.1 ml H_2O, 1 g DTT.

SDS-PAGE

For protein separation NuPAGE 4-12% Bis-Tris Gels (NuPAGE, NP0336BOX, Invitrogen) and the corresponding MES SDS running buffer (NuPAGE, NP0002, Invitrogen) were used. Lysate of 100,000 cells was loaded per sample (normally 10 µl). 5 µl of the Precision Plus Protein Standards Dual Color (161-0374, Biorad) was used and gels were run at 80 V for 5 minutes and then at 150 V for 60 minutes.

Protein transfer and signal detection

Separated proteins were transferred by semi-dry transfer onto a 0.45 µm PVDF membrane (1060023, GE Healthcare) (activated in methanol just before transfer) for 50 minutes at 110 mA. Gel and membrane were 'sandwiched' in blotting paper soaked in 1x transfer buffer incl. 20 % methanol just before (10x transfer buffer: 30 g trisbase, 144 g glycine, filled up to 1 l with deionized water). Subsequently, the membrane was blocked by shaking in 5 % milk powder in PBS for 60 minutes at room temperature. Then, the membrane was washed 3 x 5 minutes in PBS-T (i.e. PBS incl. 0.05 % Tween20) and incubated in 10 ml 0.2 µg/ml polyclonal anti-transaldolase antibody (rabbit, ab187689, Abcam) in PBS-T at 4 °C over night. On the next morning, the membrane was washed 3 x 5 minutes in PBS-T before incubating in 1:2000 secondary HRP-conjugated goat anti-rabbit antibody in PBS-T for 1 hour shaking at room temperature. Then, the membrane was washed again for 3 x 5 minutes in PBS-T. Subsequently, the protein signal was amplified by 1 minute incubation in 1:1 peroxide solution (1859701, Thermo Scientific) and luminol enhancer solution (1859698, Thermo Scientific). Chemiluminescence was detected using high performance chemiluminescence film (28906837, Amersham Hyperfilm ECL, GE Healthcare).

2.2.11 Generation of guideRNA specific lentiviral transfer plasmids

To obtain specific lentiviral transfer plasmids, the protocol 'sgRNA cloning' published by Feng Zhang on https://www.addgene.org/crispr/reference/#protocols was used with adaptations. 'sgRNA cloning' is based on material and methodology developed and published by Feng Zhang's group (Sanjana et al. 2014; Shalem et al. 2014).

Digestion and dephosphorylation of lentiCRISPRv2 plasmid

The lentiCRISPR v2 plasmid was a gift from Feng Zhang (Addgene plasmid #52961; http://n2t.net/addgene:52961; RRID: Addgene_52961).

Table 21 | Digestion and dephosphorylation

	Volume	Catalogue Number, Supplier
5 µg lentiCRISPR v2	x	Feng Zhang, Broad Institute
FastDigest Esp31 (BsmBI)	3 µl	FD0454, Thermo Scientific
FastAP Thermosensitive Alkaline Phosphatase	3 µl	EF0654, Thermo Scientific
10x Fast Digest Green Buffer	6 µl	Thermo Scientific
100 mM DTT (freshly prepared in H_2O)	0.6 µl	ALX-280001-GO25, ENZO Life Sciences
ddH_2O	x	
total	60 µl	

The digestion and dephosphorylation reaction was performed in an Eppendorf tube for 30 minutes at 37 °C. The reaction product was gel purified (see below).

Gel purification of digested and dephosphorylated lentiCRISPRv2 plasmid

The reaction product was loaded onto a 1 % agarose gel and run for 30 minutes at 100 V. Subsequently, the top band ('back bone') was cut out and the contained plasmid DNA was recovered using a Zymoclean gel DNA recovery kit (D4002, ZymoResearch) according to the manufacturer's instructions. The DNA concentration was measured using a Nanodrop-device and the digested plasmid was stored at – 20 °C until further use.

Annealing and phosphorylation of oligonucleotides

Table 22 | Annealing and phosphorylation

	Volume	Catalogue Number, Supplier
10x Buffer T4 DNA Ligase incl. 10 mM ATP	1 µl	B0202S, NEB
T4 Polynucleotide Kinase	0.5 µl	M0201L, NEB
ddH_2O	6.5 µl	
100 µM forward & reverse oligo	1 µl each	Sigma-Aldrich
total	10 µl	

Single guide RNAs were designed using either http://www.e-crisp.org/E-CRISP/ (Heigwer et al. 2014) or https://chopchop.cbu.uib.no/ (Labun et al. 2016). Corresponding oligonucleotides were ordered at Sigma-Aldrich (see Table 13 for sequences).

The annealing and phosphorylation reaction was set up in PCR tubes in a thermal cycler (S1000, Biorad) as follows: 30 minutes at 37 °C, followed by 5 minutes at 95 °C and subsequent temperature decreases of 5 °C per minute until 25 °C. Obtained oligo duplexes were diluted 1:200 in UltraPure H_2O and stored at – 20 °C.

Ligating oligonucleotides into vector

Table 23 | Ligation reaction

	Volume	Catalogue Number, Supplier
50 ng/µl BsmBI-digested plasmid lentiCRISPRv2	1 µl	See above
1 µM oligo duplex	1 µl	See above
10x T4 DNA Ligase buffer	1 µl	Thermo Scientific
ddH_20	7 µl	
T4 DNA Ligase 200 Weiss U (5 Weiss U/µl)	0.4 µl	EL0014, Thermo Scientific
total	10.4 µl	

The ligation reaction was set up in Eppendorf tubes and incubated for 30 minutes at room temperature. Subsequently, the reaction product was immediately transformed into heat-shock competent Stbl3 bacteria.

Transformation into heat-shock competent Stbl3 bacteria

20 µl frozen solution of competent bacteria (thawed on ice) were added to the ligation product of the previous reaction and kept on ice for 20 minutes. Subsequently, bacteria were heat shocked for 90 seconds at 42 °C, then placed on ice for 1 minute, before 200 µl LB medium was added and transformed bacteria were left to 'recover' for 30 minutes at 37 °C, mildly shaking.

Finally, transformed bacteria were plated out on ampicillin containing LB plates and grown over night at 37 °C.

Isolation of guideRNA-carrying lentiCRISPRv2 plasmid

Plasmids were isolated using the Invisorb Spin Pasmid Mini Two kit (1010140300, Stratec Molecular). Concentration of obtained plasmid DNA was measured on a nanodrop device. DNA samples were sent out for sequencing at a concentration of 50-100 ng/µl in 15 µl ddH_2O to Eurofins Genomics. The primer used for sequencing was hU6-F (5'- AGGGCCTATTTCCCATGATT- 3') as suggested on the addgene plasmid repository for lentiCRISPR v2 (Plasmid #52961) insertions (https://www.addgene.org/52961/).

2.2.12 HEK-293 transfection and PLB-985 transduction

HEK-293 cell transfection

HEK cells were grown up to 75-85 % confluence in HEK cell medium in 6-well plates. Medium was removed and 1.5 ml optimum medium was carefully added. After 1-2 hours transfection mixes A and B were prepared as follows:

- Mix A (volumina per well): 125 µl optimem medium + 7.5 µl lipofectamine 3000 reagent (L3000008, invitrogen).
- Mix B (volumina per well): 125 µl optimem medium + 0.5 µg psPAX + 1.5 µg pMD2.G + 9 µl P3000 reagent (100022057, invitrogen). Mix B was well mixed by pipetting and distributed onto Eppendorf tubes.

Subsequently, 2.2 µg target specific plasmid DNA was added to respective Eppendorf tubes before adding 125 µl of mix A to each tube. The transfection solution was mixed and incubated for 10-15 minutes at room temperature before carefully adding the whole mix to the HEK cells. Transfected HEK cells were incubated overnight at 37 °C in 5 % CO_2.

Medium was removed on the following morning and discarded as virus contaminated, 1.2 ml fresh HEK medium was added to cells very carefully. HEK cells were incubated overnight at 37 °C in 5 % CO_2.

Virus containing supernatant was collected on the following day, centrifuged at 250 xg to remove HEK cells and cell debris and immediately used for PLB-985 cell transduction (see below). The virus titer was tested using Lenti-X GoStix (631281, Clontech Laboratories).

PLB-985 transduction

PLB-985 cells were suspended at a concentration of $3*10^5$/ml fresh PLB medium and 1 ml cell suspension was seeded per well in a 12-well plate and incubated for 1 hour at 37 °C in 5 % CO_2. Virus containing supernatant was carefully given to PLB-985 cell suspension and cells were incubated for 48 hours at 37 °C in 5 % CO_2.

Subsequently, PLBs were collected and centrifuged at 365 xg for 5 minutes. Then, cells were resuspended in 2 ml PLB medium incl. 2.5 µM puromycin and plated out in 6-well plates in 2 ml per well.

About a week after the transduction, the PLBs were collected and centrifuged at 365 xg for 5 minutes again. Then, resuspended in 2 ml PLB medium, again incl. 2.5 µM puromycin and plated out in 6-well plates in 2 ml per well. Untransduced control cells were completely dead at this time point whereas the transduced cells were clearly recovering from the puromycin treatment.

On day 10-14 after the transduction, cells were collected and 288 single cells per guideRNA construct were seeded in 100 µl PLB medium per well, respectively, in round-bottom 96-well plates and grown for 2-3 weeks at 37 °C in 5 % CO_2. Subsequently, 32 grown clones per construct were picked, provided with fresh PLB medium, transferred to a new plate and grown for an additional 1-2 days at 37 °C in 5 % CO_2. Subsequently, cells were genotyped (see below).

Genotyping of PLB single cell clones

Genotyping of transduced PLB single cell clones was done based on slightly adapted procedures and the OutKnocker web-tool developed by Jonathan Schmid-Burgk (Schmid-Burgk et al. 2014). Half the cells of each PLB single cell clone colony were frozen down in FCS incl. 10 % DMSO at -80 °C.

To the other half 30 µl lysis buffer was added per well (composition: 0.2 mg/ml proteinase K, 1 mM $CaCl_2$, 3 mM $MgCl_2$, 1 mM EDTA, 1 % Triton X-100, 10 mM Tris (ph 7.5)).

Cells were then transferred to PCR tubes and lysed for 10 minutes at 65 °C, followed by 15 minutes at 95 °C. Then, lysates were stored at 4 °C until further processing for deep sequencing.

Subsequently, the targeted DNA loci were amplified using loci specific primer pairs. Primers were designed using the web tool http://www.browsergenome.org/ (Schmid-Burgk et al. 2014); see Table 15 for primer sequences. The amplification PCR set-up and conditions are described in the two tables below.

Table 24 | Amplifying PCR composition

	Volume for 1 reaction
5 x HF buffer	1.25 µl
dNTP (10 mM each)	0.125 µl
Forward primer (10 µM)	0.3125 µl
Reverse primer (10 µM)	0.3125 µl
DMSO	0.1875 µl
Phusion polymerase	0.0625 µl
ddH_2O	3 µl
genomic DNA	1 µl
total	6.25 µl

Table 25 | Amplifying PCR conditions

	Step	Temperature in °C	Time in seconds
	Initial Denaturation	98	180
20x	Denaturation	98	10
	Annealing	65	30
	Elongation	72	15
	Final Extension	72	600
	Hold	12	

The obtained DNA of the amplified loci was used for a second PCR and “a combination of barcode primers that is unique for each clone to be analysed” (Schmid-Burgk et al. 2014). The barcode PCR set-up and conditions are described in the two tables below.

Table 26 | Barcoding PCR composition

	Volume for 1 reaction
5 x HF buffer	1.25 µl
dNTP (10 mM each)	0.125 µl
Primer mix (10 µM)	0.3125 µl
DMSO	0.1875 µl
Phusion polymerase	0.0625 µl
ddH_2O	3.3125 µl
Amplified genomic DNA	1 µl
total	6.25 µl

Table 27 | Barcoding PCR conditions

	Step	Temperature in °C	Time in seconds
	Initial Denaturation	98	180
20x	Denaturation	98	10
	Annealing	60	30
	Elongation	72	15
	Final Extension	72	600
	Hold	12	

The obtained PCR products were pooled (2 µl per PCR sample, i.e. approximately 1.5 ml total volume) and loaded on a 1.5 % agarose gel which was run at 100 V for 70 minutes. DNA of 300-450 kb size was cut out of the gel, using UV light and a scalpel. Subsequently, DNA was recovered from the gel using the Zymoclean gel DNA recovery kit (D4002, Zymo Research) according to the supplier's instructions.

DNA clean-up was done based on Schmid-Burgk et al., 2014. Adding 0.1 volumes of 3 M NaOAc (pH5.2) and 1.1 volumes of isopropanol precipitated DNA. Then, centrifuging the sample for 30 minutes at 4 °C at 12,000 xg produced a DNA pellet which was washed once in 70 % ethanol and subsequently centrifuged for 15 minutes at 4 °C. The resulting pellet was resuspended in 30 µl ddH_2O, before spinning down and removal of the non-soluble fraction by 1 minute centrifugation. DNA concentration was measured in the remaining supernatant using a nanodrop device. The DNA was sent out for next generation sequencing ("250 bp single read dual index run") at Atlas Biolabs GmbH in Berlin.

Sequencing results were analysed using the OutKnocker web tool http://www.outknocker.org/ (Schmid-Burgk et al. 2014).

2.2.13 Sample preparation for (external) metabolome measurement

Sample preparation and shipping was done based on the sample preparation and shipping guidelines of Metabolon, Inc. (Morrisville, NC, USA).

Material & Methods

10^7 neutrophils per sample were suspended in 3.5 ml Seahorse XF RPMI medium, without phenol red (103336-100, Agilent) incl. 10 mM HEPES, 10 mM glucose and 2 mM glutamine and incubated in 5 ml FACS tubes for 10-15 minutes in rotator at 37 °C. Subsequently, four samples per donor (unstimulated control at time 0, and 100 nm PMA-stimulated samples after 15, 30 & 45 minutes incubation, respectively) were taken. PMA was added 45, 30 and 15 minutes before collecting the samples, respectively. This way all samples were collected at the same time. Cells were centrifuged at 300 xg for 5 minutes, then resuspended and transferred to 1.5 ml-Eppendorf tubes. Subsequently, cells were centrifuged at 400 xg for 2 minutes, supernatants were discarded completely to minimize buffer residual. Cell pellets were shock frozen in liquid nitrogen and stored at –80 °C until shipment.

Metabolon, Inc. performed mass spectrometry-based global metabolite measurement and provided an analysis of the resulting data including a heat map and statistical results for each sample group.

3 Results

The main focus of this work is the role of the enzyme transaldolase 1 (TAL) in neutrophil extracellular trap (NET) formation. The gene encoding for transaldolase 1 is *TALDO1* and the commonly used name for the disease caused by transaldolase 1-deficiency is TALDO. Accordingly, throughout this work, I will use 'transaldolase 1' or the abbreviation 'TAL' when referring to the protein. The italic '*TALDO1*' will be used when referring to the gene whereas 'TALDO' or 'transaldolase 1-deficiency' will refer to the genetic disease.

3.1 TALDO primary neutrophils

Individuals with a genetic transaldolase 1-deficiency (TALDO patients) are, with only 30-40 known cases to date, very rare (Lipinski et al. 2017; Williams et al. 2019). I obtained blood samples from three different TALDO patients who are in treatment with Dr Robin Kobbe at the Universitätsklinikum Eppendorf in Hamburg (one patient) and with Dr Pascale de Lonlay at the Hôpital Necker-Enfants malades in Paris (two patients). All patients were male and between 15 and 20 years old. Due to unavailability of equipment, technical restraints, limited availability of cell material and/or limited viability of neutrophils, I could only perform some assays with each of the TALDO patients. The origin of the sample(s) used for an assay will be indicated as *HH* (Hamburg patient) or *Paris 1* or *2* (Paris patient 1 or 2, respectively) where applicable.

3.1.1 Transaldolase 1 expression in TALDO neutrophils

I determined transaldolase 1 expression in a control sample and in a TALDO patient sample by Western Blot (Figure 3). I used a polyclonal anti-transaldolase 1 antibody which did not recognize any presence of transaldolase 1 in the TALDO sample whereas there was a clear tubulin signal, which was used as a loading control. The healthy donor sample presented a clear transaldolase 1 signal as well as a tubulin signal which was comparable to that of the TALDO sample. Thus, these data show that transaldolase 1 is either not expressed or efficiently degraded in TALDO patient cells.

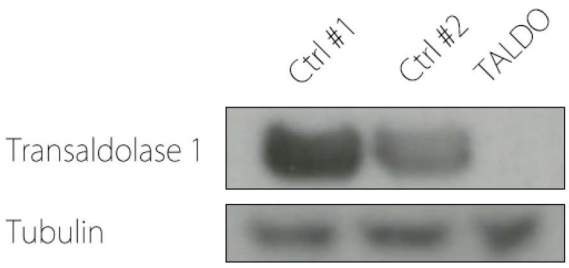

Figure 3 | TALDO patient neutrophils do not express transaldolase 1.
Cell lysate of 10^5 cells was loaded per SDS polyacrylamide gel lane. The separated proteins were transferred by semi-dry transfer onto a PVDF membrane. Transaldolase 1 and tubulin were detected by Western blot. Cell lysate of one patient (Paris 1).

3.1.2 TALDO neutrophil viability

To document fundamental characteristics of TALDO neutrophil *in-vitro* behaviour I assessed the neutrophil viability of TALDO patients by either staining isolated neutrophils directly after an overnight LPS treatment with annexin V/propidium iodide (HH) or, if no flow cytometer was available, by fixing the cells first in 70 % ethanol after the treatment and subsequently measuring the hypodiploid DNA content (Paris1) (also compare section 2.2.5). The viability results are layed out in Table 28 as percent of viable cells.

Table 28 | The viability of neutrophils (as % viable cells) from TALDO patients is comparable to that of healthy donors.
Viability measured for samples of two donors (HH & Paris 1).

Condition \ Patient	HH		Paris 1	
	Control	TALDO	Control	TALDO
unstimulated	31.2	20.6	22.5	28.7
200 ng/ml LPS (15 hours)	36.9	36.1	41.8	27

TALDO neutrophils showed a similar viability compared to control cells. The LPS treatment did only have a minor, if any, effect on neutrophil viability. I conclude from this data that *in-vitro* TALDO and healthy donor neutrophil viability is similar.

3.1.3 TALDO neutrophils do not form NETs after PMA stimulation

Based on the observation that TALDO patients present recurrent infections (Balasubramaniam et al. 2011; Wamelink et al. 2008, Robin Kobbe, personal communication) and to test the role of the non-oxPPP in the mechanism of NET formation, I assessed whether TALDO neutrophils form PMA-induced NETs (Figure 4 & Figure 5).

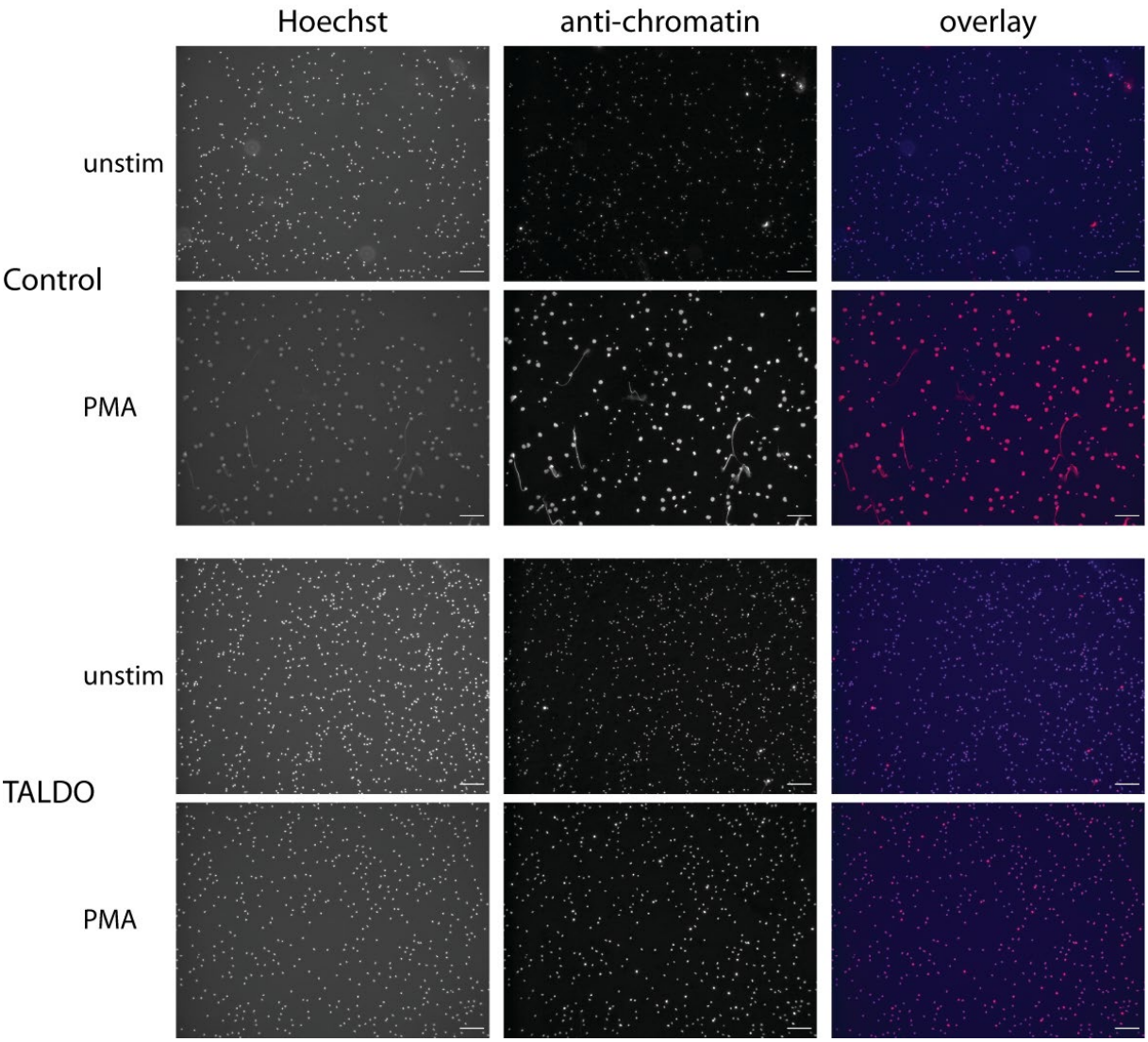

Figure 4 | TALDO neutrophils do not form PMA-induced NETs (representative microscopy images). Neutrophils were treated with 100 nM PMA for 180 minutes and fixed in 2 % PFA overnight. Samples were stained with Hoechst 33342 and the chromatin detecting anti-PL2-3 antibody and subsequently imaged using fluorescence microscopy. Scale bars represent 100 µm. Microscopy image of one patient (HH)

Hoechst binds to DNA and thus stains cell nuclei. The PL2-3 antibody (*anti-chromatin* in Figure 4) recognizes an epitope formed by Histone 2A, Histone 2B and DNA that is exposed in NETs. As expected, unstimulated neutrophils remain dim for both TALDO and the healthy control. Adding 100 nM PMA to the healthy control for 3 hours led to the expected NET formation and therefore bright PL2-3 signal. In stark contrast, the PMA stimulated TALDO cells remain dim despite the stimulation although the signal does seem stronger than that of the unstimulated sample (Figure 4).

I quantified the data using an operator independent quantification protocol (Brinkmann et al. 2012). The mean percentage of control cells that underwent NET formation was at 65 % +- 17 % SEM compared to 2.4 % +- 1.5 % SEM in the TALDO group (Figure 5).

These data show that TALDO neutrophils do not form NETs in response to PMA.

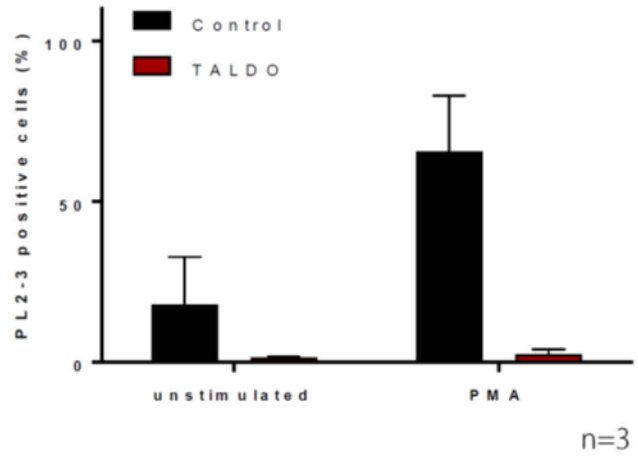

Figure 5 | TALDO neutrophils do not form PMA-induced NETs (image quantification).
Neutrophils were treated with 100 nM PMA for 180 minutes and fixed in 2 % PFA overnight. Samples were stained with Hoechst 33342 and the chromatin detecting anti-PL2-3 antibody and subsequently imaged using fluorescence microscopy. Images were quantified using the ratio of the PL2-3 to Hoechst 33342 positive cells after applying size and intensity thresholds as described in the methods section. NET formation of three patients was measured (HH, Paris 1, Paris 2).

3.1.4 TALDO neutrophils do not produce PMA-induced oxidative burst

Since I observed deficient NET formation in TALDO neutrophils and the canonical NET generating pathway relies on an oxidative burst producing ROS, I measured the capability of TALDO neutrophils to produce ROS in response to PMA treatment (Figure 6). I used a well established protocol which detects the production of the ROS superoxide and hydrogen peroxide as luminol-amplified chemiluminescence (Bedouhène et al. 2017, also compare section 2.2.7 ROS measurement).

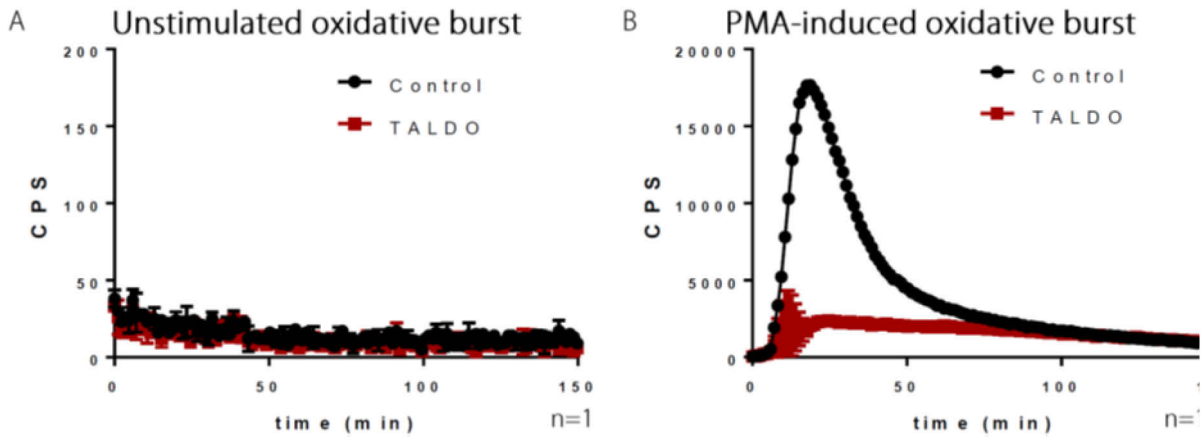

Figure 6 | TALDO neutrophils do not produce oxidative burst in response to PMA.
10^5 neutrophils in 100 µl per well were distributed in 96-well plates and stimulated with 100 nM PMA A, ROS production as counts per second (CPS) in unstimulated neutrophils. B, ROS production as counts per second (CPS) in PMA-stimulated neutrophils. Oxidative burst of one patients was measured (HH).

There is no oxidative burst in PMA-induced TALDO neutrophils (Figure 6 B). Although there is a reaction of those cells to PMA, it is very minor and very brief compared to the control cell´s reaction. As negative control I included unstimulated cells, which as expected, do not show any reaction (Figure 6 A).

3.1.5 The PMA-induced OCR and ECAR are differently affected in TALDO neutrophils

I confirmed ROS formation with a different method. The cellular oxygen consumption upon PMA stimulation can be used as a proxy of neutrophil's NOX2 activity since it is absolutely unaffected by mitochondrial inhibition which make a mitochondrial contribution unlikely (Chacko et al. 2013). Furthermore, the steady-state oxygen consumption in neutrophils is negligibly low (Kramer et al. 2014).

The oxygen consumption rate in PMA-stimulated TALDO neutrophils is reduced to 50 % of the healthy control (Figure 7 A). This was a surprising result, given that the oxidative burst was almost completely absent in TALDO neutrophils (Figure 6). Nevertheless, it shows a severe defect in the machinery responsible for the oxidative burst in neutrophils. In addition, this result indicates that possibly neutrophils need to reach a certain threshold to form NETs. However, this data stems from a single patient.

ECAR is a commonly used measurement used as an approximation for the glycolysis rate. The ECAR of TALDO neutrophils is not different from the ECAR of control neutrophils (Figure 7 B). For both samples the steady-state rate is at a low rate of below 5 mpH/min, as expected for neutrophils and increases to a peak of 10 mpH/min upon PMA-stimulation before slowly decreasing and returning to the steady-state level 120 minutes after the stimulation.

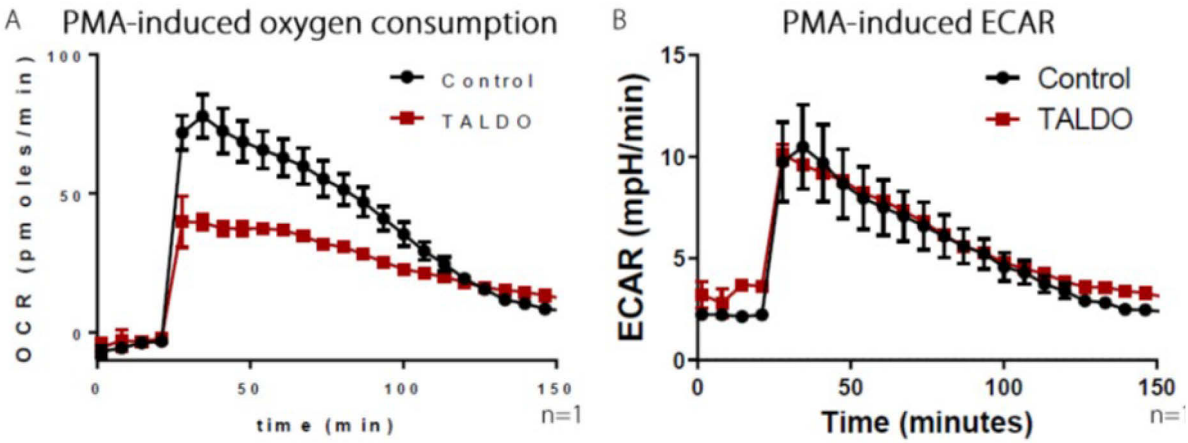

Figure 7 | PMA-induced OCR is strongly reduced and ECAR remains unaltered in TALDO neutrophils of one patient (HH).
Cells were distributed and stimulated with 100 nM PMA after 30 minutes incubation time, ie after the fourth measured time point. A, Seahorse measurement of the OCR. B, Seahorse measurement of ECAR. Experiments were performed with sample of one patient (HH).

3.1.6 NE does not translocate to nuclei in PMA-stimulated TALDO neutrophils

The translocation of NE is a hallmark of canonical ROS-dependent NET formation (Papayannopoulos et al. 2010). Since I observed a deficient ROS-response and NET formation in TALDO neutrophils, I tested whether the translocation of NE to the nucleus would also be inhibited. Whereas 180 minute PMA-stimulation leads to NE presence in almost the entire cell nucleus, this was not the case in TALDO neutrophils (Figure 8). The TALDO neutrophil nuclei did not only, not expand but also do not present any NE staining co-localizing with the DNA stain Hoechst. There does seem to be a relocalization of NE around the nucleus or in vicinity to the cell membrane.

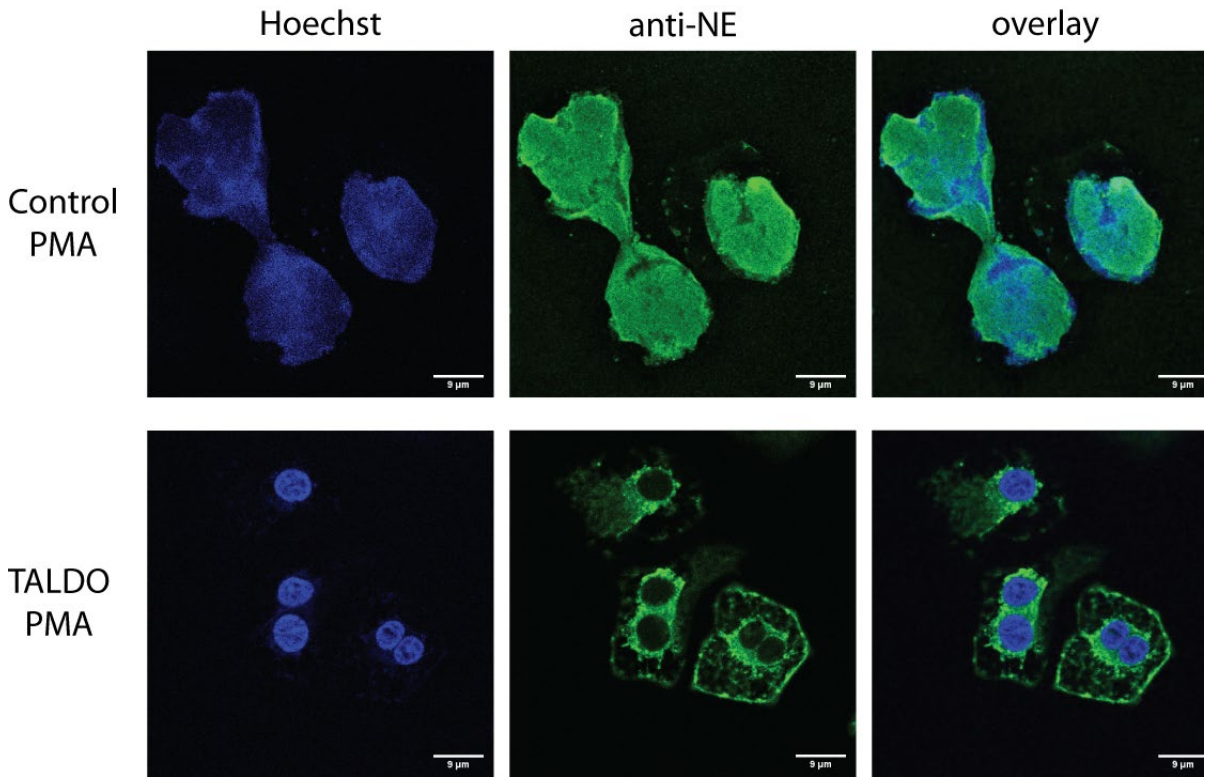

Figure 8 | NE does not translocate to the nucleus of PMA-stimulated TALDO neutrophils
Neutrophils were treated with 100 nM PMA for 180 minutes and fixed in 2 % PFA overnight. Samples were stained with Hoechst 33342 and the anti-NE antibody and subsequently imaged using a SP8 confocal microscope. NE translocation in neutrophils of one patients was imaged (Paris 1).

3.1.7 TALDO neutrophil cytokine secretion

I measured secretion of the neutrophil cytokines IL-8 and MIP-1ß in unstimulated and LPS-stimulated neutrophils (Figure 9). LPS-stimulated TALDO neutrophils secreted 120 pg IL-8 per 10^5 cells which amounts to 40 % of what control neutrophils secreted. MIP-1ß secretion was very similar between the two samples with 350 pg MIP-1ß secretion per 10^5 cells for both control and TALDO neutrophils.

These data show that the secretion of IL-8 but not that of MIP-1ß is affected in TALDO neutrophils.

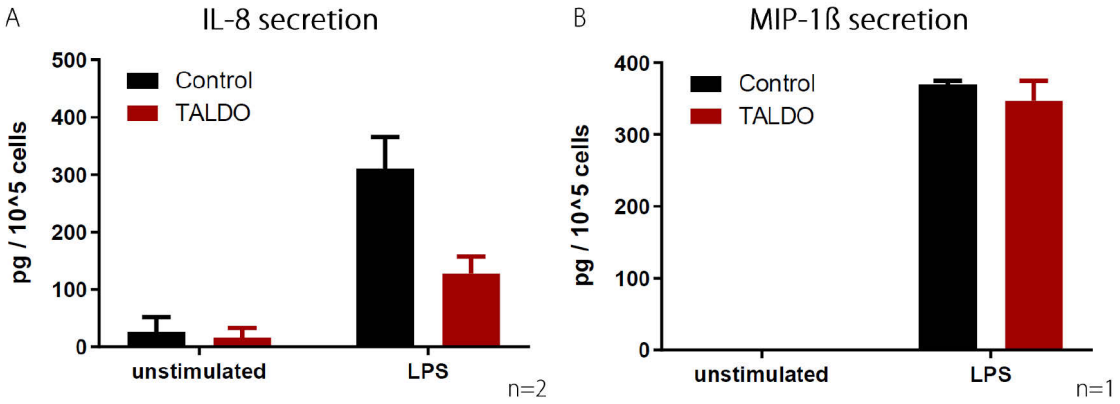

Figure 9 | LPS-induced IL-8 secretion is reduced in TALDO neutrophils. MIP-1ß secretion remains unaltered. 10^5 cells were distributed per 200 µl medium and stimulated with 200 ng/ml LPS overnight. Cytokine concentration was measured in the cell supernatants. A, IL-8 secretion of two donors. B, MIP-1ß secretion of one donor. Cytokine secretion in neutrophils was measured for two patients in the case of IL-8 (HH & Paris 1) and for one patient in the case of MIP-1ß (Paris 1).

3.2 Genetic knockouts in neutrophil-like cell line PLB-985

I reported the results I obtained from analysing samples of only three patients. This, as stated above, was due to the fact that transaldolase 1-deficient individuals (TALDO patients) are extremely rare.

To confirm the results in a different experimental approach, I chose the cell-line PLB-985 which has neutrophil-like features. PLB-985 cells can be differentiated into a post-mitotic state in which they undergo PMA-induced cell death and oxidative burst. In addition, PLB-985 cells can be genetically-engineered and therefore allow experiments assessing the role of specific proteins by generating knock-out cells. Those features make PLB-985 cells a useful cell model to study the underlying mechanism of neutrophil functions, e.g. NET formation.

I generated PLB-985 knock-out cells, using the CRISPR-Cas9 system as indicated in sections 2.2.11 & 2.2.12. In brief, I designed guideRNAs (gRNA) against early exons of the genes *TALDO1*, as primary topic of investigation, *TKT*, since it codes for transaldolase 1's partner enzyme TKL in the non-oxidative PPP and of *MPO* as a positive control. *MPO* codes for the peroxidase MPO which is known to be required for PMA-induced cell death in PLB-985 cells. Furthermore, I designed a scramble control (SCR) which does not have a target in the human genome and which was used as a negative control. PLB-985 cells containing successfully cloned gRNAs and Cas9 were selected via puromycin resistance and per gRNA 32 single cells were plated and grown for 2-3 weeks. Subsequently, genetic knock-outs were

identified using the *OutKnocker* system (Schmid-Burgk et al. 2014) before growing cells up and performing experiments.

3.2.1 Confirmation of out-of-frame mutation and absent protein

Figure 10 | Sequencing results of *TALDO1S, TALDO1L and TKT* CRISPR knock-out PLB-985 clones.
TALDO1S CRISPR knock-out PLB clones with out of frame mutations were chosen for further experiments

TALDO1 is the gene encoding for transaldolase 1 and has two different start codons which result in the expression of a short and a long version of the enzyme. I generated PLB-985 knock-outs for the short transaldolase 1 version which results in complete protein depletion (*TALDO1S* KO). In addition, I targeted the first start codon, i.e. resulting in knock-outs for the long transaldolase 1 version which results in expression of just the short transaldolase 1 (*TALDO1L* KO).

Out of the many out-of-frame mutated PLB clones which were confirmed by sequencing, I randomly picked one clone per guide, i.e. two clones per targeted gene for further experiments (Figure 10). To establish that those clones did not only present out-of-frame mutations on the DNA level but were indeed deficient on the protein level, I assessed their transaldolase 1 expression by Western blot analysis (Figure 11). Whereas the samples in the lanes 'SCR' as well as 'TALDO1L KO1' and '2' (on the right) express at least residual amounts of transaldolase 1, the short transaldolase 1 knock-outs 'TALDO1S KO1' and '2' are completely transaldolase 1-deficient.

The tubulin signal in the second row confirms that all western blot lanes contained cell lysate.

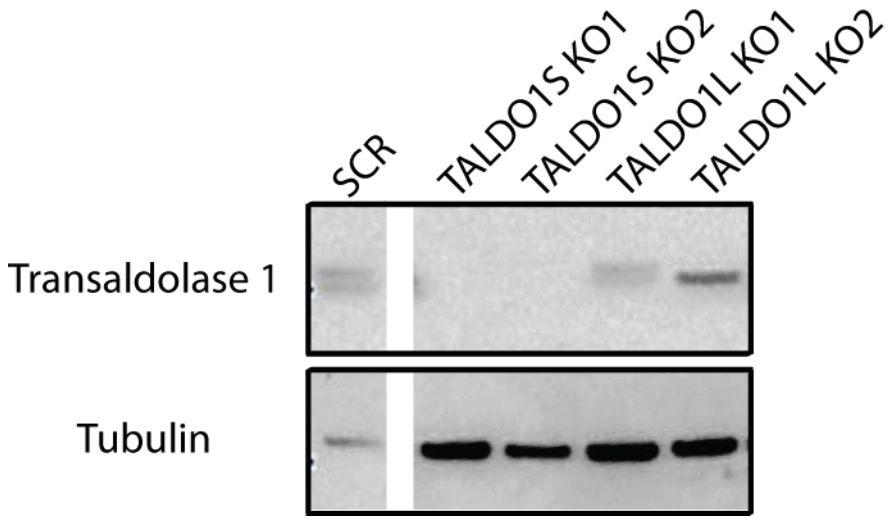

Figure 11 | TALDO1S CRISPR knock-out PLB cells are fully deficient in transaldolase 1. TALDO1L CRISPR knock-outs have a reduced level of transaldolase 1 expression.
Cell lysate of 10^5 cells was loaded per SDS polyacrylamide gel lane. The separated proteins were transferred by semi-dry transfer onto a PVDF membrane. Transaldolase 1 and tubulin were detected by Western blot. Lanes with lysates of different PLB-985 mutant cells for other proteins were run on the same gel and are not shown.

3.2.2 Knock-out of short and long form of transaldolase 1 in PLB-985 cells

Since absent NET formation and oxidative burst in response to PMA stimulation were the main findings in TALDO neutrophils, I assessed the PLB KO's ability to execute these two functions (Figure 12). As mentioned earlier, I used SCR as negative and MPO as a positive control for PMA-induced cell death.

All four, i.e. both *TALDO1S* KO and both *TALDO1L* KO cell clones have a clearly reduced oxidative burst after PMA stimulation (Figure 12 A & B). Similarly, their ability to undergo PMA-induced cell death is strongly decreased (Figure 12 C & D). Interestingly, all four clone's cell death rate decreased to 25 % of the SCR clone.

These data show that full length transaldolase 1 is needed for PMA-induced oxidative burst and cell death in PLB-985 cells confirming the results I obtained with the TALDO patients.

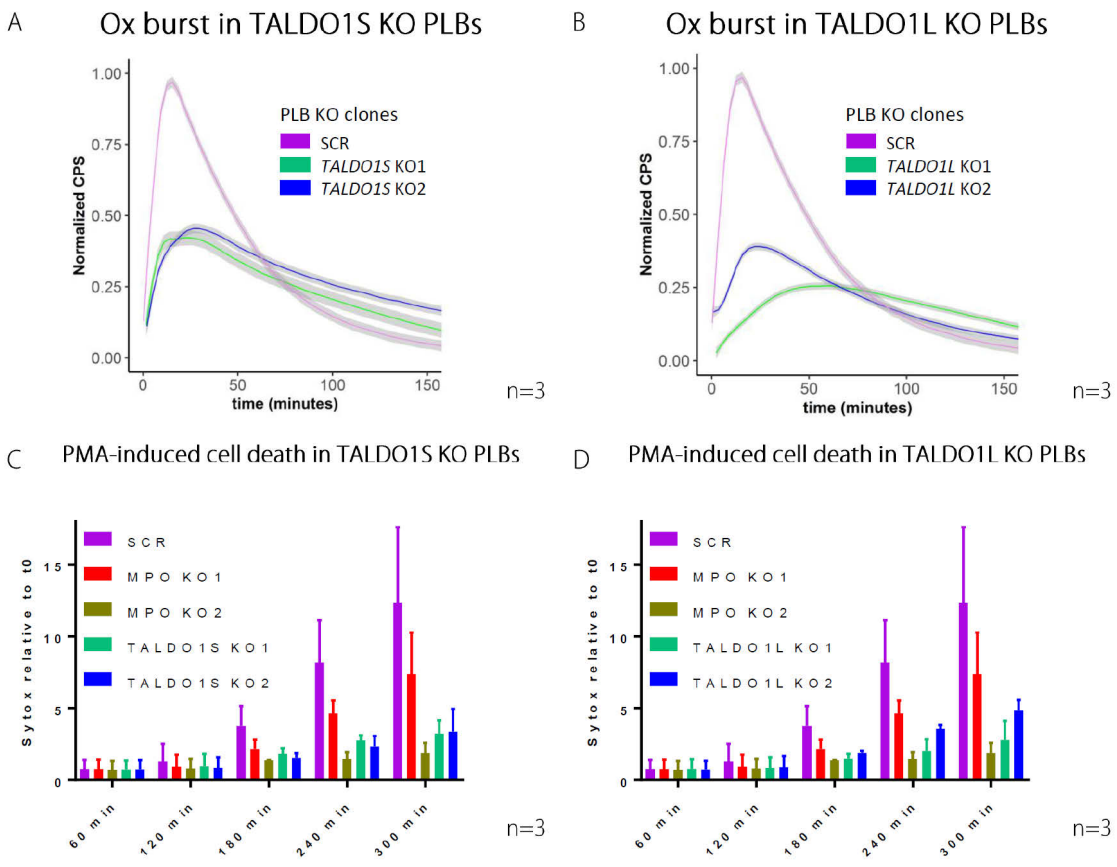

Figure 12 | Full length transaldolase 1 is required for PMA-induced oxidative burst and cell death in PLB-985 cells.
SCR, *MPO* KO1 & 2, *TALDO1S* KO1 & 2 and *TALDO1L* KO2 & 2 PLB-985 cells were plated and stimulated with 100 nM PMA. **A & B,** oxidative (Ox) burst, measured as luminescence-reaction (CPS). Measurements of different experiments were normalized and are shown as regression model. The oxidative burst was measured in the short transaldolase 1 KO mutant (*TALDO1S* KO), ie total transaldolase 1 deficiency (panel A) and in the long transaldolase 1 KO mutant (*TALDO1L* KO), ie partial transaldolase 1 deficiency (panel B). **C & D,** PMA-induced cell death during a 300 minutes time course measured as multiples of Sytox fluorescence immediately after stimulation. NET formation was measured in the short transaldolase 1 KO mutant (*TALDO1S* KO), ie total transaldolase 1 deficiency (panel C) and in the long transaldolase 1 KO mutant (*TALDO1L* KO), ie partial transaldolase 1 deficiency (panel D). MPO deletions serve as controls.

3.2.3 Knock-out of TKL in PLB-985 cells

TKL is an enzyme of the non-oxidative pentose phosphate pathway (PPP) which functions alongside transaldolase 1 and is encoded by the *TKT* gene. As opposed to *TALDO1,* no human genetic deficiency for *TKT* has ever been reported (Stincone et al. 2015), indicating either a much milder or, on the contrary, a lethal phenotype for a functional defect in TKL.

To confirm the notion that transaldolase 1 is required for NET formation and the oxidative burst due to its role in the non-oxidative PPP, I assessed whether TKL is also required for these two processes (Figure 13). *TKT* knock-outs cells were generated by CRISPR/Cas9 as described earlier. The deficient cells had a strongly decreased oxidative burst upon PMA stimulation

(Figure 13 C). Furthermore, *TKT* knock-out cells did react poorly to PMA and after 300 minutes multiplied Sytox positivity to only 2-4 times the Sytox signal at t_0 compared to an 11 times increase of the *SCR* cells (Figure 13 D). Unstimulated *TKT* knock-out cells did not show any ROS production or cell death (Figure 13 A & B).

Thus, *TKT* knock-outs cells showed a very similar phenotype to that of *TALDO1* knock-out cells upon PMA stimulation indicating that TKL, as transaldolase 1, is required for the PMA-induced oxidative burst and cell death in PLB-985 cells.

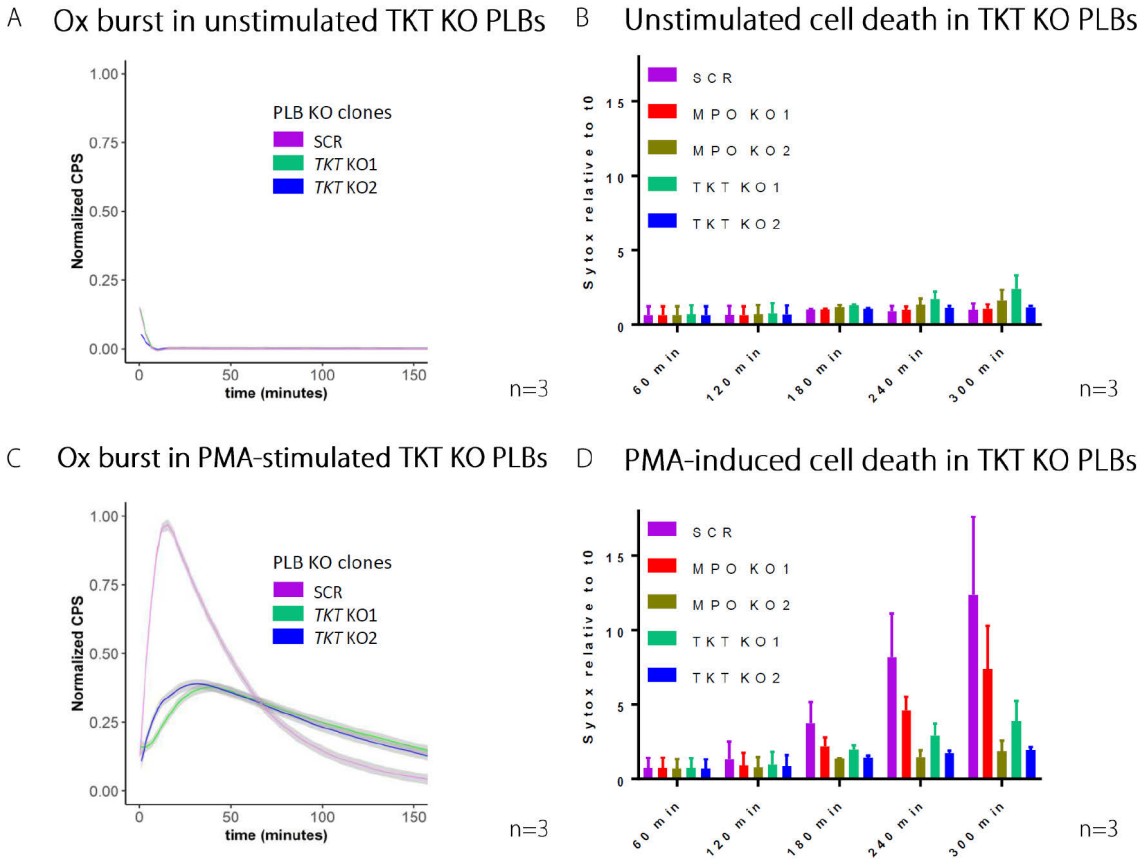

Figure 13 | TKL is required for PMA-induced oxidative burst and cell death in PLB-985 cells.
SCR, *MPO* KO1 & 2, *TKT* KO1 & 2 PLB-985 cells were plated and stimulated with 100 nM PMA. **A & C**, oxidative (Ox) burst in unstimulated (panel A) and PMA-stimulated (panel C) TKT KO mutants, measured as luminescence-reaction [CPS]. Measurements of different experiments were normalized and are shown as regression model. **B & D**, PMA-induced cell death during 300 minutes time course measured for unstimulated control (panel B) and PMA-stimulated (panel D) cells as multiples of Sytox fluorescence immediately after stimulation (t_0).

3.3 Metabolomics of PMA-stimulated primary neutrophils

Since metabolic activity affects the oxidative burst and NET formation, I investigated the metabolomic dynamics during NET formation.

I prepared neutrophil samples of 10 healthy donors at different time points of early NET formation, i.e. 15, 30 and 45 minutes after PMA stimulation (Figure 14). Mass spectrometry-based global metabolite measurement and subsequent analysis was performed externally by Metabolon, Inc. Metabolites of selected metabolism pathways are presented below.

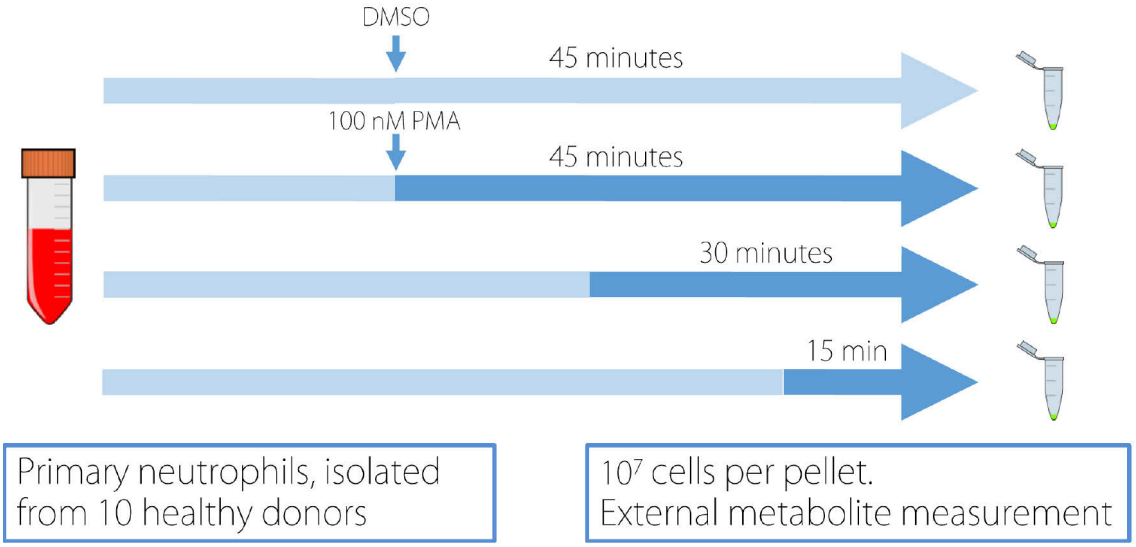

Figure 14 | Experimental set-up for PMA-induced neutrophil metabolomic measurements.
10^7 cells were distributed in 3.5 ml medium and stimulated with 100 nM PMA for 15-45 minutes. Subsequently, cells were washed and the cell pellet shock frozen and stored until shipment.

3.3.1 Glycolysis and Pentose Phosphate Pathway

Glycolysis and the PPP are part of the central cellular metabolism. Metabolome analysis revealed a statistically significant mild increase of glucose which lies at the very beginning of the glycolysis pathway 30 and 45 minutes after PMA stimulation (Figure 15 A). Interestingly, glucose-6-phosphate which is the metabolite immediately following uptake of glucose into the cell was not detected in the global metabolomic measurement (not shown).

3-phosphoglycerate is a metabolite further downstream during glycolysis and showed a significant increase at all three time points (Figure 15 B). Similarly, the abundance of phosphoenolpyruvate (PEP) which lies at the end of the glycolytic pathway was significantly higher at all three time points (Figure 15 C).

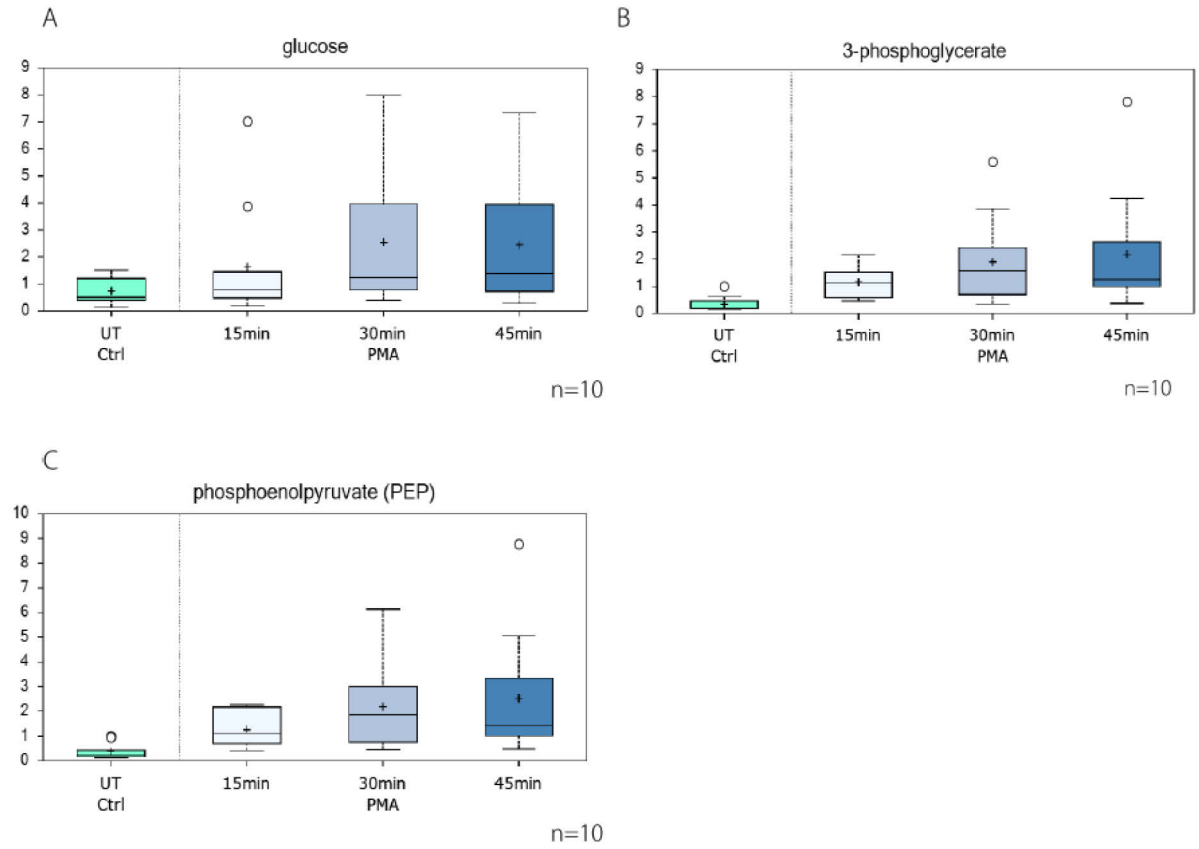

Figure 15 | Abundance of the glycolysis metabolites glucose, 3-phosphoglycerate and phosphoenolpyruvate significantly increases over time in PMA-stimulated neutrophils.
The box plot line indicates the median value and the cross indicates the mean value. Statistical significance was determined performing one-way ANOVA with repeated measurements. **A,** Glucose concentration is significantly increased at time points 30 and 45 minutes. **B,** The 3-phosphoglycerate concentration is significantly higher at all three time points. **C,** The phosphoenolpyruvate (PEP) concentration is significantly higher at all three time points.

6-phosphogluconate and sedoheptulose-7-phosphate are intermediate metabolites of the oxidative and non-oxidative PPP, respectively. Both show an increase upon PMA stimulation (Figure 16) indicating increased PPP activity. Whereas the increase in 6-PG reaches statistical significance after already 15 minutes and stays high throughout the measured time span (Figure 16 A), S7P reaches a significant level of increase only after 45 minutes (Figure 16 B).

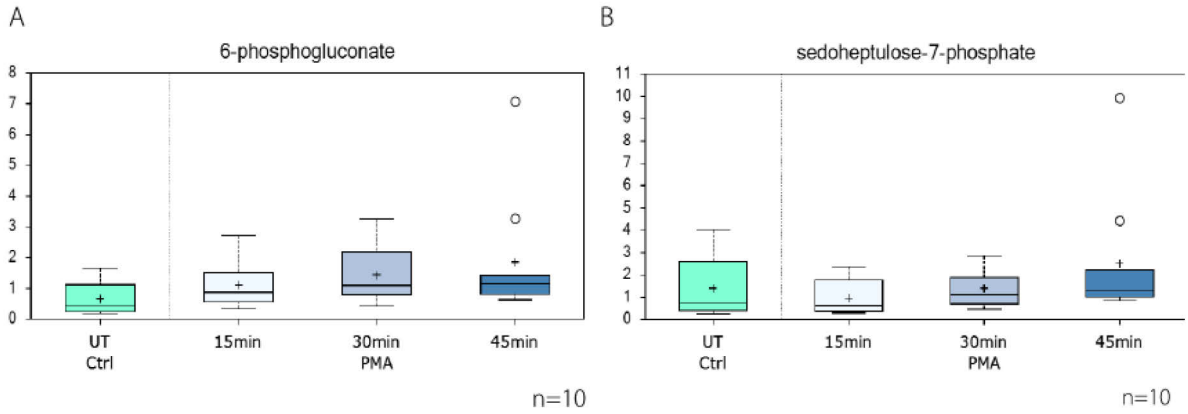

Figure 16 | Abundance of the pentose phosphate pathway metabolites 6-phosphogluconate and sedoheptulose-7-phosphate increases over time compared to the control cells.
The box plot line indicates the median value and the cross indicates the mean value. Statistical significance was determined performing one-way ANOVA with repeated measurements. **A,** the concentration of 6-phosphogluconate is significantly higher at all three time points. **B,** the sedoheptulose-7-phosphate concentration is significantly higher after 45 minutes.

3.3.2 Redox Balance

Maintaining a stable redox balance is crucial for cellular homeostasis. PMA stimulation and NET formation go hand in hand with a rapid and massive production of ROS in neutrophils. The glutathione redox system plays an important role in keeping the cellular redox balance.

Surprisingly, the amount of GSH remained unaltered throughout all time points (Figure 17 A) whereas GSSG significantly decreased after 30 minutes (Figure 17 B). Interestingly, the degradation product of GSH, cysteinylglycine, was significantly reduced after 30 and 45 minutes (Figure 17 C).

Methionine sulfoxide, an early precursor molecule of GSH is significantly increased already after 15 minutes of PMA stimulation and decreases subsequently, although it remains significantly above the baseline level (Figure 17 D).

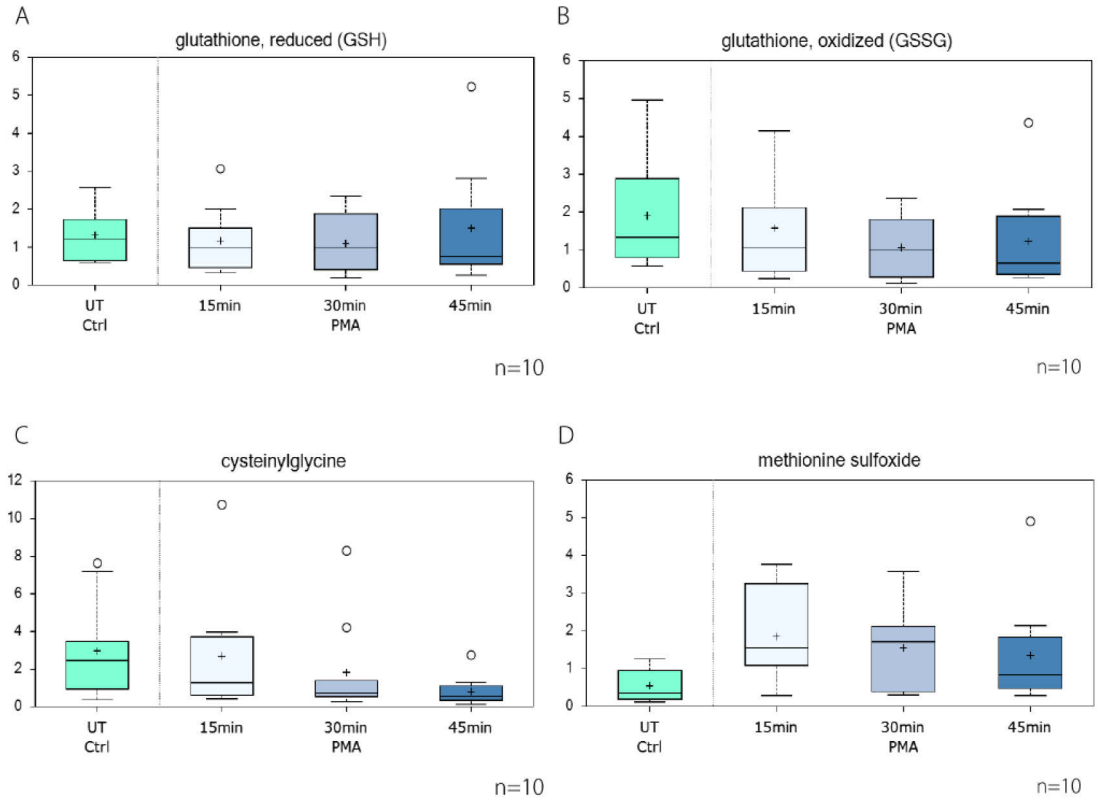

Figure 17 | Abundance of compounds in the oxidative stress and redox balance pathway.
The box plot line indicates the median value and the cross indicates the mean value. Statistical significance was determined performing one-way ANOVA with repeated measurements. **A,** the concentration of reduced GSH is not significantly altered at any time point. **B,** the concentration of GSSG is significantly reduced after 30 minutes and shows a decreasing trend after 45 minutes. **C,** the concentration of cysteinylglycine is significantly reduced after 30 and 45 minutes. **D,** the methionine sulfoxide concentration is significantly increased at all three time points.

3.3.3 Nucleotide metabolism

Metabolites of the nucleotide metabolism were also included in the global metabolome analysis. Adenosine 3-monophosphate (3-AMP) abundance is significantly increased 15 minutes after PMA stimulation and subsequently returns to baseline levels (Figure 18 A). Other nucleotide precursors on the contrary, such as guanine, uracil and guanosine were significantly reduced in their concentration over the course of 45 minutes PMA stimulation (Figure 18 B-D).

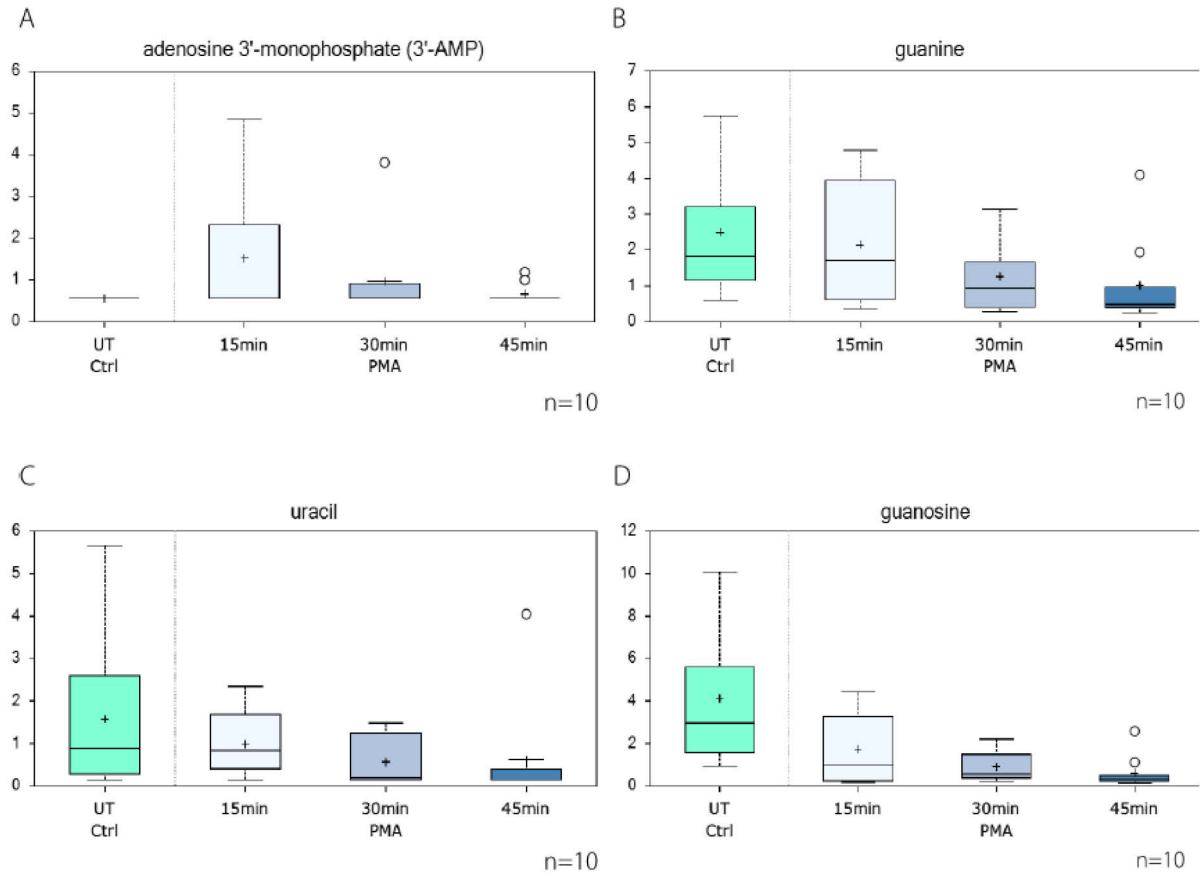

Figure 18 | Abundance of compounds in the nucleotide metabolism pathway are significantly altered in PMA-stimulated neutrophils.
The box plot line indicates the median value and the cross indicates the mean value. Statistical significance was determined performing one-way ANOVA with repeated measurements. **A,** the concentration of adenosine 3'-monophosphate (3'-AMP) is significantly increased after 15 minutes and returns to baseline thereafter. **B,** the concentration of guanine is significantly reduced after 30 and after 45 minutes. **C,** the concentration of uracil is significantly reduced after 30 and 45 minutes. **D,** the guanosine concentration is significantly reduced at all three time points.

3.3.4 Phospholipid metabolism

Phospholipids are the building stones of cellular membranes and play a role in cellular signalling. Choline phosphate, choline and glycerophosphoethanolamine underwent the highest concentration changes among the phospholipids. Whereas choline phosphate was steadily and significantly reduced over the 45 minutes to only 30 % of the baseline abundance, the choline concentration went the opposite way and tripled already after 15 minutes without subsequent further increases (Figure 19 A & B).

Glycerophosphoethanolamine increased significantly over the time course and more than quadrupled after 15 minutes before reaching more than 8 and more than 10 times the base line level after 30 and 45 minutes, respectively (Figure 19 C).

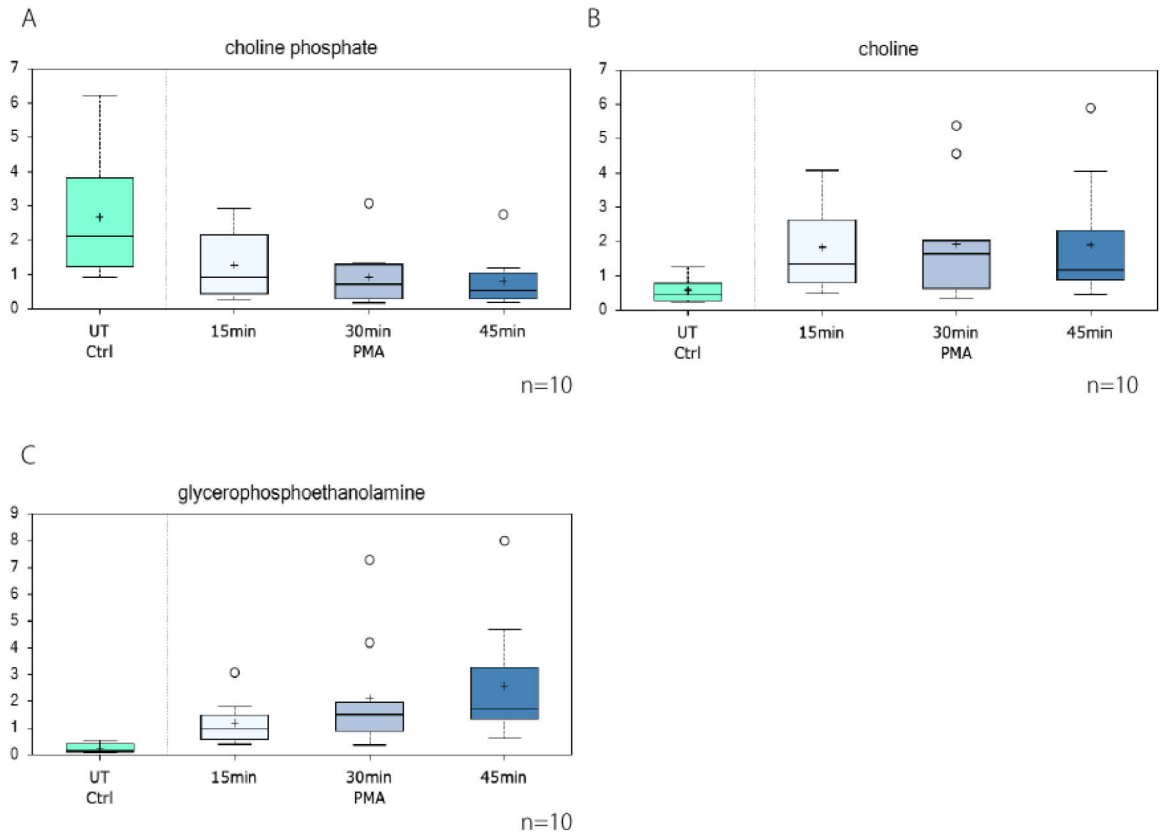

Figure 19 | Abundance of compounds in the phospholipid metabolism.
The box plot line indicates the median value and the cross indicates the mean value. Statistical significance was determined performing one-way ANOVA with repeated measurements. **A,** the concentration of choline phosphate is significantly decreased after 15, 30 and 45 minutes. **B,** the concentration of choline is significantly increased after 15, 30 and 45 minutes. **C,** the concentration of glycerophosphoethanolamine is very significantly increased at all three time points.

3.4 Assessing metabolic requirements of NETs by pharmacological inhibition

Based on my observations in transaldolase 1-deficient primary neutrophils and PLB-985 cells and in order to broaden our understanding of the metabolism-NET formation interplay, I assessed how pharmacologic inhibition of central metabolic pathways affects NET formation. I used the inhibitors 2-deoxyglucose (2-DG), 6-aminonicotinamide (6-AN) and diphenyleneiodonium (DPI) which act on different reactions of glycolysis, PPP and ROS formation (Figure 20).

Furthermore, another aim of this part of the study was to elucidate a threshold of ROS production that might be required to induce NET formation *in-vitro* in primary neutrophils. Therefore, I measured oxygen consumption (a proxy of NOX 2 activity) in parallel with ROS

production in a luminescence-based assay and NET formation based on nuclear enlargement and Sytox Green positivity.

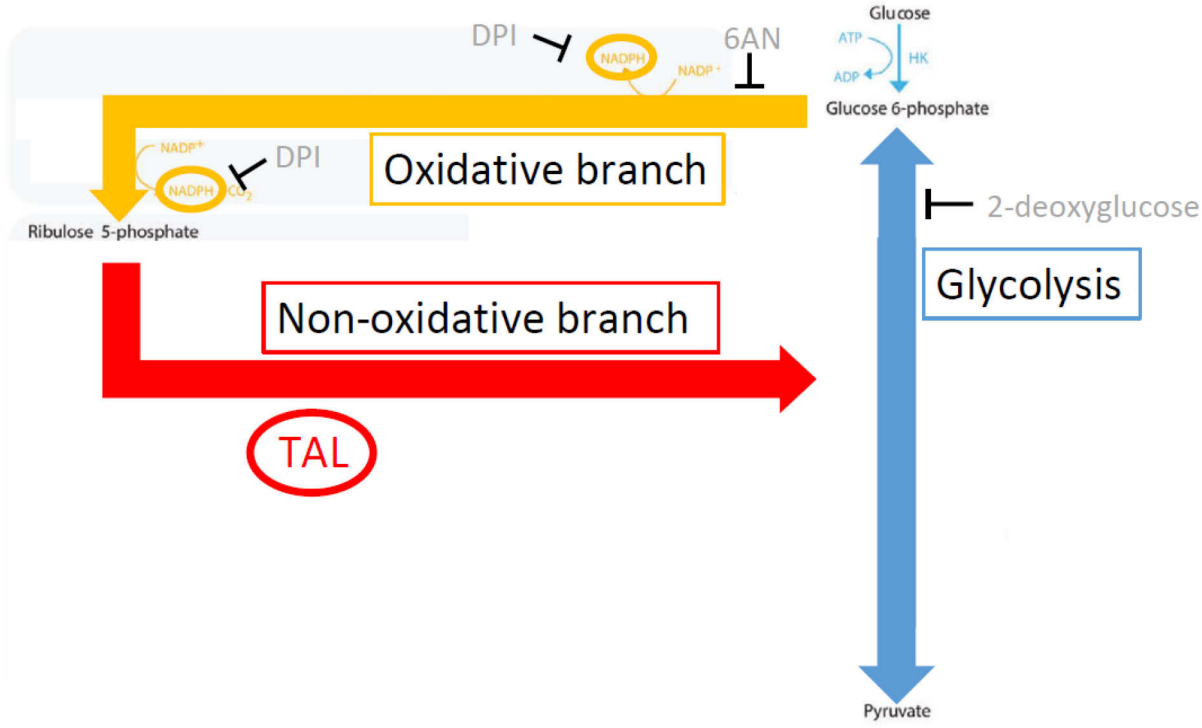

Figure 20 | Overview of the Pentose-Phosphate-Glycolysis Interplay and the location of action of the pharmacological inhibitors used in this study.

3.4.1 Scavengers and inhibitors of oxidative burst

The NOX2 inhibitor DPI inhibits NET formation by abolishing the PMA-induced ROS burst. I used DPI inhibition here to assess the similarities between inhibition of the metabolic pathways and inhibition of the ROS generating machinery, i.e. NOX2 that lay downstream of it. NOX2 inhibition by DPI potently inhibits oxygen consumption in a concentration dependent way with more than 90 % OCR abolition with 300 nM DPI. (Figure 21 A).

Accordingly, I observed a DPI concentration-dependent oxidative burst inhibition (Figure 21 B). Interestingly, DPI had a stronger effect on the oxidative burst than on the OCR with already the smallest concentration of 3.7 nM DPI showing a clear reduction and the highest concentration of 300 nM completely abolishing ROS production.

Similarly, DPI showed a strong effect on NET formation (Figure 21 C). The NET formation rate was reduced from 90 % NET forming neutrophils to less than 50 % at 3.7 nM DPI and to 0 % at 100 nM DPI.

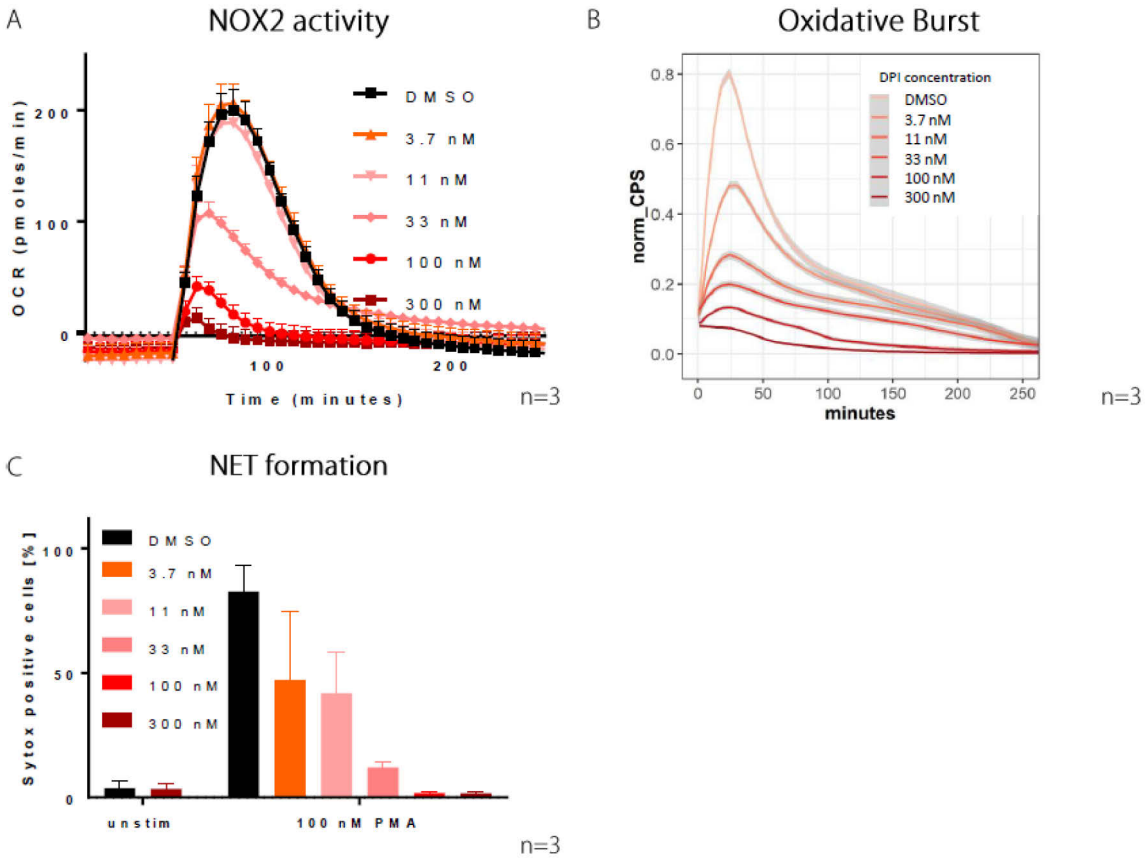

Figure 21 | DPI inhibits NOX2 activity, the oxidative burst and NET formation in PMA-stimulated neutrophils. Cells were distributed and incubated with respective inhibitor concentration for 30 minutes, then stimulated with 100 nM PMA and measured at respective indicated time points. **A,** the OCR was measured as a proxy for NOX2 activity using a Seahorse device. **B,** Oxidative burst, measured as luminescence-reaction [CPS]. Measurements of different donors were normalized and are shown as regression model. **C,** NET formation after 3 hours measured as percent of Sytox-positive and expanded nuclei of total amount of Draq5-positive nuclei.

3.4.2 Metabolic inhibitors

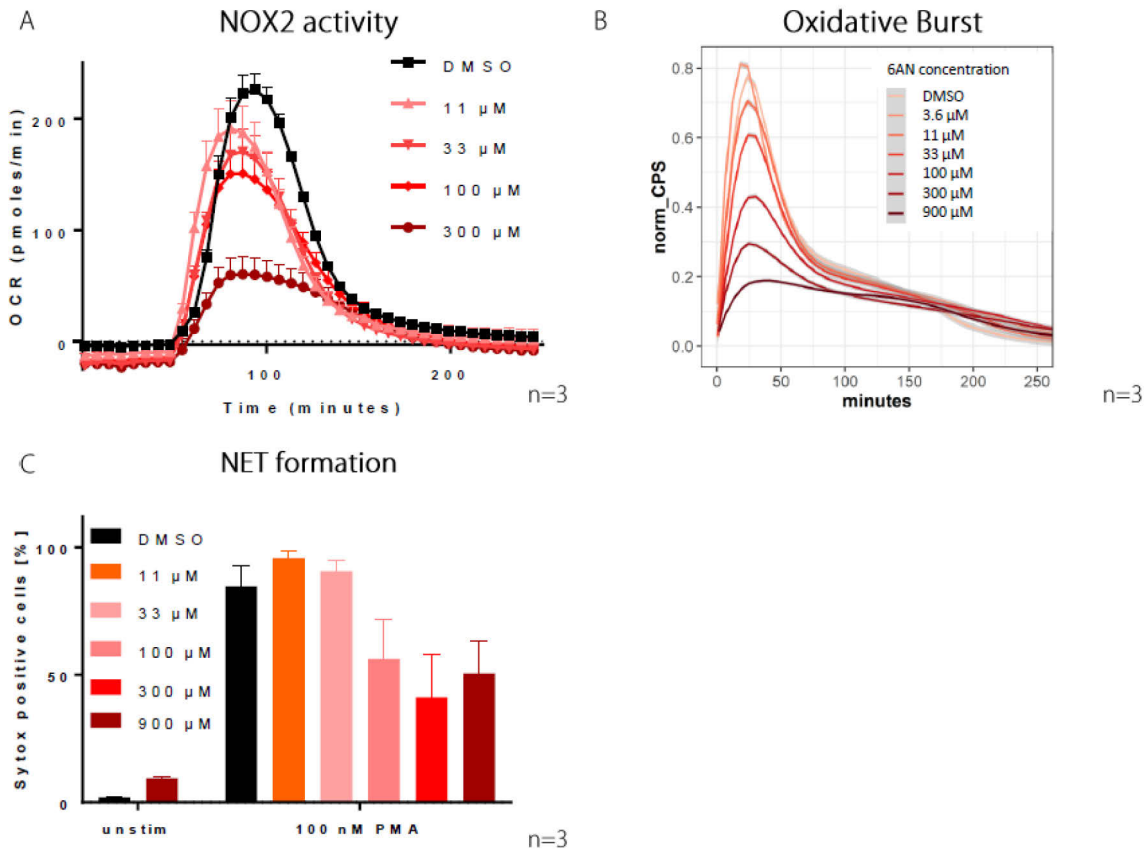

Figure 22 | The oxPPP inhibitor 6-AN inhibits NOX2 activity and the oxidative burst and reduces NET formation to 50 %.
Cells were distributed and incubated with the respective concentration of 6-AN for 30 minutes, then stimulated with 100 nM PMA and measured at respective indicated time points. **A,** the OCR was measured as a proxy for NOX2 activity using a Seahorse device. **B,** oxidative burst, measured as luminescence-reaction [CPS]. Measurements of different donors were normalized and are shown as regression model. **C,** NET formation after 3 hours measured as percent of Sytox-positive and expanded nuclei of total amount of Draq5-positive nuclei.

The pharmacological inhibitor 6-aminonicotinamide (6-AN) acts on the oxidative PPP. 6-AN reduces oxygen consumption in PMA-stimulated primary neutrophils mildly at a low concentration of 11 µM 6-AN up to 75 % reduction at the highest concentration of 300 µM (Figure 22 A). 6-AN also inhibits the oxidative burst in a concentration dependent way, reducing the oxidative burst peak to 35 % of the DMSO control at 300 µM 6-AN and 25 % at 900 µM but not completely abolishing it (Figure 22 B). Furthermore, NET formation is inhibited by 6-AN in a concentration dependent manner and drops from around 85 % NET forming neutrophils to 45 % at 300 µM (Figure 22 C). Interestingly, inhibition of NET formation by 6-AN reaches a plateau at 40-50 % NET forming cells and does not further drop when applying a concentration above 300 µM.

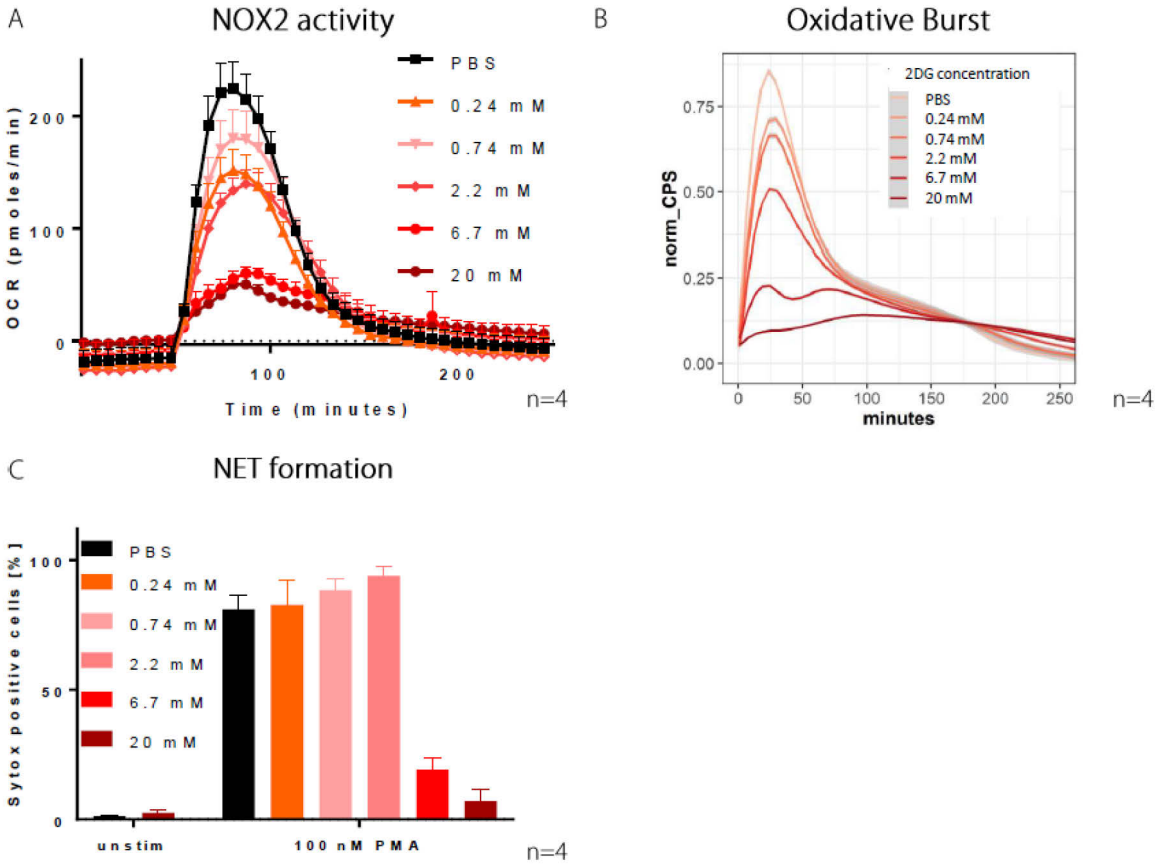

Figure 23 | The glycolysis and PPP inhibiting glucose analogue 2-deoxyglucose (2-DG) strongly inhibits NOX2 activity, the oxidative burst and NET formation.
Cells were distributed and incubated with respective 2-DG concentration for 30 minutes, then stimulated with 100 nM PMA and measured at respective indicated time points. **A**, the OCR was measured as a proxy for NOX2 activity using a Seahorse device. **B**, oxidative burst, measured as luminescence-reaction [CPS]. Measurements of different donors were normalized and are shown as regression model. **C**, NET formation after 3 hours measured as percent of Sytox-positive and expanded nuclei of total amount of Draq5-positive nuclei.

2-deoxyglucose (2-DG) is a glucose analogue and used as an inhibitor of glycolysis. 2-DG gets phosphorylated to 2-DG-6-phosphate in the cell and as such competitively inhibits the enzyme phosphoglucoseisomerase (GPI). Therefore, 2-DG is both an inhibitor of glycolysis and of closing the full circle of the PPP.

2-DG reduces the PMA-induced NOX2 activity in a dose dependent manner, decreasing the OCR to below 50 pmoles/min at the maximum concentration of 20 mM 2-DG (Figure 23 A). The oxidative burst is also reduced in a concentration dependent way and shows no peak at 20 mM 2-DG (Figure 23 B).

Interestingly, the approximately linear 2-DG dose-dependent reduction observed for the oxygen consumption and the oxidative burst is not reflected in the reduction of NET formation. The lower doses of 0.24-2.2 mM 2-DG do not affect NET formation which stays at

the control level of 80-90 % whereas 6.7 mM and 20 mM 2-DG reduce NET formation to 21 % and 7 % NET forming neutrophils, respectively.

3.4.3 Requirement of carbon sources for the oxidative burst and NET formation

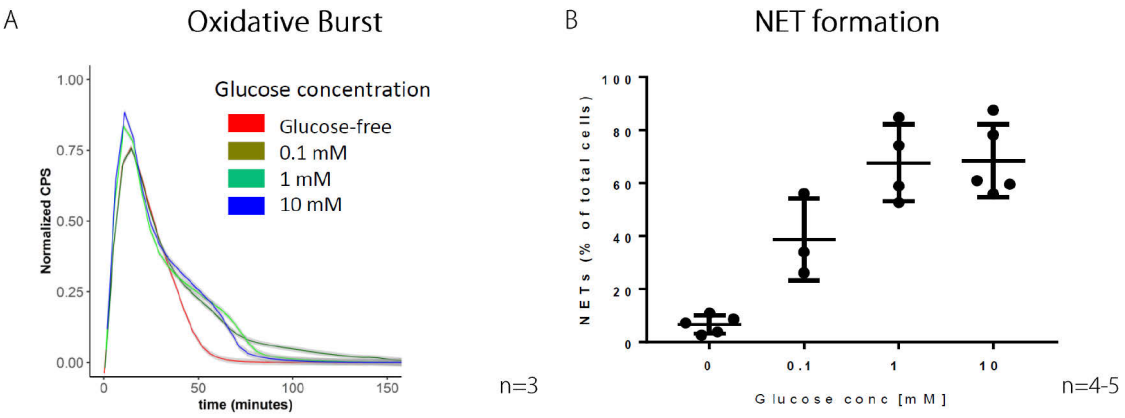

Figure 24 | Glucose is needed for NET formation but not for the oxidative burst.
Cells were distributed in freshly prepared medium with respective glucose concentrations and stimulated with 100 nM PMA. **A,** oxidative burst, measured as luminescence-reaction [CPS]. Measurements of different donors were normalized. **B,** NET formation after 3 hours measured as percent of Sytox-positive and expanded nuclei of total amount of Draq5-positive nuclei.

Based on the previously reported findings in transaldolase 1-deficient cells, the metabolome results and the inhibitor studies, I wanted to further assess the role and level of requirement of glucose in the NET formation process. I therefore measured ROS production and NET formation in media with varying concentrations of glucose (Figure 24). Whereas the peak of the oxidative burst was not affected by a reduced amount of glucose or even glucose-free medium a different kinetic of the glucose-free medium burst compared to the glucose containing media can be observed at the end of the burst, around 50 minutes after stimulating the cells (Figure 24 A). The glucose-free burst reaches the baseline level after just above 50 minutes and thus around 25 minutes before the other media. Interestingly, despite the considerable glucose concentration differences in the other media, their ROS production reach baseline levels at roughly the same time.

Intriguingly, the above described pattern does not repeat for NET formation (Figure 24 B). NET formation does not take place in glucose-free medium. A glucose level of 0.1 mM allows 40 % of neutrophils to form NETs and 1 mM glucose is already sufficient to reach 70 % NET forming neutrophils and thus the level of the control sample which contains the standard medium glucose concentration of 10 mM.

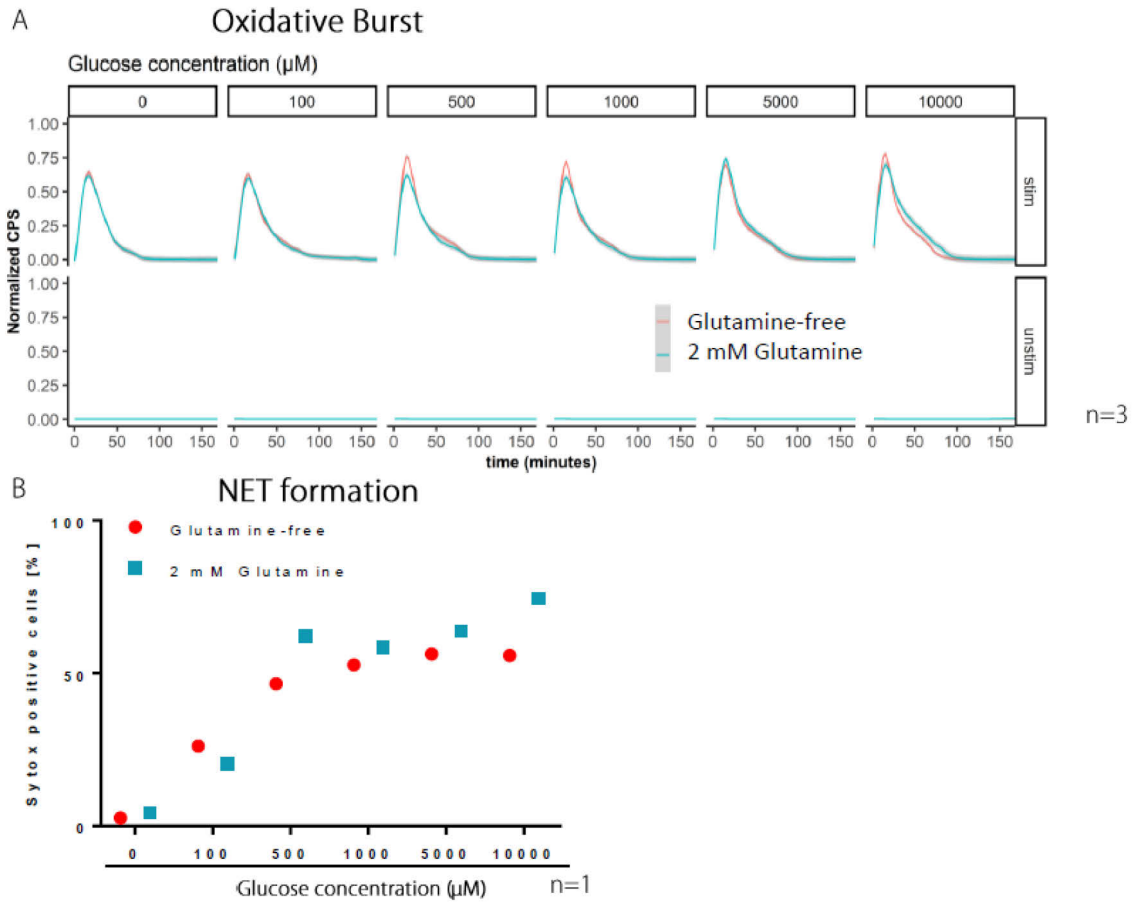

Figure 25 | Glutamine has no effect on the oxidative burst and does not rescue NET formation in glucose-free medium.
Cells were distributed in freshly prepared medium with respective glucose and glutamine concentrations and stimulated with 100 nM PMA. **A,** oxidative burst, measured as luminescence-reaction [CPS]. Measurements of different donors were normalized and are shown as regression models in sub-panels according on the glucose concentration and the stimulation-status. **B,** NET formation after 3 hours measured as percent of Sytox-positive and expanded nuclei of total amount of Draq5-positive nuclei.

Since glucose seemed to be required for NET formation but I did not provide a different carbon source in the respective media, such as glutamine, I aimed to assess whether providing glutamine would rescue the NET defect in glucose-free medium (Figure 25).

Glutamine did not have an effect on the oxidative burst in any glucose concentration or in glucose-free medium (Figure 25 A). Also, glutamine did not rescue the absent NET formation in glucose-free medium but also did not show any effect on NET formation in different media of between 0.1 and 10 mM glucose, yet with an n=1 this result does not allow a confident conclusion (Figure 25 B).

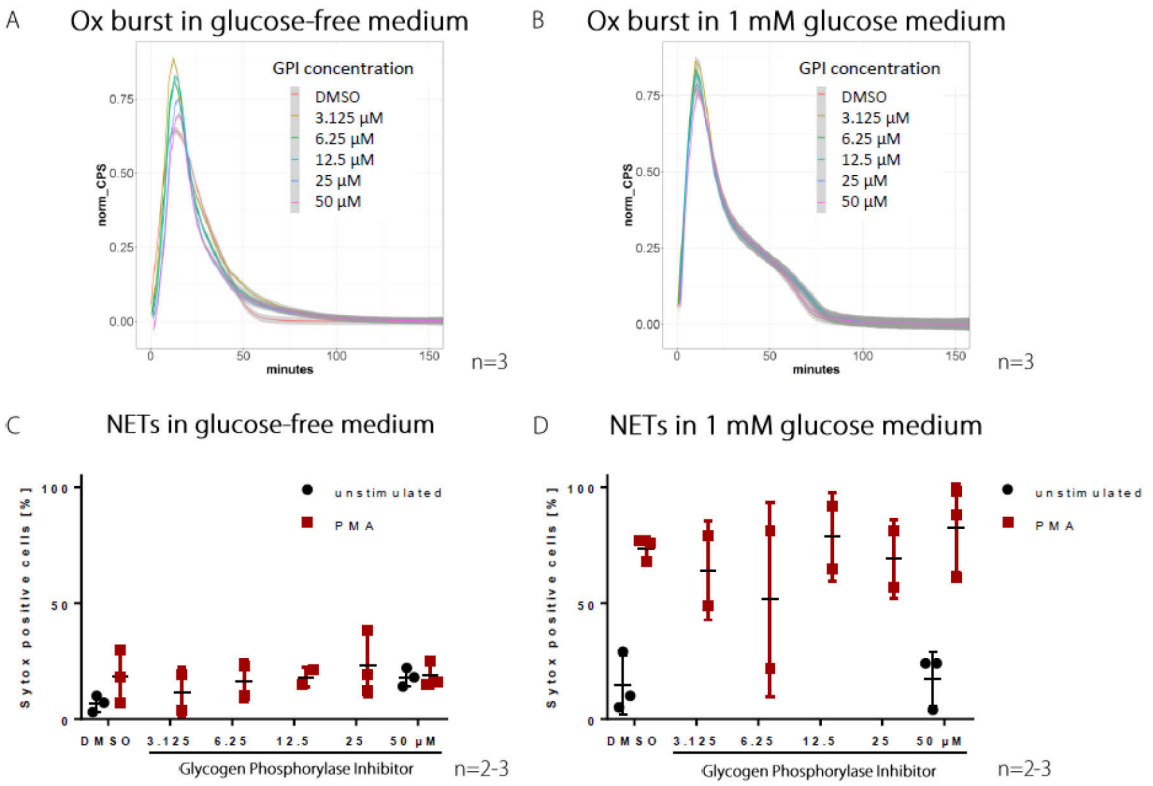

Figure 26 | Glycogen degradation is not required for the oxidative burst in Glucose-free medium. Cells were distributed in either glucose-free or 1 mM glucose medium and with respective glycogen phorsphorylase inhibitor (GPI) concentration and stimulated with 100 nM PMA. **A & B,** Oxidative (Ox) burst was measured as luminescence-reaction [CPS]. Measurements of different donors were normalized and are shown as regression model. **C & D,** NET formation after 3 hours measured as percent of Sytox-positive and expanded nuclei of total amount of Draq5-positive nuclei.

The observation that an external glucose supply is needed for NET formation but not for the PMA-induced oxidative burst in neutrophils together with the, speculative, notion that *some* carbon source *must* be needed for the oxidative burst as well, led me to hypothesize that this carbon source could be a neutrophil *internal* one. Glycogen is a glucose polymer which is classically known as a glucose storage in hepatocytes or neurons. However, neutrophils and other immune cell have been known for decades to store glycogen as well.

Thus, I measured the oxidative burst and NET formation in glucose-free and 1 mM glucose medium supplied with different amounts of glycogen phosphorylase inhibitor (GPI) (Figure 26). GPI inhibits the glycogen phosphorylase and thus the first step in glycogen degradation required to provide single glucose molecules.

There was no GPI effect on the oxidative burst independent of whether glucose was present in the medium or not (Figure 26 A & B). Similarly, GPI did not affect NET formation in glucose-free or 1 mM glucose medium (Figure 26 C &D).

Thus, I can conclude that the neutrophil oxidative burst in glucose-free medium does not depend on the degradation of glycogen.

3.5 Technical considerations of the luminescence-based ROS measurement

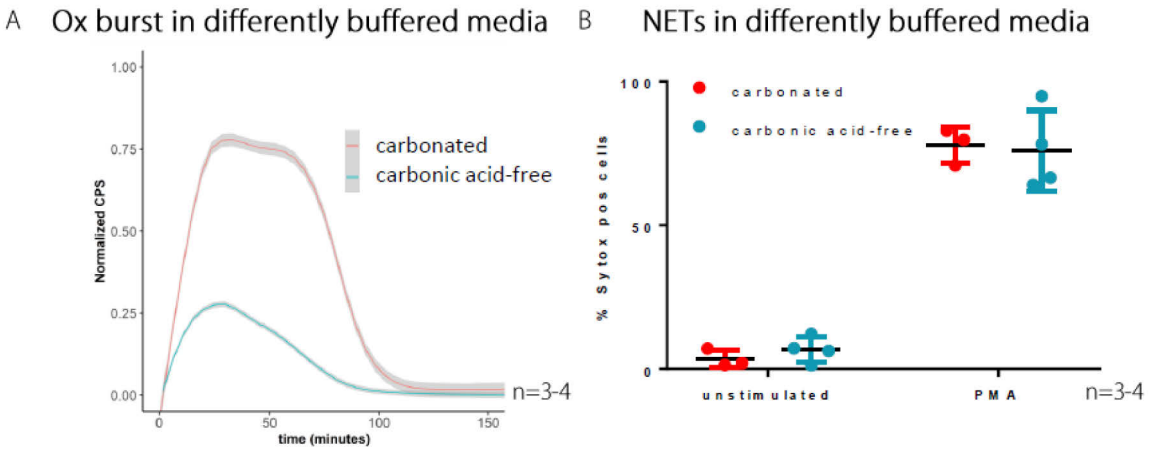

Figure 27 | Carbonated medium strongly enhances the PMA-induced oxidative burst measured in a not-CO_2 buffered environment.
The two different media used in these assays contain the same amount of glucose and human serum albumin and are 10 mM HEPES buffered. **A,** the oxidative (Ox) burst was measured as luminescence-reaction [CPS] for H_2CO_3-buffered medium ('carbonated') and H_2CO_3-free ('carbonic acid-free') medium. Cells were kept in the not CO_2-buffered luminometer for the duration of the time course. Measurements of different experiments were normalized and are shown as regression model. **B,** NET formation after 3 hours for H_2CO_3-buffered medium ('carbonated') and H_2CO_3-free ('carbonic acid-free') medium was measured as percent of Sytox-positive and expanded nuclei of total amount of Draq5-positive nuclei. Cells were kept in the not CO_2-buffered incuabtor for the duration of the experiment.

The production of ROS is an important feature of neutrophils and therefore a widely used parameter to assess neutrophil functions. The assay that we use here, directly measures luminescence which is used as a proxy for the production of hydrogen peroxide. These measurements are carried out continually for the duration of the experiment which is why the samples remain in the, not CO_2-buffered, luminescence reader for the entire time of the experiment. Besides enhancing the NET formation rate, basic conditions have been shown to increase NOX2 activity, thus magnifying and prolonging the oxidative burst (Khan et al. 2018; Maueröder et al. 2016).

Based on these observations, I tested the effect of carbonate-buffered versus carbonate-free 0.1 % HSA supplemented medium. All media used were buffered with 10 mM HEPES independent of whether carbonate was also supplied as a buffer or not.

The oxidative burst peak in the carbonate-free medium was decreased to roughly one third as compared to the carbonate-buffered one (Figure 27 A). Furthermore, kinetics were

slightly altered, with the carbonate-buffered oxidative burst increasing to a maximum after 30 minutes and subsequently plateauing for 30-40 minutes before sharply decreasing to base line levels. The carbonic acid-free medium in contrast has a sharper peak which is also reached after 30 minutes but then immediately starts decreasing although with a flatter downward slope.

In contrast to the effect on the oxidative burst, the formation of NETs was not affected by using carbonate-free versus carbonate-buffered medium (Figure 27 B).

I assessed whether adding 0.1 % HSA to the medium causes any difference regarding the oxidative burst and NET formation in carbonated or carbonate-free medium (Figure 28). I did not observe any difference in the PMA-induced oxidative burst (Figure 28 A & C) or PMA-induced NET formation (Figure 28 B & D). A small increase in spontaneous NET formation did take place in carbonated and HSA-free medium which I did not observe in any of the other conditions (Figure 28 A).

In addition I assessed the PMA dose-dependency of the oxidative burst (Figure 29). Our standard ROS and NET inducing concentration is 100 nM PMA which was the minimum required concentration out of the range I tried. A 10-fold decreased amount of PMA induced an already clearly attenuated oxidative burst.

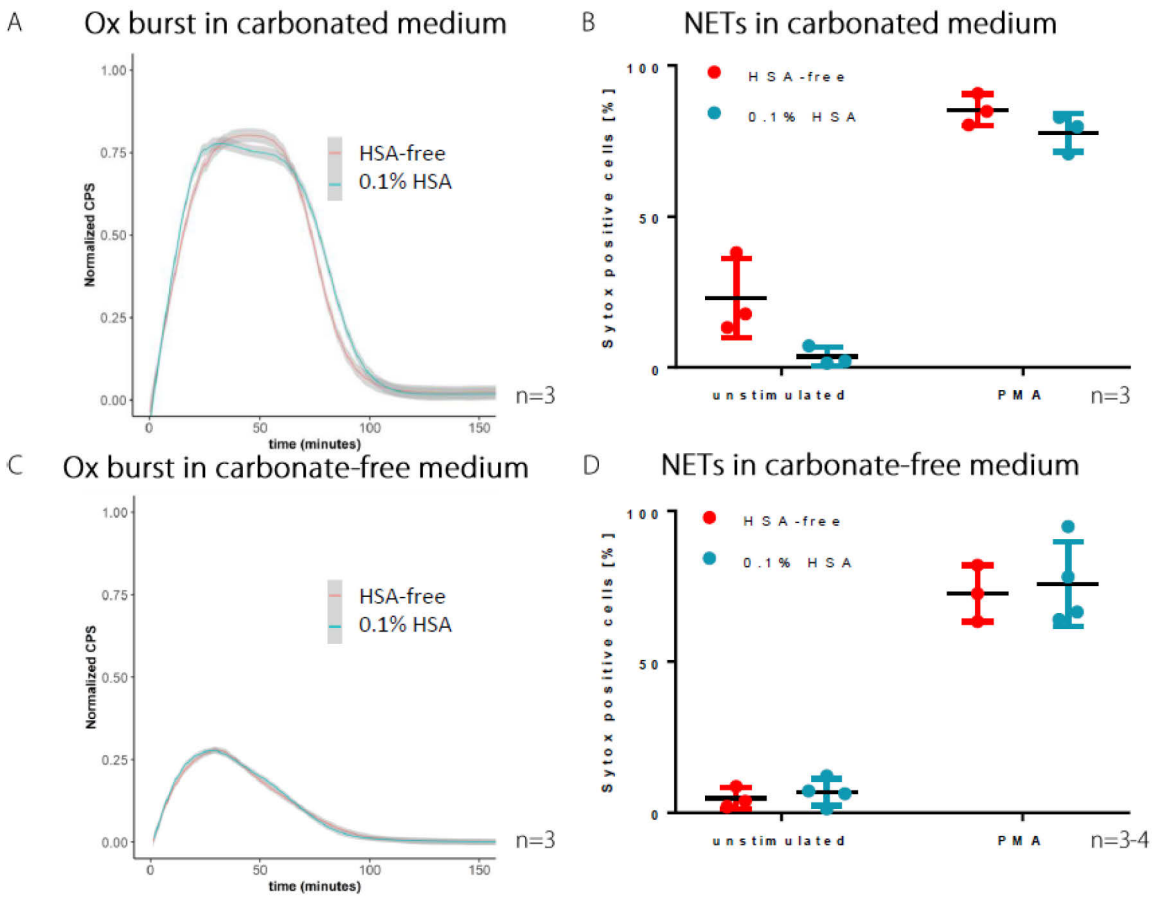

Figure 28 | Human serum albumin (HSA) does not affect the oxidative burst or NET formation in carbonated or carbonate-free medium.
The different media used in these assays contain the same amount of glucose and are 10 mM HEPES buffered. They differ, as indicated, in the amount of HSA and H_2CO_3. **A & C,** the oxidative (Ox) burst was measured as luminescence-reaction [CPS] with and without 0.1 % HSA in H_2CO_3-buffered ('carbonated') medium (panel A) and H_2CO_3-free ('carbonic acid-free') medium (panel B). Cells were kept in the not CO_2-buffered luminometer for the duration of the time course. Measurements of different experiments were normalized and are shown as regression model. **B & D,** NET formation with and without 0.1 % HSA after 3 hours for H_2CO_3-buffered medium ('carbonated') (panel B) and H_2CO_3-free ('carbonate-free') medium (panel D) was measured as percent of Sytox-positive and expanded nuclei of total amount of Draq5-positive nuclei. Cells were kept in the not CO_2-buffered incuabtor for the duration of the experiment.

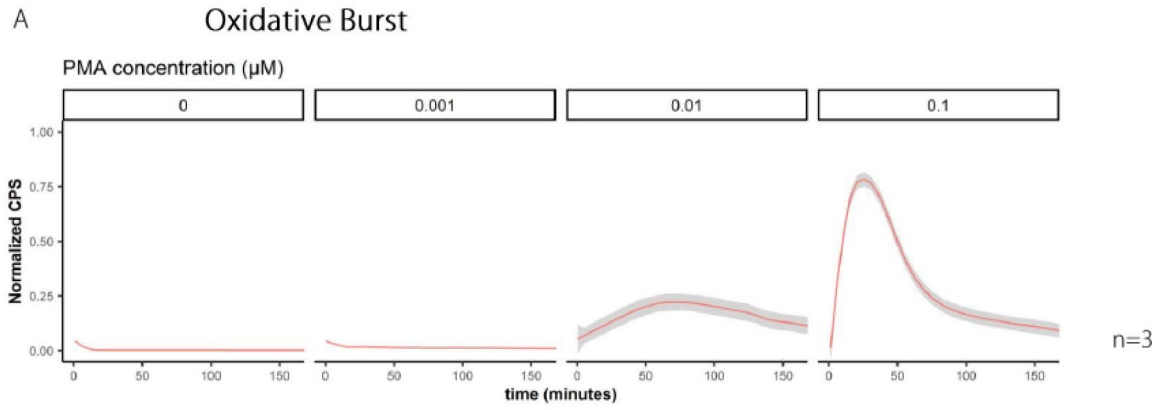

Figure 29 | More than 10 nM 12-myristate 13-acetate (PMA) is required to mount a whole oxidative burst response in neutrophils.
PMA titration for oxidative burst induction. Cells were distributed and stimulated with 100 nM PMA. The oxidative burst was measured as luminescence-reaction [CPS]. Measurements of different experiments were normalized and are shown as regression models in different sub-panels according to the respective concentration of PMA.

4 Discussion

4.1 Primary TALDO neutrophils stimulated with PMA do not make NETs

Inborn transaldolase 1-deficiency is a very rare metabolic defect which to-date has been described in only 34 patients (Williams et al. 2019). The spectrum of clinical manifestations is broad and reaches from early lethality to asymptomatic. Consequently, clinical symptoms vary hugely. However, most patients experience hepatomegaly and liver dysfunction is the reason for initial clinical consultation in many cases.

Thus far, for five patients (15 %) an increased level of infection was described, including the first patient we assessed who suffers from recurrent respiratory tract infections (Williams et al. 2019; Kobbe, personal communication). No malfunctioning of immune cells has been reported for TALDO patients until now. However, transaldolase 1 plays a crucial role in the non-oxPPP (Perl et al. 2011). Furthermore, both the oxPPP and the non-oxPPP are required for the rapid generation of the reducing equivalent NADPH in cells under oxidative stress and the oxPPP was shown to be required for the neutrophil oxidative burst and subsequent NOX2-dependent NET formation (Riyapa et al. 2019; Siler et al. 2016). No clear evidence exist regarding the involvement of the non-oxPPP. Taking into consideration the aforementioned observations and published findings I assessed several parameters in TALDO neutrophils.

I obtained blood in EDTA-treated tubes and started with neutrophil isolations one (Paris I & II) to three (HH) hours after blood drawing. This timing is the longest possible given the short life of neutrophils and the lag period was controlled with blood obtained from a healthy donor. We obtained only 5-15 ml of blood from the patients which limits the availability of neutrophils. Hence, no transaldolase 1 expression could be detected by Western Blot for the patient where enough material was obtained for lysate preparation (Figure 3). The neutrophil viability of two TALDO patients is very similar to that of the respective healthy controls, suggesting that a potential immune defect is not caused by shorter life span of TALDO neutrophils (Table 28).

I determined TALDO PMNs' ability to undergo netosis as one of the main antimicrobial processes in neutrophils. I used the mitogen PMA as a NET inducer which activates NET formation through the classical NOX2-dependent signalling cascade and is therefore widely used in mechanistic NET research (Amulic et al. 2017). Using a standardized NET quantification protocol (Brinkmann et al. 2012) NET formation of three patients was consistently below the

background level (Figure 4 & Figure 5). Accordingly, I also analysed ROS formation and oxygen consumption, a proxy for NOX2 activity, in one TALDO patient (Figure 6 & Figure 7 A). Testing ROS formation in the Paris patients was not possible because of technical limitations. The oxidative burst as determined by ROS formation was almost completely absent. Interestingly, oxygen consumption was strongly reduced but still reached a level of about 50 % after PMA stimulation. Since these two assays supposedly measure substrate and product, oxygen and superoxide, respectively, of the same NOX2-mediated reaction, i.e. oxygen reduction, a *true* biological discrepancy would be unexpected. However, since the source of the substrate oxygen is exclusively cytosolic and the product superoxide on the contrary is released extra-cytosolically, i.e. into phagosomes or extracellularly, it is conceivable of course that differential NOX2 localization could explain this inconsistency. Alternatively, the measured difference between ROS formation and oxygen consumption could have a technical explanation and just reflect the different sensitive ranges of the respective assays.

In conclusion, the observed absent NET and ROS-formation in TALDO neutrophils provide the very first genetic evidence of non-ox PPP requirement for these two antimimicrobial neutrophil effector functions. In addition, these data align well with the current knowledge of the literature regarding PPP's involvement in PMA-induced NET formation. Pharmacological inhibition suggests a requirement of the oxPPP, namely glucose-6-phosphate dehydrogenase (G6PDH) (Azevedo et al. 2015). This was genetically confirmed by analysing neutrophils of patients with an inherited G6PDH-defect, the most frequent human enzymatic deficiency (Cappellini & Fiorelli 2002; Nkhoma et al. 2009; Siler et al. 2016). The defect in G6PDH results in susceptibility to infection and absent netosis (Siler et al. 2016). Furthermore, pharmacologically inhibiting the non-oxPPP enzyme TKL , and TAL partne enzyme, led to reduced ROS- and NET formation, although no genetic evidence was provided (Riyapa et al. 2019).

The extracellular acidification rate is a proxy of glycolysis activity and its increase upon PMA stimulation is similar in the TALDO sample and in the healthy control, suggesting that a reduced flow through the PPP does not automatically lead to an increase in the glycolytic flow (Figure 7 B).

NE translocation to the nucleus during NOX2-dependent ROS formation is an important step preceeding chromatin decondensation. In TALDO neutrophils stimulated for 3 hours with PMA, NE did not enter the nucleus but localized to the plasma and, even more so, to the

nuclear membrane (Figure 8). This phenotype is reminiscent of NOX2-deficient CGD patients and is consistent with the crucial role of transaldolase 1 in the early events of NET formation.

Neutrophils produce a number of cytokines and chemokines, including IL-8 and MIP-1ß (Tecchio et al. 2014). I assessed secretion of those chemokines and observed no change for MIP-1ß in one tested patient and a reduced secretion of IL-8 in two tested patients (Figure 9). This discrepancy is interesting and could be based on ROS' reported involvement in the upregulation of IL-8 expression (Ye et al. 2009). However, with an "n" of two, further experiments are needed to verify the consistency of this trend.

4.2 PLB-986 CRISPR knock-outs

The TALDO neutrophils provided genetic evidence of transaldolase 1's requirement for ROS generation and NET formation. I wanted to assess transaldolase 1's role in NET formation in a different model and thus used the human neutrophil-like cell line PLB-985. Consequently, I generated different PLB-985 knock-out clones using the CRISPR-Cas9 system. I used different gRNAs targeting different sites in the short and long version of the TALDO1 gene as well as the *TKT* gene, the *MPO* gene as positive control and a SCR gRNA as negative control.

Transaldolase 1 was completely undetectable by Western Blot in the two *TALDO1S* KO clones whereas in the *TALDO1L* KO clones, some protein expression could be detected (Figure 11). Considering the double bands which can be seen for SCR and the *MPO* KO controls, it seems likely that the single band transaldolase 1 expression oberseved in the TALDO1L KO clones is just the lower running band and thus shorter version of TAL-S.

Similar to the assays I performed with the primary TALDO neutrophils, I assessed ROS formation and PMA-induced cell death, as a proxy for NETs, in the *TALDO1S* and *TALDO1L* knockout clones (Figure 12). The SCR control clone showed the highest rate of PMA-induced oxidative burst and cell death, thus confirming the ability of single cell clone-selected and fully differentiated PLB-985 cells to respond to PMA. For both versions of transaldolase 1, both selected clones showed a decrease in the oxidative burst compared to SCR controls cells. Similary, *TALDO1S* and *TALDO1L* knockout clones had a decreased rate of PMA-induced cell death. After 300 minutes, their Sytox positivity rate had multiplied 2.5 to maximum 5 times, whereas the SCR control reached 12 times the t_0 level. Interestingly, the transaldolase 1 requirement for PMA-induced cell death was even more pronounced than that of the positive control, i.e. *MPO* knockout. Importantly, these data are in line with the above reported results

in primary TALDO neutrophils as well as with the previously mentioned studies (Azevedo et al. 2015; Riyapa et al. 2019; Siler et al. 2016).

Furthermore, observing that full TAL knockout clones (*TALDO1S* KO) and clones just deficient for the long version TAL-L (*TALDO1L* KO) show basically the same phenotype with regard to PMA-induced cell death and ROS generation, indicates that the long version is required for those cellular events. Further experiments would be needed to assess whether just the long version would be sufficient but it is at least conceivable that nucleoplasmic transaldolase 1 activity, as suggested for TAL-L (Moriyama et al. 2016) is required for successful NET formation.

In addition to functionally testing the *TALDO1* KO clones, I also assessed the role of TAL's non-oxPPP partner enzyme TKL in NET formation and ROS generation (Figure 13). Of note, targeting the TKL-encoding *TKT* gene using the CRISPRCas9 system produced only one viable KO clone per gRNA. Together with the absence of a human TKL-deficiency, this emphasizes the crucial role of TKL on the organism and cellular level. *TKT* KO PLB-985 cells had a strongly reduced PMA-oxidative burst and cell death rate. These data align well with the finding of reduced ROS-generation and NET formation upon pharmacological TKT inhibition (Riyapa et al. 2019). Furthermore, these data provide the very first genetic evidence of TKL's requirement in these neutrophil functions.

4.3 Metabolomics of PMA-stimulated neutrophils

The findings on transaldolase 1`s requirement for NET formation prompted an analysis of the global metabolic landscape in PMA-stimulated neutrophils. The oxidative burst as crucial step previous to chromatin decondensation and nuclear expansion takes place in the first 10-25 minutes following PMA stimulation. Consequently, we decided to analyse the metabolome 15, 30 and 45 minutes after PMA stimulation in order to detect the global metabolic dynamics during and following the oxidative burst (Figure 14).

Global metabolite measurements are commonly done applying nuclear magnetic resonance (NMR) spectroscopy- or mass spectrometry (MS)-based approaches (Lu et al. 2017). Although other methods exist, NMR and MS stand out because of their cost effective, truly unbiased (NMR) or highly sensitive (MS) approaches, respectively (Emwas 2015).

Recently, two NMR-based global metabolite studies were published, assessing the neutrophil metabolome in cytokine-treated or aged neutrophils (Richer et al. 2018) and in 5 or 15 minutes PMA-stimulated neutrophils (Chokesuwattanaskul et al. 2018).

Discussion

We opted for a MS-based commercial metabolomics technology with the company Metabolon, Inc. Thus, the method combines MS-inherent high sensitivity with an expanded chemical reference library of more than 4000 known and 8000 unknown metabolites, thus allowing an almost unbiased metabolome analysis. Consequently, to my knowledge this is the first MS-based global metabolome study in PMA-stimulated neutrophils.

PMA stimulation resulted in statistical significant up/down regulation of 21/22 metabolites at 15, 21/70 metabolites at 30 and 23/102 metabolites after 45 minutes compared to the untreated control. I will discuss a few of those results regarding their potential relevance in NET formation.

Glycolysis and PPP

Glucose levels in PMA stimulated neutrophils were already increased to more than 2-fold after 15 minutes and were significantly increased to more than 3-fold after 30 and 45 minutes (Figure 15 A). This result is in line with a recently reported strong increase of neutrophil glucose abundance after 5 and, although less pronounced, 15 minutes of PMA stimulation (Chokesuwattanaskul et al. 2018). The increased glucose levels could be caused by a reduced cellular glucose consumption upon PMA-stimulation although that seems like a counter intuitive conclusion which is, to my knowledge, not supported by the literature. Conversely, the source of this increased glucose could be an upregulation of glucose transport into the cell, supported by a, previously reported, PMA-induced translocation of GLUT3 from intracellular vesicles to the cellular membrane (Simpson et al. 2008). Additionally, it has been speculated that the increased glucose could be due to glycogenolysis (Chokesuwattanaskul et al. 2018), based on the long known presence of glycogen in neutrophils (Valentine et al. 1953; Wagner 1945). However, it is not known whether neutrophils could produce glucose upon glycogen degradation or whether the final glycogenolysis product would be G6P because the phosphatase producing glucose from G6P is widely assumed to be only expressed in hepatocytes.

Unfortunately, G6P was not detected in the metabolome analysis despite being part of the library.

Levels of PEP and 3-phosphoglycerate, two glycolysis metabolites, were consistently and significantly increased at all three time points (above 3-fold, 5-fold 6-fold increased, respectively) (Figure 15 B & C). 3-phosphogycerate is a metabolite of both, glycolysis and PPP, and its increase would align with a hypothesized PMA-induced shift from glycolysis to PPP

(Azevedo et al. 2015; Chokesuwattanaskul et al. 2018). PEP however, is a metabolite of the lower glycolysis and its increase could only be explained by an increase in the glycolytic pathway.

The significant increase in PPP metabolites 6-phosphogluconate (oxPPP, for all three time points) and sedoheptulose-7-phosphate (non-oxPPP, only for the last time point) indicates an increased requirement of shuffling through the PPP upon PMA-stimulation, also described elsewhere (Chokesuwattanaskul et al. 2018). Nevertheless, the fold change increase of maximally 2.8 times seems surprisingly mild.

Redox balance pathway

As discussed before, PMA induces NOX2 activation and consequently a strong ROS formation. ROS damage is counteracted in most cells by the glutathione redox system which, as NOX2 relies on the reducing equivalent NADPH. Disappointingly, NADP was not detected in the metabolomics analysis.

Interestingly, abundance of GSH was not affected upon PMA stimulation (Figure 17 A). Due to the massive NADPH consumption by activated NOX2 (thus not available for reducing GSSG to GSH) taken together with an assumed stronger need for ROS damage control (oxidizing GSH to GSSG), my expectation was a reduced GSH level. Similarly, if anything, I would have expected an increase in GSSG, the analysis however revealed a significant reduction to 56 % after 30 minutes (Figure 17 B), thus leading to an increased GSH:GSSG ratio. Taken together, these data indicate a more reduced cellular environment upon PMA stimulation in neutrophils. This is a very interesting and, considering the strong PMA-induced ROS formation, rather unexpected result. Of note, a recent study using a genetically encoded redox sensor to assess the cellular redox state in PMA-stimulated neutrophil-like PLB-985 cells made an opposing observation, i.e. a trend towards a more oxidizing cellular environment (Xie et al. 2020). More research in this area is needed to determine the true nature of the matter, also with regard to the different kinds of ROS and the likely relevance of subcellular localization which was not assessed by my study or the just cited one. Additionally, I detected a significant reduction of cysteinylglycine, a degradation product of GSH, after 30 and 45 minutes (Figure 17 C).

A general conclusion regarding the described findings remains speculative. The data seem to indicate that despite its presumambly very high consumption by PMA activated NOX2, NADPH is not limited and still sufficiently available to recycle GSSG to GSH. Furthermore, the

reduced levels of cysteinglycine indicate decreased GSH degradation, logically contributing to stabilizing or elevating GSH abundance. This could indicate a strong cellular requirement for the glutathione redox stress balancing system. The fact that ROS stress is occurring in PMA induced neutrophils is emphasized by the more than 3-fold increase of methionine sulfoxide after 15 minutes which subsequently mitigates but remains significantly above base line levels (Figure 17 D). Methionine, together with cysteine, is the easiest oxidizable amino acid because of the sulfur it contains and thus indicates elevated levels of ROS stress (Lee & Gladyshev 2011).

Nucleotide metabolism pathway

Assessing the PMA-induced dynamics of compounds in the nucleotide metabolism provided a multifaceted picture (Figure 18). Whereas the adenine precursor 3-AMP was significantly increased to a level of 2.74-fold the base line level after 15 minutes and subsequently returned to base line levels, the bases guanine and uracil as well as the nucleoside guanosine were significantly and progressively reduced during PMA stimulation.

Given that those compound are potential building blocks for/degradation products of DNA, these data suggest that either DNA synthesis was increased or DNA degradation came to a halt. However, these interpretations have to be taken with care and further experiments are needed to assess the cellular relevance of the above described findings.

Phospholipid metabolism

Compounds in the phospholipid metabolism are essential for cellular membrane building and in a range of cell regulatory processes. The levels of choline, choline phosphate and glycerophosphoethanolamine were most dramatically affected in this compound group (Figure 19). As described above, choline phosphate was steadily and significantly reduced over the 45 minutes to only 30 % of the baseline abundance, the choline concentration went the opposite way and tripled already after 15 minutes without subsequent further increases (Figure 19 A & B). The PMA-induced choline phosphate decrease and accompanying choline level increase induced by PMA aligns well with previously made observations by others (Pédruzzi et al. 1998). Choline phosphate and choline are products of degradation of phosphatidylcholine, a very frequent membrane lipid and source of second messengers (Pédruzzi et al. 1998). The physiological implications of choline phosphate and choline in neutrophils do not seem fully elucidated but in a recent report an attenuating effect of choline on bovine neutrophils activation was observed (Garcia et al. 2018).

Glycerophosphoethanolamine is a glycerolipid derivative with, to my knowledge, no identified cellular function. Its levels increased significantly over the time course and more than quadrupled after 15 minutes before reaching more than 8 and more than 10 times the base line level after 30 and 45 minutes, respectively (Figure 19 C).

4.4 Inhibition of NETs by pharmacological manipulation

I aimed to verify the previously described results we observed by pharmacologically inhibiting metabolic and other reactions upstream of NOX2-dependent NET formation (Figure 20). Besides confirming the previous results, I was also interested in determining a potential *NOX2-activity/ROS threshold* required for NET formation. Therefore, and in addition to the classically used luminescence-based ROS formation assay, I also assessed oxygen consumption of NET forming neutrophils as a more quantitative proxy for NOX2 activity. The three used inhibitors DPI, 6-AN and 2-DG respectively inhibit NOX2, the oxPPP enzyme G6PDH and the glycolysis/PPP enzyme GPI. Unfortunately, at the moment no commercially available transaldolase 1 inhibitor exists.

DPI decreases OCR and ROS formation levels to near 0 at 300 nM whereas NET formation was already absent at 100 nM (Figure 21). These data recapitulate the previously reported inhibitory effect of DPI on ROS generation and NET-formation (Fuchs et al. 2007) and confirm it with the additional observation of reduced PMA-induced oxygen consumption.

The G6PDH inhibitor 6-AN strongly reduces OCR and ROS formation and decreases NET formation to roughly 50 % at a concentration of 300 µM (Figure 22). This data confirms the crucial role of G6PDH and consequently the oxPPP in NOX2-dependent NET formation. A previous study had already reported 6-AN`s inhibitory effect on ROS- and NET formation, although at a more than 30 times higher concentration (Azevedo et al. 2015).

The glucose analogous inhibitor 2-DG strongly reduces OCR and ROS-generation followed by a pronounced reduction in NET formation to 21 % and 7 % NET forming neutrophils at concentrations of 6.7 and 20 mM, respectively (Figure 23). The effect of 2-DG on ROS- and NET-formation has been assessed before and was reported to be inhibitory in several studies (Azevedo et al. 2015; Rodríguez-Espinosa et al. 2015). Controversally, one study also observed a NET formation enhancing effect of 2-DG, although this was only observed in unphysiologically high glucose concentrations of 30 mM (Joshi et al. 2013).

Commonly, 2-DG`s inhibitory role on ROS- and NET-formation is interpreted as a dependence on glycolysis, i.e. energy in the form of ATP, of those mechanisms. In addition, a

recently study suggested that glycolytic ATP is required for NET formation (Amini et al. 2018). Of note however, the unusual NET-inducer used in that study makes it hard to translate the results to the mostly studied NOX2-dependent NET formation. Furthermore, taking into consideration the thus far scarce evidence regarding ATP requirement for netosis and 2-DG´s mechanism of inhibition, an ATP-independent inhibiting effect seems conceivable. 2-DG is a non-competitive hexokinase (HK) and a competitive phosphoglucose isomerase (PGI) inhibitor (Ralser et al. 2008; Wick et al. 1956). Both enzymes are required for glycolysis. Conversely, both enzymes are needed for the PPP as well. HK catalyzes the initial glucose phosphorylation step after which G6P goes either through glycolysis or through the PPP. The observation that glucose levels after PMA stimulation are increased (section 4.3) make it seem unlikely that HK inhibition would be the NET-impairing 2-DG effect. GPI however is not needed for initially providing G6P to the PPP but does catalyze the last step of the `cyclic` PPP, namely the conversion of F6P to G6P.

Therefore, I propose the hypothesis that 2-DG´s inhibiting effect on NOX2-dependent netosis is ATP and glycolysis-independent and mainly consists of impairing the fully closed PPP cycle.

Furthermore, taking together the data obtained with the three inhibitors DPI, 6-AN and 2-DG, I could not establish a clear NOX2 activity-/ROS-threshold required for a full NET response.

4.5 ROS formation is only relevant for NETs 50 minutes after PMA stimulation

Based on the observation that PMA-stimulation of neutrophils results in an increased level of glucose (section 4.3), I analyzed the effect of glucose on ROS generation and NET formation. That relationship has been analyzed before and the consistent observation is that glucose is required for NETs and for ROS formation although controversial interpretations of this finding remain, especially regarding the question of whether the crucial glucose-dependent factor required for NETs is the glycolysis-derived ATP or the PPP-derived NADPH (Amini et al. 2018; Azevedo et al. 2015; Menegazzo et al. 2015; Rodríguez-Espinosa et al. 2015).

I supplied neutrophils with a range of different glucose concentrations and observed no effect on the oxidative burst peak but a clear positive correlation between glucose concentration and NET formation (Figure 24). Absent glucose results in absent netosis. Interestingly, a very low glucose concentration of only 0.1 mM is enough for already 50 % of control level NET formation and 1 mM (still ten times below normal experimental standards)

was sufficient for a normal NET response. This fits nicely to the fact that, similar to very glucose-dependent brain cells, neutrophils express high amounts of glucose transporter 3 (GLUT3), the GLUT isoform with the highest glucose affinity (Vrhovac et al. 2014). Surprisingly, the oxidative burst peak was not affected by the absence of glucose. Of note, the oxidative burst kinetics of the tree samples with different glucose concentrations were very similar, returning to baseline levels after 75 minutes, whereas the glucose-free sample presented a more rapid return to baseline levels after approximately 55 minutes. A previous study had shown that ROS formation is significantly reduced in glucose-free conditions, although no time resolution was provided (Azevedo et al. 2015).

To my knowledge the here presented data show for the first time that the peak height of the oxidative burst, as measured in the widely used luminescence-based ROS formation assay, is irrelevant for NET formation. Importantly, the glucose-fuelled *shoulder* of ROS production after around 50 minutes makes all the difference for NET formation. The different mechanisms potentially underlying the shoulder and the main peak are unknown and deciphering them would surely provide crucial insights into the netosis mechanism. Noteworthy, these data fit nicely with preliminary data obtained in our laboratory, indicating that NET formation can be inhibited with the NOX-2 inhibitor DPI as late as 50 minutes after PMA stimulation (Foti, personal communication). Furthermore, the potentially crucial role of the 50 minutes ROS shoulder sheds a different light on the metabolomics data discussed before (section 4.3), since the last analzyed time point was at 45 minutes PMA stimulation.

4.6 Carbonated medium enhances PMA-induced oxidative burst measured in a not-CO_2 buffered environment

In this part I assessed a technical feature of the ROS formation assay I used throughout this project. The respective assay is a widely applied luminol-amplified chemiluminescence technique used for the detection of ROS production in neutrophils (Bedouhène et al. 2017). I determined the effect of carbonate-buffered versus carbonic acid-free medium during the ROS formation assay which is carried out in a not CO_2-buffered luminometer. In addition, I assessed an effect of these two media on NET formation. ROS formation in carbonated medium presented a much higher oxidative burst peak and was more prolonged as compared to carbonic acid-free medium (Figure 27 A). There was no difference between the media with regard to NET formation (Figure 27 B).

These data indicate that the choice of medium for the not-CO_2-buffered ROS assay has to be carefully taken into consideration. Carbonate and HEPES buffered, human serum albumin (HSA)-complemented medium ('Neutrophil medium', compare Table 5 | Media composition) is commonly used for this assay in our laboratory. Since CO_2 is constantly released from the medium under normal atmospheric CO_2 concentration (0.04 %), the carbonate to water plus CO_2 equilibrium ($H_2CO_3 \leftrightarrow CO_2 + H_2O$) is shifted towards $CO_2 + H_2O$, subsequently pushing the medium into a more basic pH. Basic conditions have been shown to increase NOX2 activity, thus magnifying and prolonging the oxidative burst and enhancing the rate of NET formation (Khan et al. 2018; Maueröder et al. 2016). Accordingly, for all experiments carried out for this project in equipment without CO_2 supply, HEPES-buffered medium was used.

4.7 Concluding remarks

Taken together the main finding of this PhD thesis is that the enzyme transaldolase 1 is as an essential enzyme in NOX2-dependent NET formation which could potentially explain some of the clinical observations in TALDO patients. This data for the very first time provides genetic evidence showing the requirement of the non-oxPPP for NET formation.

Furthermore, this work shows that the oxidative burst peak is irrelevant for NET formation and that in fact the ROS formation starting 50 minutes after PMA stimulation is essential for netosis.

In addition, the present data indicate, that 2-DG´s inhibitory effect on NETs is likely glygolysis and ATP-independent and rather PPP and NADPH-mediated.

References

Agledal L, Niere M, Ziegler M. 2010. The phosphate makes a difference: cellular functions of NADP. *Redox Rep.* 15(1):2–10

Agmon-Levin N, Lian Z, Shoenfeld Y. 2011. Explosion of autoimmune diseases and the mosaic of old and novel factors. *Cell. Mol. Immunol.* 8(3):189–92

Amini P, Stojkov D, Felser A, Jackson CB, Courage C, et al. 2018. Neutrophil extracellular trap formation requires OPA1-dependent glycolytic ATP production. *Nat. Commun.* 9(1):

Amulic B, Cazalet C, Hayes GL, Metzler KD, Zychlinsky A. 2012. Neutrophil Function: From Mechanisms to Disease. *Annu. Rev. Immunol.* 30(1):459–89

Amulic B, Knackstedt SL, Abu Abed U, Deigendesch N, Harbort CJ, et al. 2017. Cell-Cycle Proteins Control Production of Neutrophil Extracellular Traps. *Dev. Cell*. 43(4):449-462.e5

Assari T. 2006. Chronic granulomatous disease; fundamental stages in our understanding of CGD. *Med. Immunol.* 5:1–8

Azevedo EP, Rochael NC, Guimarães-Costa AB, De Souza-Vieira TS, Ganilho J, et al. 2015. A metabolic shift toward pentose phosphate pathway is necessary for amyloid fibril- and phorbol 12-myristate 13-Acetate-induced neutrophil extracellular trap (NET) formation. *J. Biol. Chem.* 290(36):22174–83

Baehner RL, Nathan DG. 1967. Leukocyte Oxidase: Defective Activity in Chronic Granulomatous Disease. *Science (80-.).* 155(3764):835–36

Balasubramaniam S, Wamelink MMC, Ngu L-H, Talib A, Salomons GS, et al. 2011. Novel heterozygous mutations in TALDO1 gene causing transaldolase deficiency and early infantile liver failure. *J. Pediatr. Gastroenterol. Nutr.* 52(1):113–16

Banki K, Hutter E, Colombo E, Gonchoroff NJ, Perl A. 1996. Glutathione levels and sensitivity to apoptosis are regulated by changes in transaldolase expression. *J. Biol. Chem.* 271(51):32994–1

Bedouhène S, Moulti-Mati F, Hurtado-Nedelec M, Dang PM-C, El-Benna J. 2017. Luminol-amplified chemiluminescence detects mainly superoxide anion produced by human neutrophils. *Am. J. Blood Res.* 7(4):41–48

Bianchi M, Hakkim A, Brinkmann V, Siler U, Seger RA, et al. 2009. Restoration of NET formation by gene therapy in CGD controls aspergillosis. *Blood*. 114(13):2619–22

Björnsdottir H, Welin A, Michaëlsson E, Osla V, Berg S, et al. 2015. Neutrophil NET formation is regulated from the inside by myeloperoxidase-processed reactive oxygen species. *Free Radic. Biol. Med.* 89:1024–35

Brinkmann V, Goosmann C, Kühn LI, Zychlinsky A. 2012. Automatic quantification of in vitro NET formation. *Front. Immunol.* 3(JAN):1–8

Brinkmann V, Reichard U, Goosmann C, Fauler B, Uhlemann Y, et al. 2004. Neutrophil extracellular traps kill bacteria. *Science*. 303(5663):1532–35

Brinkmann V, Zychlinsky A. 2012. Neutrophil extracellular traps: Is immunity the second function of chromatin? *J. Cell Biol.* 198(5):773–83

Burgener SS, Schroder K. 2019. Neutrophil Extracellular Traps in Host Defense. *Cold Spring Harb. Perspect. Biol.* (November):

Cappellini MD, Fiorelli G. 2002. Glucose-6-phosphate dehydrogenase deficiency. *Lancet*. 37(6):64–74

Chacko BK, Kramer PA, Ravi S, Johnson MS, Hardy RW, et al. 2013. Methods for defining distinct bioenergetic profiles in platelets, lymphocytes, monocytes, and neutrophils, and the oxidative burst from human blood. *Lab. Investig.* 93(6):690–700

Chang GG, Tong L. 2003. Structure and Function of Malic Enzymes, A New Class of Oxidative Decarboxylases. *Biochemistry*. 42(44):12721–33

Chapman EA, Lyon M, Simpson D, Mason D, Beynon RJ, et al. 2019. Caught in a trap? Proteomic analysis of neutrophil extracellular traps in rheumatoid arthritis and systemic lupus erythematosus. *Front. Immunol.* 10(MAR):

Chen G, Zhang D, Fuchs TA, Manwani D, Wagner DD, Frenette PS. 2014. Heme-induced neutrophil extracellular traps contribute to the pathogenesis of sickle cell disease. *Blood*. 123(24):3818–27

References

Chen KW, Monteleone M, Boucher D, Sollberger G, Ramnath D, et al. 2018. Noncanonical inflammasome signaling elicits gasdermin D–dependent neutrophil extracellular traps. *Sci. Immunol.* 3(26):

Chokesuwattanaskul S, Phelan MM, Edwards SW, Wright HL. 2018. A robust intracellular metabolite extraction protocol for human neutrophil metabolic profiling. *PLoS One*. 13(12):1–20

Collins SJ, Gallo RC, Gallagher RE. 1977. Continuous growth and differentiation of human myeloid leukaemic cells in suspension culture. *Nature*. 270(November):347–49

Corbin BD, Seeley EH, Raab A, Feldmann J, Miller MR, et al. 2008. Metal Chelation and Inhibition of Bacterical Growth in Tissue Abscesses. *Science (80-.).* 319(February):962–66

De Oliveira S, Rosowski EE, Huttenlocher A. 2016. Neutrophil migration in infection and wound repair: Going forward in reverse. *Nat. Rev. Immunol.* 16(6):378–91

Desai J, Kumar S V., Mulay SR, Konrad L, Romoli S, et al. 2016. PMA and crystal-induced neutrophil extracellular trap formation involves RIPK1-RIPK3-MLKL signaling. *Eur. J. Immunol.* 46(1):223–29

Donato H, Krupenko NI, Tsybovsky Y, Krupenko SA. 2007. 10-Formyltetrahydrofolate Dehydrogenase Requires a 4 ¯-Phosphopantetheine Prosthetic Group for Catalysis *. *J. Biol. Chem.* 282(47):34159–66

Douda DN, Yip L, Khan MA, Grasemann H, Palaniyar N. 2014. To the editor: Akt is essential to induce NADPH-dependent NETosis and to switch the neutrophil death to apoptosis. *Blood*. 123(4):597–600

Dupré-Crochet S, Erard M, Nüβe O. 2013. ROS production in phagocytes: why, when, and where? *J. Leukoc. Biol.* 94(4):657–70

Ehrlich P. 1879. Ueber die specifischen Granulationen des Blutes

Ehrlich P. 1880. Methodologische Beiträge zur Physiologie und Pathologie der verschiedenen Formen der Leukocyten. *Z. Klin. Med.* 1:553–60

Emwas A-HM. 2015. The Strengths and Weaknesses of NMR Spectroscopy and Mass Spectrometry with Particular Focus on Metabolomics Research. In *Metabolomics - Methods and Protocols*, Vol. 1277, pp. 161–93

Faget J, Boivin G, Ancey P-B, Gkasti A, Mussard J, et al. 2018. Efficient and specific Ly6G+ cell depletion: A change in the current practices toward more relevant functional analyses of neutrophils. *bioRxiv*. 498881

Filio-Rodríguez G, Estrada-García I, Arce-Paredes P, Moreno-Altamirano MM, Islas-Trujillo S, et al. 2017. In vivo induction of neutrophil extracellular traps by Mycobacterium tuberculosis in a Guinea pig model. *Innate Immun.* 23(7):625–37

Foote JR, Patel AA, Yona S, Segal AW. 2019. Variations in the phagosomal environment of human neutrophils and mononuclear phagocyte subsets. *Front. Immunol.* 10(MAR):1–11

Fridlender ZG, Sun J, Kim S, Kapoor V, Cheng G, et al. 2009. Polarization of Tumor-Associated Neutrophil Phenotype by TGF-β: “N1” versus “N2” TAN. *Cancer Cell*. 16(3):183–94

Fuchs TA, Abed U, Goosmann C, Hurwitz R, Schulze I, et al. 2007. Novel cell death program leads to neutrophil extracellular traps. *J. Cell Biol.* 176(2):231–41

Garcia M, Mamedova LK, Barton B, Bradford BJ. 2018. Choline regulates the function of bovine immune cells and alters the mRNA abundance of enzymes and receptors involved in its metabolism in vitro. *Front. Immunol.* 9(OCT):1–14

Hakkim A, Fuchs TA, Martinez NE, Hess S, Prinz H, et al. 2011. Activation of the Raf-MEK-ERK pathway is required for neutrophil extracellular trap formation. *Nat. Chem. Biol.* 7(2):75–77

Haley PJ. 2003. Species differences in the structure and function of the immune system. *Toxicology*. 188(1):49–71

Halverson TWR, Wilton M, Poon KKH, Petri B, Lewenza S. 2015. DNA Is an Antimicrobial Component of Neutrophil Extracellular Traps. *PLoS Pathog.* 11(1):1–23

Harbort CJ, Soeiro-Pereira PV, Bernuth H von, Kaindl AM, Costa-Carvalho BT, et al. 2015. Neutrophil oxidative burst activates ATM to regulate cytokine production and apoptosis. *Blood*. 126(26):2842–52

Hasenberg A, Hasenberg M, Männ L, Neumann F, Borkenstein L, et al. 2015. Catchup: A mouse model for imaging-based tracking and modulation of neutrophil granulocytes. *Nat. Methods*. 12(5):445–

52
Hatefi Y, Osborn MJ, Kay LD, Huennekens FM. 1957. Hydroxymethyl tetrahydrofolic dehydrogenase. *J. Biol. Chem.* 637–49
Heigwer F, Kerr G, Boutros M. 2014. E-CRISP: Fast CRISPR target site identification. *Nat. Methods*. 11(2):122–23
Hirsch JG. 1958. Bactericidal Action of Histone. *J. Exp. Med.* 1960(2):925–44
Hoppenbrouwers T, Autar ASA, Sultan AR, Abraham TE, Van Cappellen WA, et al. 2017. In vitro induction of NETosis: Comprehensive live imaging comparison and systematic review. *PLoS One*. 12(5):1–29
Isles HM, Loynes CA, Hamilton N, Muir CF, Kadochnikova A, et al. 2019. Endogenous pioneer neutrophils release NETs during the swarming response in zebrafish
Jie Z, Zhang Y, Wang C, Shen B, Guan X, et al. 2017. Large-scale ex vivo generation of human neutrophils from cord blood CD34+ cells. *PLoS One*. 12(7):1–18
Joshi MB, Lad A, Bharath Prasad AS, Balakrishnan A, Ramachandra L, Satyamoorthy K. 2013. High glucose modulates IL-6 mediated immune homeostasis through impeding neutrophil extracellular trap formation. *FEBS Lett.* 587(14):2241–46
Kawakami T, He J, Morita H, Yokoyama K, Kaji H, et al. 2014. Rab27a is essential for the formation of neutrophil extracellular traps (NETs) in neutrophil-like differentiated HL60 cells. *PLoS One*. 9(1):
Kenny EF, Herzig A, Krüger R, Muth A, Mondal S, et al. 2017. Diverse stimuli engage different neutrophil extracellular trap pathways. *Elife*. 6:e24437
Khallaf H Al. 2017. Isocitrate dehydrogenases in physiology and cancer : biochemical and molecular insight. *Cell Biosci.* 1–18
Khan MA, Philip LM, Cheung G, Vadakepeedika S, Grasemann H, et al. 2018. Regulating NETosis: Increasing pH Promotes NADPH Oxidase-Dependent NETosis. *Front. Med.* 5(February):
Klebanoff SJ. 2005. Myeloperoxidase: friend and foe. *J. Leukoc. Biol.* 77(5):598–625
Klein C. 2016. Children with rare diseases of neutrophil granulocytes: From therapeutic orphans to pioneers of individualized medicine. *Hematology*. 2016(1):33–37
Kramer PA, Ravi S, Chacko B, Johnson MS, Darley-Usmar VM. 2014. A review of the mitochondrial and glycolytic metabolism in human platelets and leukocytes: Implications for their use as bioenergetic biomarkers. *Redox Biol.* 2(1):206–10
Labun K, Montague TG, Gagnon JA, Thyme SB, Valen E. 2016. CHOPCHOP v2: a web tool for the next generation of CRISPR genome engineering. *Nucleic Acids Res.* 44(W1):W272–76
Lawrence SM, Corriden R, Nizet V. 2018. The Ontogeny of a Neutrophil: Mechanisms of Granulopoiesis and Homeostasis. *Microbiol. Mol. Biol. Rev.* 82(1):1–22
Lee BC, Gladyshev VN. 2011. The biological significance of methionine sulfoxide stereochemistry. *Free Radic. Biol. Med.* 50(2):221–27
Lee WL, Harrison RE, Grinstein S. 2003. Phagocytosis by neutrophils. *Microbes Infect.* 5(14):1299–1306
Lennartz MR. 1999. Phospholipases and phagocytosis: The role of phospholipid-derived second messengers in phagocytosis. *Int. J. Biochem. Cell Biol.* 31(3–4):415–30
Lichtenberg D, Pinchuk I. 2015. Oxidative stress, the term and the concept. *Biochem. Biophys. Res. Commun.* 461(3):441–44
Lipinski P, Pawlowska J, Stradomska T, Ciara E, Jankowska I, et al. 2017. Long-Term Systematic Monitoring of Four Polish Transaldolase Deficient Patients. *JIMD Rep.*
Liu X, Zhang Z, Ruan J, Pan Y, Magupalli VG, et al. 2016. Inflammasome-activated gasdermin D causes pyroptosis by forming membrane pores. *Nature*. 535(7610):153–58
Loeffen YGT, Biebuyck N, Wamelink MMC, Jakobs C, Mulder MF, et al. 2012. Nephrological abnormalities in patients with transaldolase deficiency. *Nephrol. Dial. Transplant.* 27(8):3224–27
Lu W, Su X, Klein MS, Lewis IA, Fiehn O, Rabinowitz JD. 2017. Metabolite Measurement: Pitfalls to Avoid and Practices to Follow. *Annu. Rev. Biochem.* 86(1):277–304
Lunt SY, Vander Heiden MG. 2011. Aerobic Glycolysis: Meeting the Metabolic Requirements of Cell Proliferation. *Annu. Rev. Cell Dev. Biol.* 27(1):441–64
Maueröder C, Mahajan A, Paulus S, Gößwein S, Hahn J, et al. 2016. Ménage-à-trois: The ratio of bicarbonate to CO2 and the pH regulate the capacity of neutrophils to form NETs. *Front. Immunol.*

7(DEC):
Mayadas TN, Cullere X, Lowell CA. 2014. The Multifaceted Functions of Neutrophils. *Annu. Rev. Pathol. Mech. Dis.* 9(1):181–218
McNamara MP, Wiessner JH, Collins-Lech C, Hahn BL, Sohnle PG. 1988. Neutrophil Death as a Defence Mechanism against Candida Albicans Infections. *Lancet*. 1163–65
Menegazzo L, Ciciliot S, Poncina N, Mazzucato M, Persano M, et al. 2015. NETosis is induced by high glucose and associated with type 2 diabetes. *Acta Diabetol.* 52(3):497–503
Metzler K, Goosmann C, Lubojemska A, Zychlinsky A, Papayannopoulos V. 2014. A Myeloperoxidase-Containing Complex Regulates Neutrophil Elastase Release and Actin Dynamics during NETosis. *Cell Rep.* 8(3):883–96
Metzler KD, Fuchs T a, Nauseef WM, Reumaux D, Roesler J, et al. 2012. Myeloperoxidase is required for neutrophil extracellular trap formation : implications for innate immunity. *Blood*. 117(3):953–59
Moriyama T, Tanaka S, Nakayama Y, Fukumoto M, Tsujimura K, et al. 2016. Two isoforms of TALDO1 generated by alternative translational initiation show differential nucleocytoplasmic distribution to regulate the global metabolic network. *Sci. Rep.* 6(1):34648
Neubert E, Senger-Sander SN, Manzke VS, Busse J, Polo E, et al. 2019. Serum and serum albumin inhibit in vitro formation of Neutrophil Extracellular Traps (NETs). *Front. Immunol.* 10(JAN):
Nkhoma ET, Poole C, Vannappagari V, Hall SA, Beutler E. 2009. The global prevalence of glucose-6-phosphate dehydrogenase deficiency: A systematic review and meta-analysis. *Blood Cells, Mol. Dis.* 42(3):267–78
Nordenfelt P, Tapper H. 2011. Phagosome dynamics during phagocytosis by neutrophils. *J. Leukoc. Biol.* 90(2):271–84
Papayannopoulos V. 2017. Neutrophil extracellular traps in immunity and disease. *Nat. Publ. Gr.* 1–14
Papayannopoulos V, Metzler KD, Hakkim A, Zychlinsky A. 2010. Neutrophil elastase and myeloperoxidase regulate the formation of neutrophil extracellular traps. *J. Cell Biol.* 191(3):677–91
Pédruzzi E, Hakim J, Giroud JP, Périanin A. 1998. Analysis of choline and phosphorylcholine content in human neutrophils stimulated by f-met-leu-phe and phorbol myristate acetate: Contribution of phospholipase D and C. *Cell. Signal.* 10(7):481–89
Perl A, Hanczko R, Telarico T, Oaks Z, Landas S. 2011. Oxidative stress, inflammation and carcinogenesis are controlled through the pentose phosphate pathway by transaldolase. *Trends Mol. Med.* 17(7):395–403
Perl A, Qian Y, Chohan KR, Shirley CR, Amidon W, et al. 2006. Transaldolase is essential for maintenance of the mitochondrial transmembrane potential and fertility of spermatozoa. *Proc. Natl. Acad. Sci. U. S. A.* 103(40):14813–18
Pilsczek FH, Salina D, Poon KKH, Fahey C, Yipp BG, et al. 2010. A novel mechanism of rapid nuclear neutrophil extracellular trap formation in response to Staphylococcus aureus. *J. Immunol.* 185(12):7413–25
Plaitakis A, Kalef-Ezra E, Kotzamani D, Zaganas I, Spanaki C. 2017. The Glutamate Dehydrogenase Pathway and Its Roles in Cell and Tissue Biology in Health and Disease. . (Figure 1):1–26
Ralser M, Wamelink MM, Struys EA, Joppich C, Krobitsch S, et al. 2008. A catabolic block does not sufficiently explain how 2-deoxy-D-glucose inhibits cell growth. *Proc. Natl. Acad. Sci. U. S. A.* 105(46):17807–11
Ray PD, Huang BW, Tsuji Y. 2012. Reactive oxygen species (ROS) homeostasis and redox regulation in cellular signaling. *Cell. Signal.* 24(5):981–90
Reczek CR, Chandel NS. 2015. ROS-dependent signal transduction. *Curr. Opin. Cell Biol.* 33:8–13
Reeves EP, Lu H, Jacobs HL, Messina CGM, Bolsover S, et al. 2002. Killing activity of neutrophils is mediated through activation of proteases by K+ flux. *Nature*. 416(6878):291–97
Richer BC, Salei N, Laskay T, Seeger K. 2018. Changes in Neutrophil Metabolism upon Activation and Aging. *Inflammation*. 41(2):710–21
Riyapa D, Rinchai D, Muangsombut V, Wuttinontananchai C, Toufiq M, et al. 2019. Transketolase and vitamin B1 influence on ROS-dependent neutrophil extracellular traps (NETs) formation. . 1–17

References

Rodríguez-Espinosa O, Rojas-Espinosa O, Moreno-Altamirano MMB, López-Villegas EO, Sánchez-García FJ. 2015. Metabolic requirements for neutrophil extracellular traps formation. *Immunology*. 145(2):213–24

Sanjana NE, Shalem O, Zhang F. 2014. Improved vectors and genome-wide libraries for CRISPR screening. *Nat. Methods*. 11(8):783–84

Schmid-Burgk JL, Schmidt T, Gaidt MM, Pelka K, Latz E, et al. 2014. OutKnocker: A web tool for rapid and simple genotyping of designer nuclease edited cell lines. *Genome Res.* 24(10):1719–23

Selmi C. 2010. The worldwide gradient of autoimmune conditions. *Autoimmun. Rev.* 9(5):A247–50

Shalem O, Sanjana EN, Hartenian E, Zhang F. 2014. Genome-Scale CRISPR-Cas9 Knockout Screening in Human Cells. *Science (80-.).* 343(January):84–88

Siler U, Romao S, Tejera E, Pastukhov O, Kuzmenko E, et al. 2016. Severe glucose-6-phosphate dehydrogenase deficiency leads to susceptibility to infection and absent NETosis. *J. Allergy Clin. Immunol.* 139(1):212-219.e3

Silk E, Zhao H, Weng H, Ma D. 2017. The role of extracellular histone in organ injury. *Cell Death Dis.* 8(5):e2812

Simpson IA, Dwyer D, Malide D, Moley KH, Travis A, Vannucci SJ. 2008. The facilitative glucose transporter GLUT3: 20 Years of distinction. *Am. J. Physiol. - Endocrinol. Metab.* 295(2):242–53

Sollberger G, Amulic B, Zychlinsky A. 2016. Neutrophil extracellular trap formation is independent of de novo gene expression. *PLoS One*. 11(6):1–10

Sollberger G, Choidas A, Burn GL, Habenberger P, Lucrezia R Di, et al. 2018. Gasdermin D plays a vital role in the generation of neutrophil extracellular traps. *Sci. Immunol.* 3(26):

Sollberger G, Streeck R, Caffrey BE, Zychlinsky A. 2019. Linker Histone H1 subtypes specifically regulate neutrophil differentiation. *bioRxiv*

Steinberg BE, Grinstein S. 2007. Unconventional roles of the NADPH oxidase: signaling, ion homeostasis, and cell death. *Sci. STKE*. 2007(379):pe11

Stincone A, Prigione A, Cramer T, Wamelink MMC, Campbell K, et al. 2015. The return of metabolism: Biochemistry and physiology of the pentose phosphate pathway. *Biol. Rev.* 90(3):927–63

Takei H, Araki A, Watanabe H, Ichinose A, Sendo F. 1996. Rapid killing of human neutrophils by the potent activator phorbol 12-myristate 13-acetate (PMA) accompanied by changes different from typical apoptosis or necrosis. *J. Leukoc. Biol.* 59(2):229–40

Tauber AI. 2003. Metchnikoff and the phagocytosis theory. *Nat. Rev. Mol. Cell Biol.* 4(11):897–901

Taylor EL, Rossi AG, Dransfield I, Hart SP. 2007. Analysis of Neutrophil Apoptosis. In *Neutrophil Methods and Protocols*, eds. MT Quinn, FR DeLeo, GM Bokoch, pp. 177–200. Totowa, NJ: Humana Press

Tecchio C, Micheletti A, Cassatella MA. 2014. Neutrophil-derived cytokines: Facts beyond expression. *Front. Immunol.* 5(OCT):1–7

Tong M, Potter JA, Mor G, Abrahams VM. 2019. Lipopolysaccharide-Stimulated Human Fetal Membranes Induce Neutrophil Activation and Release of Vital Neutrophil Extracellular Traps. *J. Immunol.* 203(2):500–510

Tottmar BSC, Petiersson H, Kiessling K. 1973. The Subcellular Distribution and Properties of Aldehyde Dehydrogenases in Rat Liver. *Biochem. J.* 135:577–86

Urban CF, Ermert D, Schmid M, Abu-Abed U, Goosmann C, et al. 2009. Neutrophil extracellular traps contain calprotectin, a cytosolic protein complex involved in host defense against Candida albicans. *PLoS Pathog.* 5(10):

Valentine WN, Follette JH, Lawrence JS. 1953. The glycogen content of human leukocytes in health and in various disease states. *J. Clin. Investig.* 32(3):251–57

Verhoeven NM, Wallot M, Huck JHJ, Dirsch O, Ballauf A, et al. 2005. A newborn with severe liver failure, cardiomyopathy and transaldolase deficiency. *J. Inherit. Metab. Dis.* 28(2):169–79

Villanueva E, Yalavarthi S, Berthier CC, Hodgin JB, Khandpur R, et al. 2011. Netting Neutrophils Induce Endothelial Damage, Infiltrate Tissues, and Expose Immunostimulatory Molecules in Systemic Lupus Erythematosus. *J. Immunol.* 187(1):538–52

Vrhovac I, Breljak D, Sabolic I. 2014. Glucose transporters in the mammalian blood cells. *Period. Biol.* 116(2):131–38

Wagner R. 1945. The estimation of glycogen in whole blood and white blood cells. *Arch. Biochem.*

11(Oct):249–58
Wamelink MM, Struys EA, Salomons GS, Fowler D, Jakobs C, Clayton PT. 2008. Transaldolase deficiency in a two-year-old boy with cirrhosis. *Mol. Genet. Metab.* 94(2):255–58
Warnatsch A, Ioannou M, Wang Q, Papayannopoulos V. 2015. Neutrophil extracellular traps license macrophages for cytokine production in atherosclerosis. *Science (80-.).* 349(6245):1–6
WHO. 2004. The global burden of disease: 2004 update
Wick AN, Drury DR, Nakada HI, Wolfe JB. 1956. Localization of the primary metabolic block produced by 2-deoxyglucose. *J. Biol. Chem.* (5):
Williams M, Valayannopoulos V, Altassan R, Chung WK, Heijboer AC, et al. 2019. Clinical, biochemical, and molecular overview of transaldolase deficiency and evaluation of the endocrine function: Update of 34 patients. *J. Inherit. Metab. Dis.* 42(1):147–58
Winterbourn CC, Kettle AJ, Hampton MB. 2016. Reactive Oxygen Species and Neutrophil Function. *Annu. Rev. Biochem.* 85:765–92
Xie K, Varatnitskaya M, Maghnouj A, Bader V, Winklhofer KF, et al. 2020. Activation leads to a significant shift in the intracellular redox homeostasis of neutrophil-like cells. *Redox Biol.* 28(October 2019):
Ye SF, Wu YH, Hou ZQ, Zhang QQ. 2009. ROS and NF-κB are involved in upregulation of IL-8 in A549 cells exposed to multi-walled carbon nanotubes. *Biochem. Biophys. Res. Commun.* 379(2):643–48
Yipp BG, Kubes P. 2013. NETosis: how vital is it? *Blood*. 122(16):2784–94
Yipp BG, Petri B, Salina D, Jenne CN, Scott BN V, et al. 2012. Infection-induced NETosis is a dynamic process involving neutrophil multitasking in vivo. *Nat. Med.* 18(9):1386–93
Zhen L, King AAJ, Xiao Y, Chanock SJ, Orkin SH, Dinauer MC. 1993. Gene targeting of X chromosome-linked chronic granulomatous disease locus in a human myeloid leukemia cell line and rescue by expression of recombinant gp91(phox). *Proc. Natl. Acad. Sci. U. S. A.* 90(21):9832–36
zur Hausen H, O'Neill FJ, Freese UK, Hecker E. 1978. Persisting oncogenic herpesvirus induced by the tumour promoter TPA. *Nature*. 272(March):6–8

Selbstständigkeitserklärung

Hiermit erkläre ich, die Dissertation selbstständig und nur unter Verwendung der angegebenen Hilfen und Hilfsmittel angefertigt zu haben.

Ich habe mich anderwärts nicht um einen Doktorgrad beworben und besitze keinen entsprechenden Doktorgrad.

Ich erkläre, dass ich die Dissertation oder Teile davon nicht bereits bei einer anderen wissenschaftlichen Einrichtung eingereicht habe und dass sie dort weder angenommen noch abgelehnt wurde.

Ich erkläre die Kenntnisnahme der dem Verfahren zugrunde liegenden Promotionsordnung der Lebenswissenschaftlichen Fakultät der Humboldt-Universität zu Berlin vom 5. März 2015.

Weiterhin erkläre ich, dass keine Zusammenarbeit mit gewerblichen Promotionsberaterinnen/Promotionsberatern stattgefunden hat und dass die Grundsätze der Humboldt-Universität zu Berlin zur Sicherung guter wissenschaftlicher Praxis eingehalten wurden.

Berlin, 20. Dezember 2019

Jakob Paul Steffen Morath

Acknowledgements

This work would not have been possible without the help and support of many people.

Above all, I would like to thank Arturo. Thank you for your trust and support throughout the last four and a half years and for giving me the chance to work on this thesis in your lab. It was for sure not always an easy ride but definitely one during which I learned a lot about science and many other things. In many moments your example served as an inspiration. It has been a privilege to be part of the Zychlinsky department. I much enjoyed its pleasant and curiosity-driven atmosphere which it has thanks to its members of course but also thanks to its head.

Also, I would like to thank Alf. Thank you for your invaluable, optimism-focused support in critical times of this project, for your much appreciated advice and important contribution to the supervision of this work.

A big thank you goes out to the Zychlinsky department as a whole for the great collaborative and supportive spirit in our group. I am deeply grateful for help, advice and critical conversations regarding experimental procedures to Gabriel, Soo, Falko, Borko (who taught me the great art of being a PMN ninja), CJ and Sebastian as well as for inspiring and open discussions to Holly, Andrey, Ale, Garth, Gerben, Thea, Robert, Florian and the other members of our department.

I would like to thank Teresa Domaszewska and Joanna Zyla for help with some of the experimental analyses and visualisations.

Importantly, I would like to thank the medical doctors in Paris and Hamburg, Pascale de Lonlay and Robin Kobbe, respectively who provided us with the TALDO samples.

Life outside of the lab, however compromised it became at times, kept me going throughout this project. I would like to thank Teresa who always and unconditionally supported me; without you I would not have managed. I am amazingly blessed with many beautiful friendships and achieving this work without my friends' comprehension, sympathy and company is unimaginable. Equally important throughout this time was my numerous, slightly complicated and dearly loved family. Again too many to all be named, I would like to express my deepest gratitude and love especially to my siblings, my grandparents, my parents and my brothers. Thank you for being here with me.

Acknowledgements